AD_____

MODELING OF THE NON-AUDITORY RESPONSE TO BLAST OVERPRESSURE

Blast Dynamics of Surrogate Models of the Gastrointestinal Tract

ANNUAL/FINAL REPORT

Edward J. Vasel
James H.-Y. Yu
James H. Stuhmiller

JANUARY 1990

Supported by

U.S. ARMY MEDICAL RESEARCH AND DEVELOPMENT COMMAND
Fort Detrick, Frederick, Maryland 21701-5012

Contract No. DAMD17-85-C-5238

JAYCOR
11011 Torreyana Road
San Diego, California 92121-1190

MODELING OF THE NON-AUDITORY RESPONSE TO BLAST OVERPRESSURE

Blast Dynamics of Surrogate Models of the Gastrointestinal Tract

JANUARY 1990

Supported by

U.S. ARMY MEDICAL RESEARCH
AND DEVELOPMENT COMMAND
Fort Detrick
Frederick, Maryland 21701-5012

Contract No. DAMD17-85-C-5238

REPORT DOCUMENTATION PAGE

1a. REPORT SECURITY CLASSIFICATION Unclassified	1b. RESTRICTIVE MARKINGS N/A
2a. SECURITY CLASSIFICATION AUTHORITY N/A	3. DISTRIBUTION / AVAILABILITY OF REPORT Approved for Public Release; Distribution unlimited
2b. DECLASSIFICATION / DOWNGRADING SCHEDULE N/A	
4. PERFORMING ORGANIZATION REPORT NUMBER(S)	5. MONITORING ORGANIZATION REPORT NUMBER(S)
6a. NAME OF PERFORMING ORGANIZATION JAYCOR Applied Sci. & Engr. Technol. Group 6b. OFFICE SYMBOL (If applicable)	7a. NAME OF MONITORING ORGANIZATION Director Walter Reed Army Institute of Research
6c. ADDRESS (City, State, and ZIP Code) 11011 Torreyana Rd. San Diego, CA 92121-1190	7b. ADDRESS (City, State, and ZIP Code) ATTN: SGRD-UWZ-C, Kenneth T. Dodd, Ph.D. Bldg. 40 Washington, DC 20307-5100
8a. NAME OF FUNDING / SPONSORING ORGANIZATION U. S. Army Medical Res. & Devel. Cmd. 8b. OFFICE SYMBOL (If applicable)	9. PROCUREMENT INSTRUMENT IDENTIFICATION NUMBER DAMD17-85-C-5238
8c. ADDRESS (City, State, and ZIP Code) Fort Detrick Frederick, MD 21701-5012	10. SOURCE OF FUNDING NUMBERS PROGRAM ELEMENT NO.: 62787A PROJECT NO.: 62787A878 TASK NO.: AB WORK UNIT ACCESSION NO.: 004

11. TITLE (Include Security Classification)

(U) Modeling of the Non-Auditory Response to Blast Overpressure

12. PERSONAL AUTHOR(S) Edward J. Vasel, James H.-Y. Yu, and James H. Stuhmiller

13a. TYPE OF REPORT	13b. TIME COVERED	14. DATE OF REPORT (Year, Month, Day)	15. PAGE COUNT
Annual/Final	FROM 8/15/85 TO 7/31/89	1990 January	158

16. SUPPLEMENTARY NOTATION

Blast Dynamics of Surrogate Models of the Gastrointestinal Tract

17. COSATI CODES			18. SUBJECT TERMS (Continue on reverse if necessary and identify by block number)
FIELD	GROUP	SUB-GROUP	RA 3,
26	14		
23	04		

19. ABSTRACT (Continue on reverse if necessary and identify by block number)

Surrogate models of gastrointestinal tract sections have been constructed and tested systematically to gain insight into the dynamics of this organ system under external blast loading. The findings provide a link in the process of producing a predictive methodology for blast injury to the abdomen.

The experimental setup consists of a water-filled chamber providing a surrogate for the abdominal cavity. Coupling to the external blast field is provided by a piston and flexible membrane. Into this chamber can be placed surrogates of the GI tract sections. The pressure fields inside the section and outside in the chamber can be measured. A clear, Plexiglas top allows direct observation of the dynamics.

A commercially prepared lamb caecum material was found to have mechanical properties similar to that of the rabbit GI tract and was used as the surrogate material. Rupture of the material was induced both under static and dynamic loading. Under static conditions the differential pressure across the membrane is directly proportional to the internal stress. Under dynamic loading, the differential pressure at rupture was nearly twice as great, establishing that local inertial effects are critical to blast injury.

20. DISTRIBUTION / AVAILABILITY OF ABSTRACT ☐ UNCLASSIFIED/UNLIMITED ☒ SAME AS RPT ☐ DTIC USERS	21. ABSTRACT SECURITY CLASSIFICATION Unclassified
22a. NAME OF RESPONSIBLE INDIVIDUAL Mary Frances Bostian	22b. TELEPHONE (Include Area Code) [301] 663-7325 22c. OFFICE SYMBOL SGRD-RMI-S

DD FORM 1473, 84 MAR

Blast Dynamics of Surrogate Models of the Gastrointestinal Tract

19. ABSTRACT *(Continued from front)*

The dynamics of the surrogate GI tract were studied under less severe loading for which hemorrhaging is known to occur. Pressures were recorded inside the surrogate (in the liquid and the bubble), near the surrogate, and far away in the chamber. The objective was to determine the physical parameters critical to the tract dynamics and to provide data to validate a previously developed computational model.

The results confirmed the mathematical model, which account was taken of the effect of walls on the flow patterns. Changes in the flow pattern can change the amplitude and frequency of the bubble oscillation and the resulting tissue stress. Once again, it was confirmed that the instantaneous differential pressure across the membrane does not correlate with the tissue stress and that a full dynamic model is required.

Parametric studies showed that the bubble dynamics depend on the bubble volume and shape, the viscosity of the gut contents, and the geometry of the gut section. The effects of neighboring gut sections and their contents did not significantly affect the results.

BLAST DYNAMICS OF SURROGATE MODELS OF THE GASTROINTESTINAL TRACT

Edward J. Vasel
James H.-Y. Yu
James H. Stuhmiller
Applied Science and Engineering Technology
JAYCOR

ABSTRACT

Surrogate models of gastrointestinal tract sections have been constructed and tested systematically to gain insight into the dynamics of this organ system under external blast loading. The findings provide a link in the process of producing a predictive methodology for blast injury to the abdomen.

The experimental setup consists of a water-filled chamber providing a surrogate for the abdominal cavity. Coupling to the external blast field is provided by a piston and flexible membrane. Into this chamber can be placed surrogates of the GI tract sections. The pressure fields inside the section and outside in the chamber can be measured. A clear, Plexiglas top allows direct observation of the dynamics.

A commercially prepared lamb caecum material was found to have mechanical properties similar to that of the rabbit GI tract and was used as the surrogate material. Rupture of the material was induced both under static and dynamic loading. Under static conditions the differential pressure across the membrane is directly proportional to the internal stress. Under dynamic loading, the differential pressure at rupture was nearly twice as great, establishing that local inertial effects are critical to blast injury.

The dynamics of the surrogate GI tract were studied under less severe loading for which hemorrhaging is known to occur. Pressures were recorded inside the surrogate (in the liquid and the bubble), near the surrogate, and far away in the chamber. The objective was to determine the physical parameters critical to the tract dynamics and to provide data to validate a previously developed computational model.

The results confirmed the mathematical model, which account was taken of the effect of walls on the flow patterns. Changes in the flow pattern can change the amplitude and frequency of the bubble oscillation and the resulting tissue stress. Once again, it was confirmed that the instantaneous differential pressure across the membrane does not correlate with the tissue stress and that a full dynamic model is required.

Parametric studies showed that the bubble dynamics depend on the bubble volume and shape, the viscosity of the gut contents, and the geometry of the gut section. The effects of neighboring gut sections and their contents did not significantly affect the results.

SUMMARY

Surrogate models of gastrointestinal tract sections have been constructed and tested systematically to gain insight into the dynamics of this organ system under external blast loading. The findings provide a link in the process of producing a predictive methodology for blast injury to the abdomen.

The experimental setup consists of a water-filled chamber providing a surrogate for the abdominal cavity. Coupling to the external blast field is provided by a piston and flexible membrane. Into this chamber can be placed surrogates of the GI tract sections. The pressure fields inside the section and outside in the chamber can be measured. A clear, Plexiglas top allows direct observation of the dynamics.

A commercially prepared lamb caecum material was found to have mechanical properties similar to that of the rabbit GI tract and was used as the surrogate material. Rupture of the material was induced both under static and dynamic loading. Under static conditions the differential pressure across the membrane is directly proportional to the internal stress. Under dynamic loading, the differential pressure at rupture was nearly twice as great, establishing that local inertial effects are critical to blast injury.

The dynamics of the surrogate GI tract were studied under less severe loading for which hemorrhaging is known to occur. Pressures were recorded inside the surrogate (in the liquid and the bubble), near the surrogate, and far away in the chamber. The objective was to determine the physical parameters critical to the tract dynamics and to provide data to validate a previously developed computational model.

The results confirmed the mathematical model, which account was taken of the effect of walls on the flow patterns. Changes in the flow pattern can change the amplitude and frequency of the bubble oscillation and the resulting tissue stress. Once again, it was confirmed that the instantaneous differential pressure across the membrane does not correlate with the tissue stress and that a full dynamic model is required.

Parametric studies showed that the bubble dynamics depend on the bubble volume and shape, the viscosity of the gut contents, and the geometry of the gut section. The effects of neighboring gut sections and their contents did not significantly affect the results.

CONTENTS

ILLUSTRATIONS

TABLES

1. INTRODUCTION

Previous field studies have shown that strong or repeated blast exposure can result in injury to the gastrointestinal (G.I.) tract. Such injury ranges from simple surface contusions to severe hemorrhage and intestinal wall rupture. Field tests have also shown that the threshold for G.I. tract injury appears to lie between that of the larynx and the lung and therefore may be a critical element in combat casualty care.

Insight into the mechanism of G.I. blast injury was gained in laboratory experiments at JAYCOR using isolated, perfused rabbit intestine that allowed direct visual observation of the G.I. tract and pressure measurement at bubble locations during blast exposure. The perfusion technique developed by Yu and Vasel [1] uses the animal's own cardiopulmonary system to oxygenate the isolated G.I. tract which is placed inside a saline-filled test chamber for blast loading tests. Results from such tests showed that the injury locations could be directly correlated with bubble locations; that violent intestinal wall surface motion correlates with internal pressure time histories; and that injury correlates more with the differential pressure across the membrane wall and bubble internal pressure than with the peak chamber loading pressures.

When an animal is exposed to blast overpressure the general sequence of events leading to G.I. injury is as illustrated in Figure 1-1. The free field blast produces body loading which produces body distortion. Body motion results in a local deformation of air-containing organs. Membrane deformation causes strain in the material which at a critical stress level will result in injury. Determining this critical wall stress is central to prediction of blast injury.

A surrogate G.I. tract model allows us to establish the dynamic relationship between blast loading and G.I. bubble response. When this information is supplemented by small animal injury threshold tests, an analytical tool for G.I. tract injury prediction can then be developed.

The first step in the development of an analytical model of intestinal response is to identify the controlling parameters for blast-induced bubble response. Because the study of bubble dynamics does not require the presence of a blood supply, a surrogate model can be used in lieu of live animals. Also, the use of a surrogate for these experiments offers distinct advantages over live animals. A surrogate with similar material properties is a more stable medium, allowing quicker test setup and turnaround time. It allows tighter control of test variables. Finally, it reduces the number and cost of animals needed by eliminating extraneous variables before verification in live animal tests.

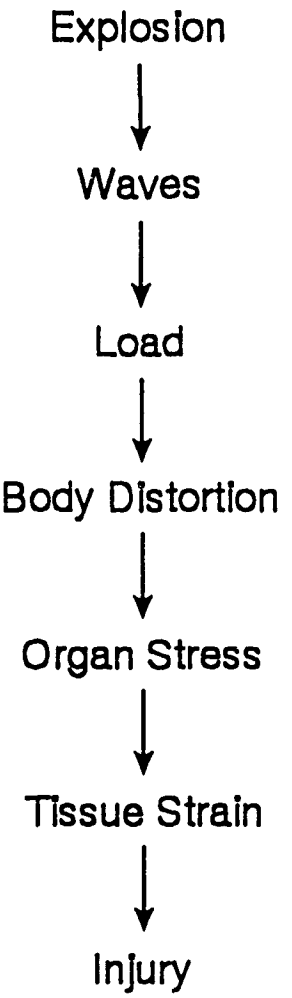

Figure 1-1. Common mechanical sequence of injury.

This report covers the results of surrogate material tests, blast loading rate effect study, and the evaluation of some of the control parameters identified. Using this data, the analytical BUBBLE code was evaluated. Implications of these results for the small animal protocol to determine blast injury thresholds is discussed.

2. BLAST LOADING TECHNIQUE

2.1 LABORATORY BLAST LOADING CHAMBER

The free field blast produces body loading which results in local organ strain and potential injury. Extensive data from free field blast loading on sheep have been taken during experiments carried out by WRAIR at the Lovelace LS-1 facility in Albuquerque, New Mexico. These experiments were designed to measure blast loading, internal organ response, and to observe injury. The external blast loading was measured by using the Blast Overpressure Orientation Module [2] and a few sheep skin gauges. Internal loading signals were gathered from abdominally instrumented sheep. Typical examples of the data from a field test are shown in Figures 2-1 and 2-2. These figures show that the blast pressure wave changes markedly as it passes through the animal. Therefore, in order to study local organ injury in the laboratory, a method to emulate internal local blast loading characteristics was needed.

The JAYCOR blast loading test chamber used for G.I. tract blast injury tests is shown in Figure 2-3. The primary design components are: the 8" diameter water-filled test chamber with cover, the flexible diaphragm, the impact piston and powder actuated impactor. The impactor uses the explosive pressure from a 22 caliber blank to push the piston into the diaphragm creating a pressure cycle in the chamber similar to field abdominal blast loading signals. There are ten blank sizes available and, depending on the amount of air bubbles in the chamber, can deliver a peak impulse between 2 and 120 psi, (14 and 800 kPa). The design was based on an estimated abdominal blast signal for a long duration blast. A typical pressure chamber loading signal and 5 cc air bubble pressure response is shown in Figure 2-4. The shape and impulse of the chamber signal are similar to the deep abdominal signals measured in sheep in the field tests and was used for all surrogate G.I. tests.

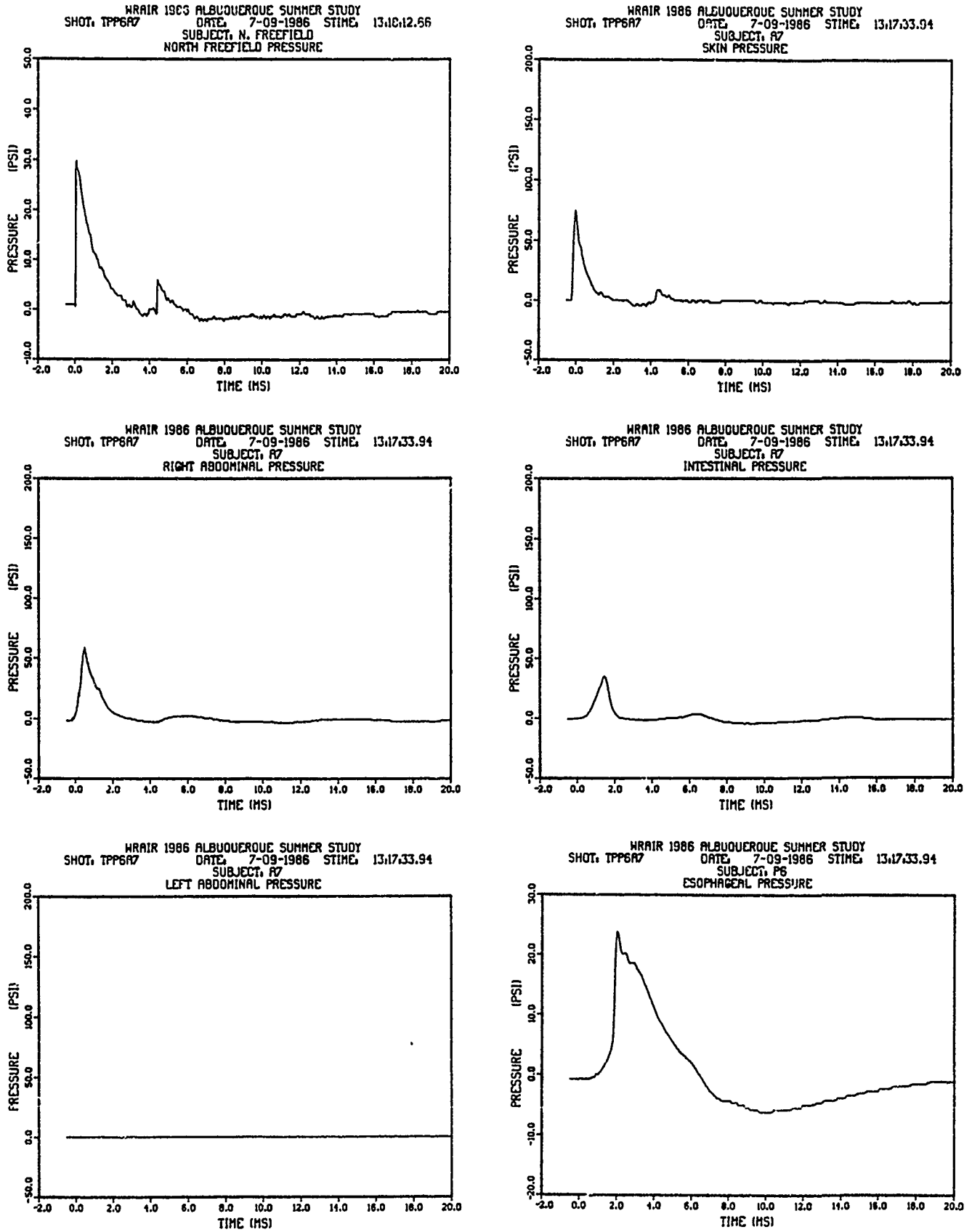

Figure 2-1. Typical sheep internal signals.

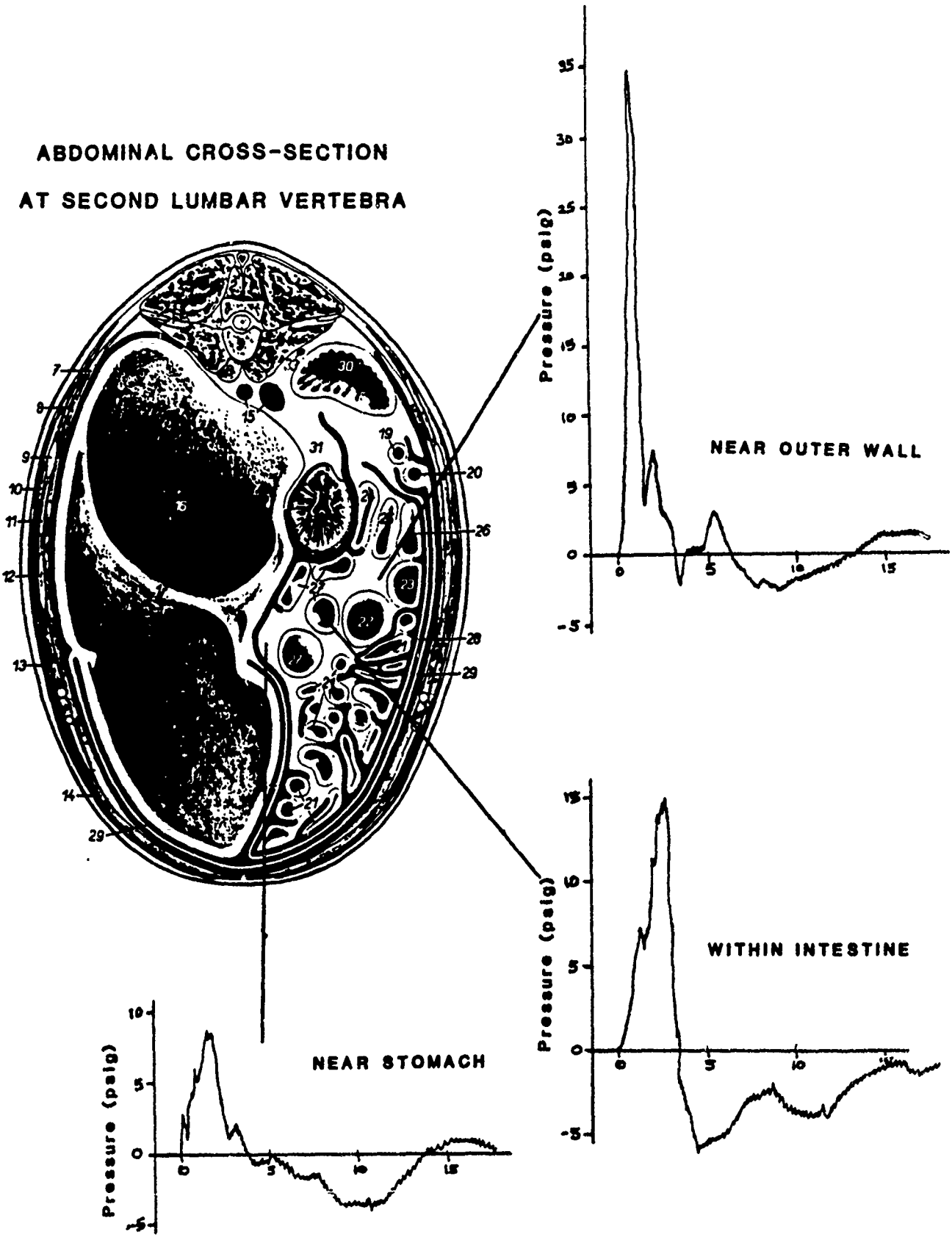

Figure 2-2. Typical sheep loading signals.

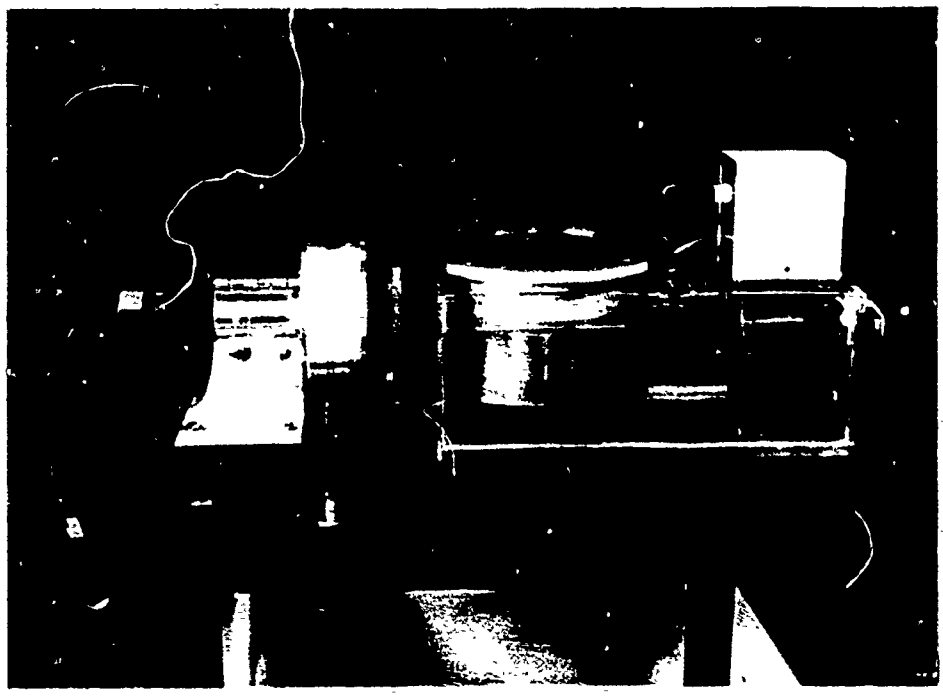

Figure 2-3a. Laboratory loading system, pressure chamber and powder actuated impactor.

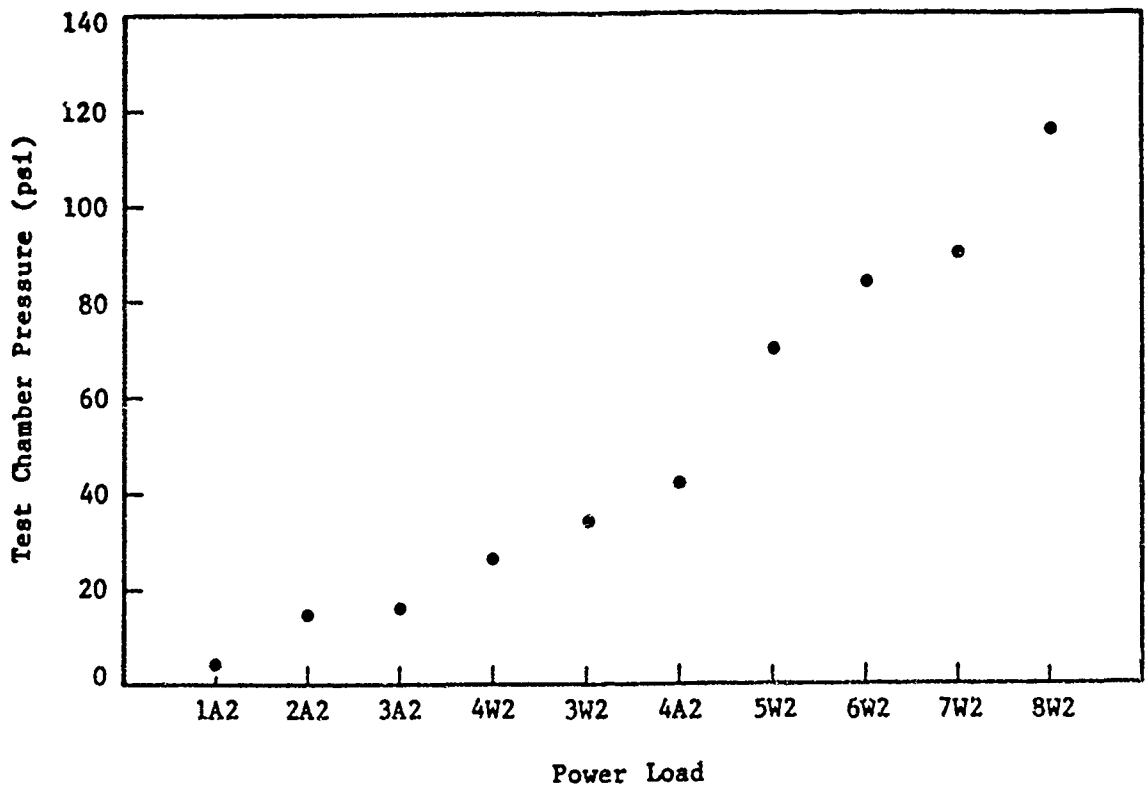

Figure 2-3b. Test chamber pressure vs power load.

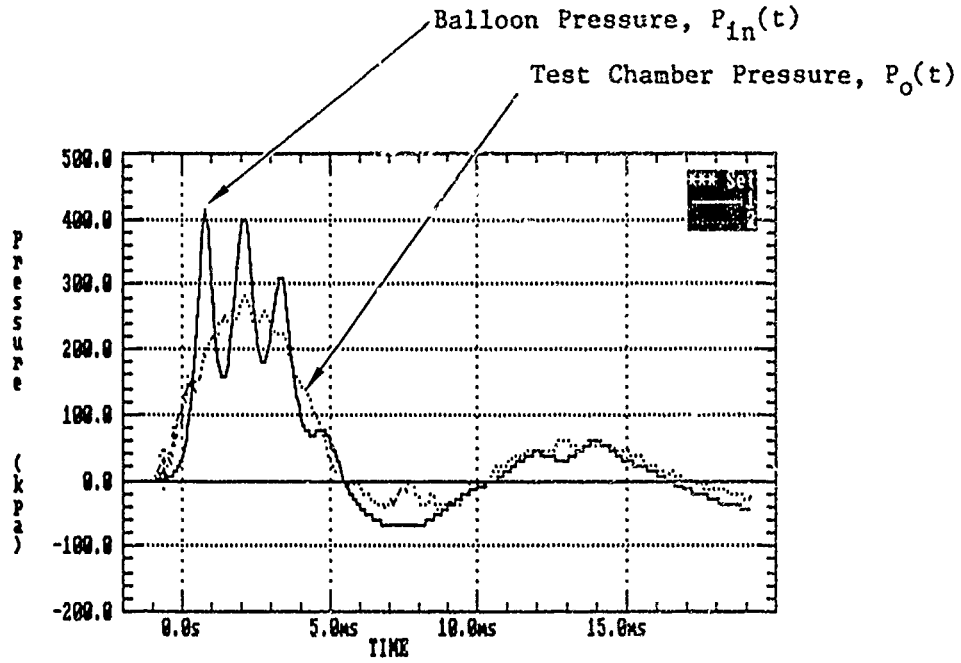

Figure 2-4. Typical pressure chamber loading signal and 5 cc bubble internal pressure response.

3. SURROGATE MATERIAL LOADING RESPONSE

3.1 SURROGATE MATERIAL SELECTION

To account for any material properties effect on loading response and bubble dynamics, a commercially processed sheep caecum material that closely models G.I. material was selected as the surrogate material.

Previously, a series of in vivo static burst pressure studies was conducted on rabbit large intestine samples to determine their material strength [3]. Table 3-1 is a summary of the data collected using the setup shown in Figure 3-1.

The same setup was used to evaluate two commercially available products which were geometrically similar to actual G.I. cross-sections. The first candidate was a thin walled, 2 in. diameter latex tube. The second sample was a 2 in. diameter tube made from commercially processed lamb caecum material. Both samples had one end sealed.

The test procedure was as follows. The sample was first filled with water to zero pressure in a water bath to neutralize shape distortion due to gravitational effects. Static pressure was then applied to the sample by injection with additional water using a syringe. The gauge pressure corresponding to the added liquid volume was read on a sphygmomanometer gauge. The change in sample circumference was also measured. The wall thickness was monitored using a Nova ultrasonic thickness gauge. The results of the latex and lambskin static pressurization tests are shown in Figures 3-2 and 3-3, respectively. As can be seen, the latex model is very elastic and distorts easily with an increase in internal pressure, whereas the lambskin has shown characteristics more similar to that of the rabbit G.I. tracts. Therefore, the lambskin was chosen as the surrogate material for our parametric studies.

3.2 DYNAMIC VERSUS STATIC LOADING

Circular stress (σ) for a thin walled cylinder is defined as:

$$\sigma = PD/2t \tag{1}$$

where P is the static differential pressure across the membrane, D is the diameter and t is the wall thickness.

Table 3-1. Summary of Bursting Properties of Rabbit Large Intestine

		Diameter (cm)		Wall Thickness (mm)		Rupture Strength (kPa)	
	Sex	D_O	D_B	t_O	t_B	P_B	σ
Caecum	M	3.28±0.191	3.84±0.188	0.406±0.052	0.295±0.041	15.58±4.55	1,014.11
	F	3.40±0.264	4.14±0.244	0.371±0.042	0.277±0.026	13.10±2.21	979.64
Ascending Colon (Proximal)	M	1.96±0.305	2.54±0.25	0.729±0.137	0.483±0.113	23.51±4.55	618.39
	F	2.01±0.137	2.74±0.20	0.726±0.112	0.480±0.082	21.79±2.28	622.53
Ascending Colon (Distal)	M	1.37±0.226	1.96±0.119	0.643±0.133	0.442±0.058	27.30±7.31	603.91
	F	1.47±0.124	2.03±0.097	0.615±0.131	0.389±0.057	23.23±2.96	607.36
Transverse Colon	M	1.30±0.122	1.68±1.65	0.394±0.066	0.296±0.061	11.44±2.41	324.02
	F	1.40±0.102	1.91±0.122	0.495±0.091	0.336±0.053	11.10±1.59	315.06
Descending Colon	M	1.40±0.175	1.85±0.183	0.406±0.076	0.285±0.052	10.41±1.86	339.19
	F	1.40±1.42	1.98±0.188	0.406±0.070	0.295±0.045	9.38±0.97	315.06

σ: $P_B D_B / 2t_B$, bursting circular stress

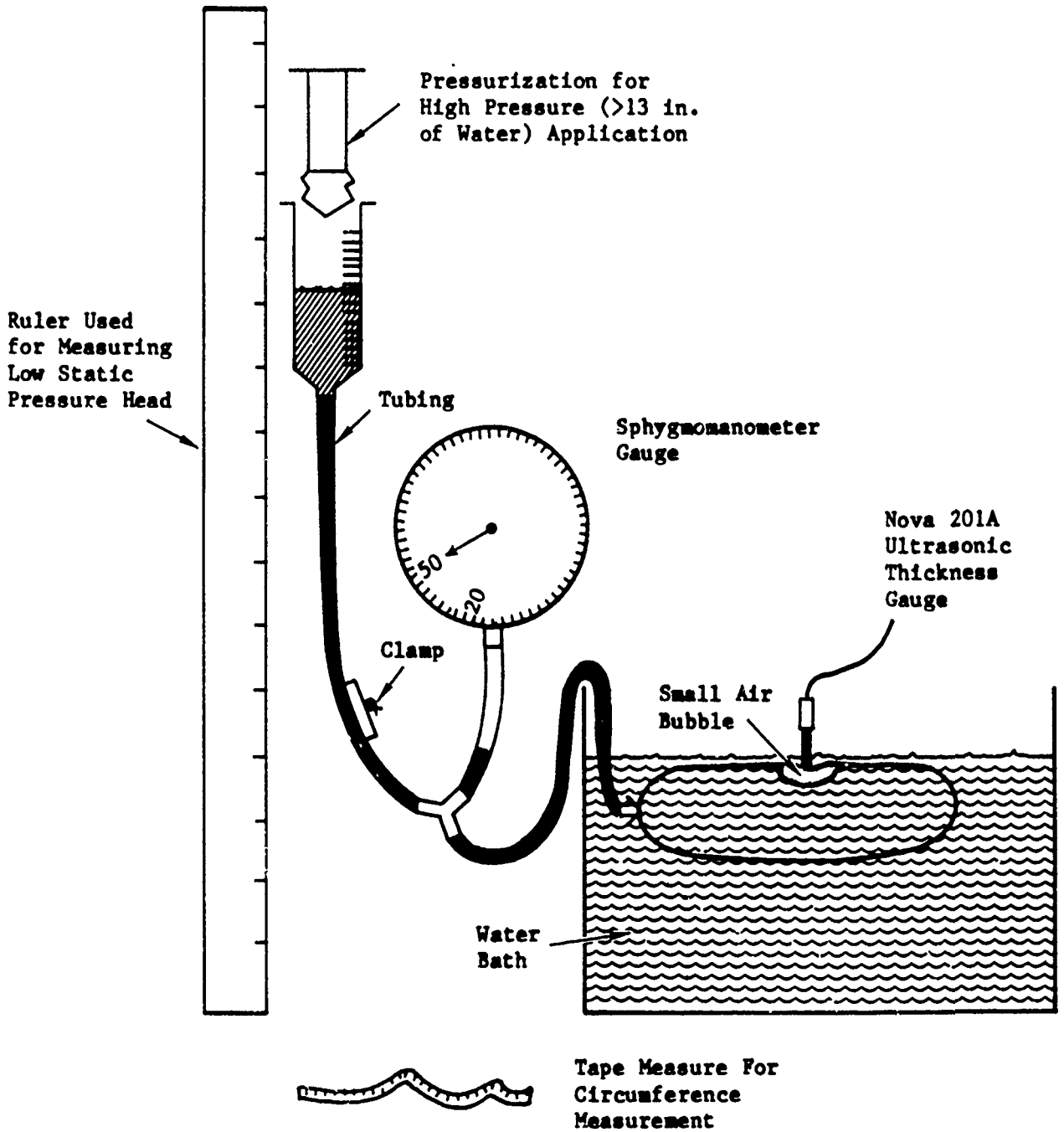

Figure 3-1. Static pressurization experimental setup.

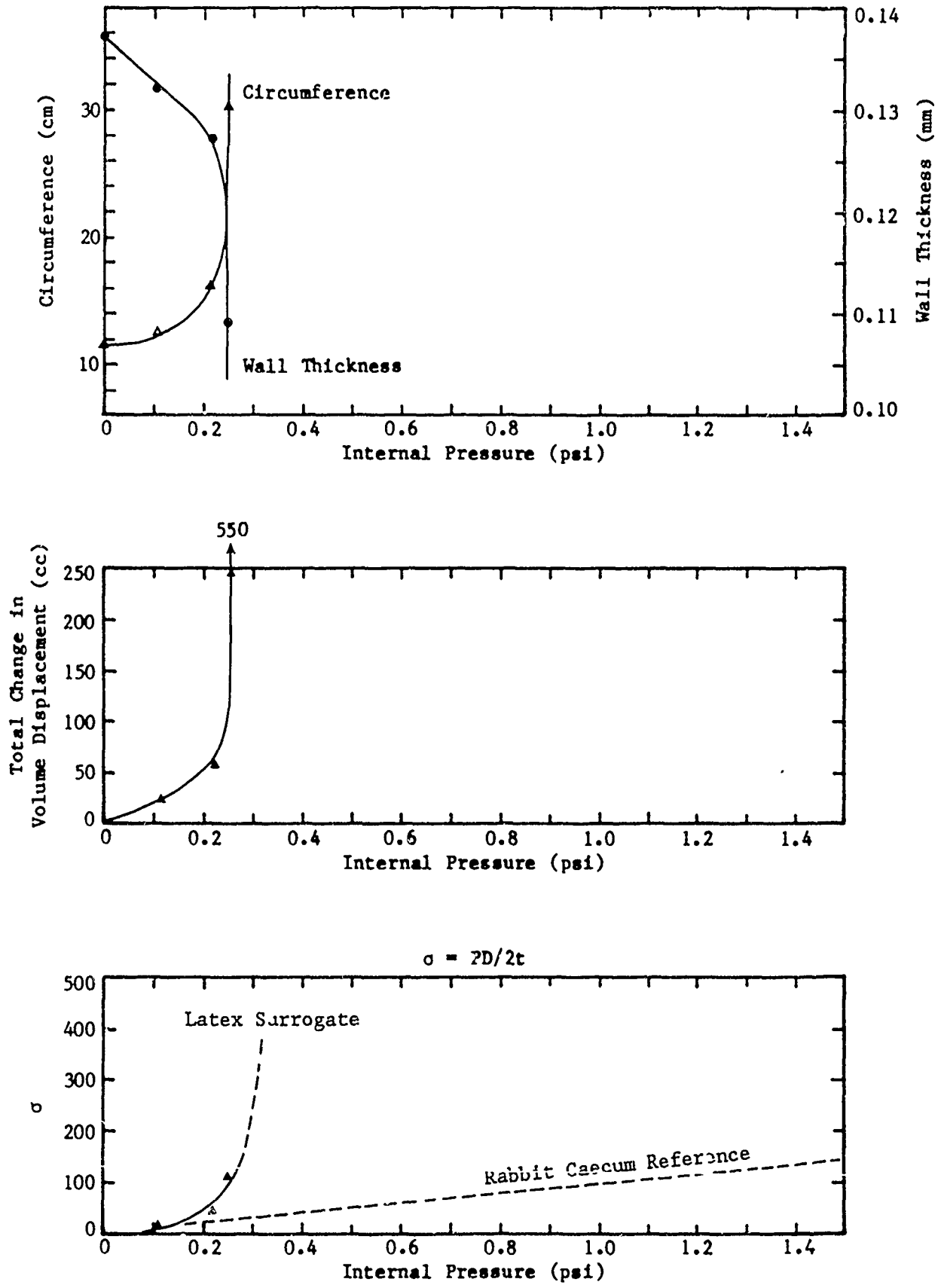

Figure 3-2. Material properties of latex tube.

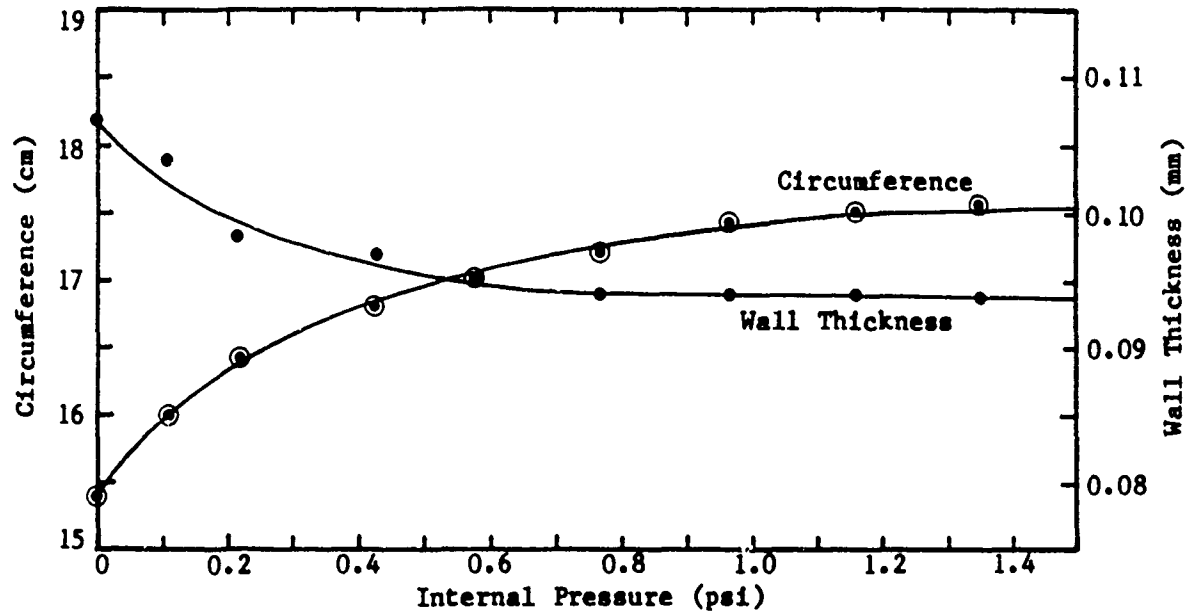

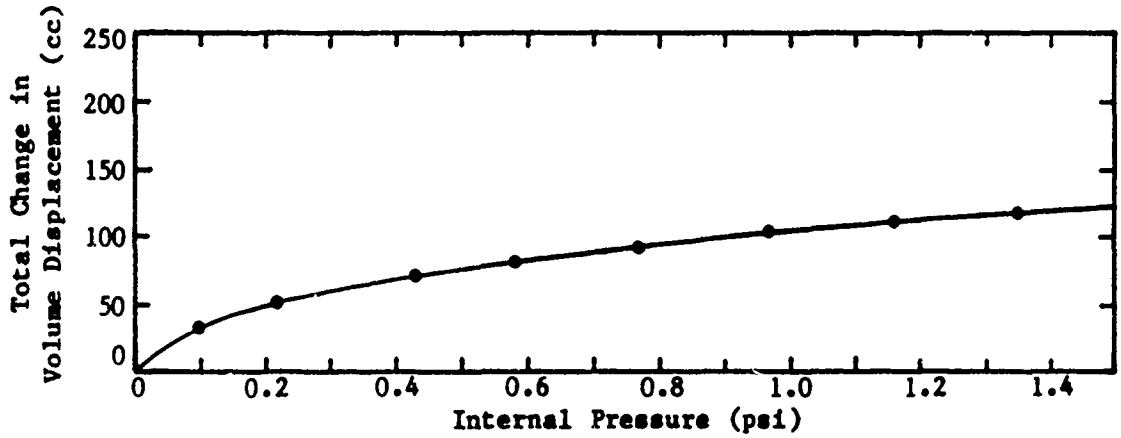

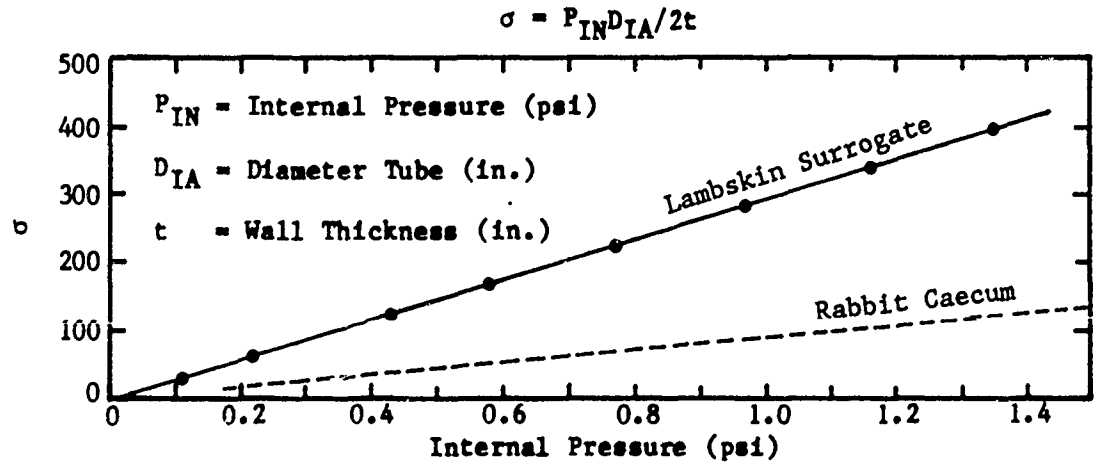

Figure 3-3. Material properties of lambskin caecum membrane.

For a sphere, the equation is:

$$\sigma = PR/2t \qquad (2)$$

As P increases, D or R increases and t decreases until the critical stress (σ_c)is reached, when the material ruptures.

An experiment was designed to test whether this critical stress (σ_c)is a constant under both dynamic and static loading conditions. To test the dynamic response property of the surrogate material, each lambskin surrogate was cut into four test sections to be used, two each, for both dynamic and static tests. These sections were installed in the test fixture as shown in Figure 3-4 and 3-5. Static pressure was slowly applied to the pressure chamber through a sidewall port. A pressure gauge monitored the static chamber pressure until the membrane ruptured.

Table 3-2 summarizes the results of the static test series. The average static burst pressure for a 0.75" diameter hole was 24.6 psi, and the average static burst pressure for a 1.50" diameter hole was 13.3 psi. Figure 3-6 shows that within each sample the results were very consistent. These results agree with Eq. (1): as membrane diameter increases, rupture pressure decreases and the critical (σ_c) remains constant.

The dynamic test setup is shown in Figure 3-7 and 3-8. The powder actuated impactor was used to deliver the loading. This configuration was designed with several goals in mind: to measure the membrane loading at burst, to prevent the impingement of the transducer by the test membrane, and to test the effect of radius of curvature on membrane stress by using a different cavity opening.

Since the dynamic pressure in the water decreases rapidly away from the oscillating bubble, the exact loading can only be measured on the membrane. However, the transducer can only be placed either at a finite distance away from the wall and measure the approximate value, or mounted on the membrane and risk altering the membrane properties and its response to blast. If the pressure transducer is placed too close to the membrane it can get hit during the expansion mode of the oscillation and produce erroneous data.

The design shown in Figure 3-7 alleviated both problems. The surrogate test sample enclosed a known air volume at pressure P_2. Instead of exposing the test membrane directly to water, an additional latex membrane was installed to provide an air chamber for the wall-mounted transducer (P_1). Since the pressure in the air cavity (P_2) is the same everywhere, the exact loading on the membrane was determined by the differential pressure measured on both sides of the membrane ($P_1 - P_2$).

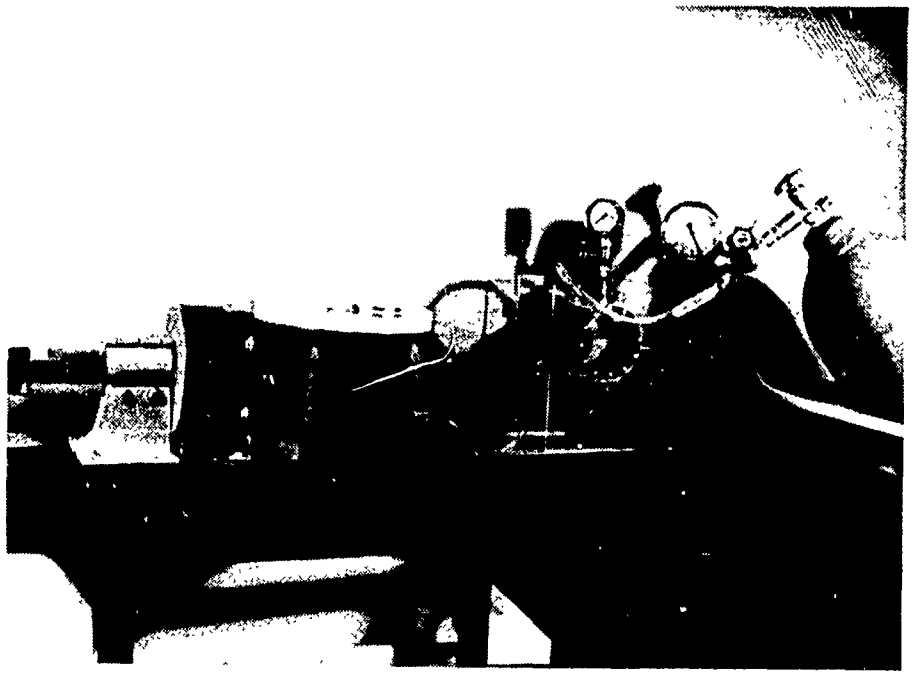

(a) Lambskin burst strength test setup

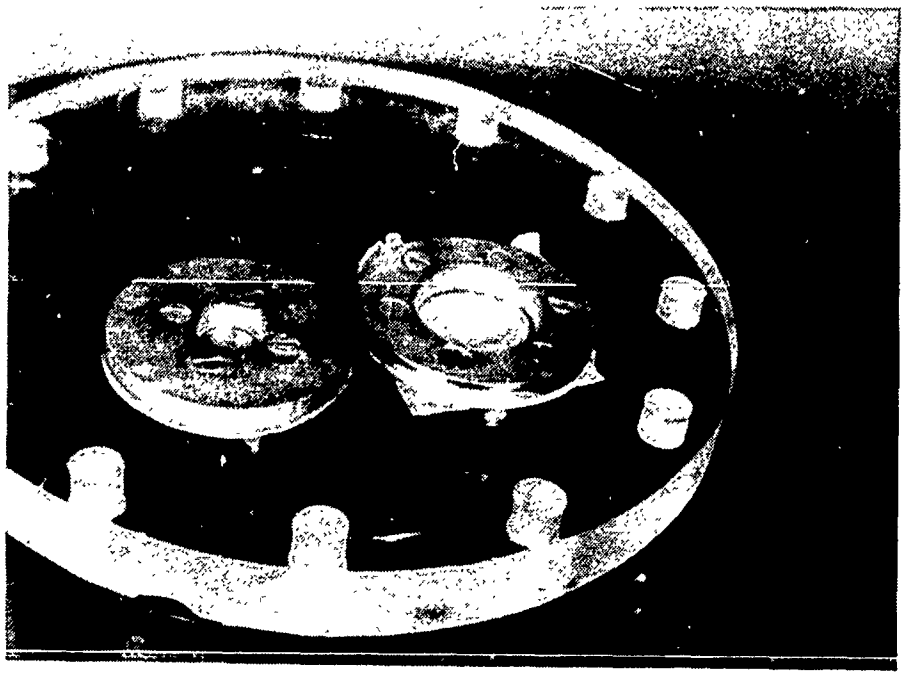

(b) Static test sample installation (1.5" diameter)

Figure 3-4. Static burst strength test setup.

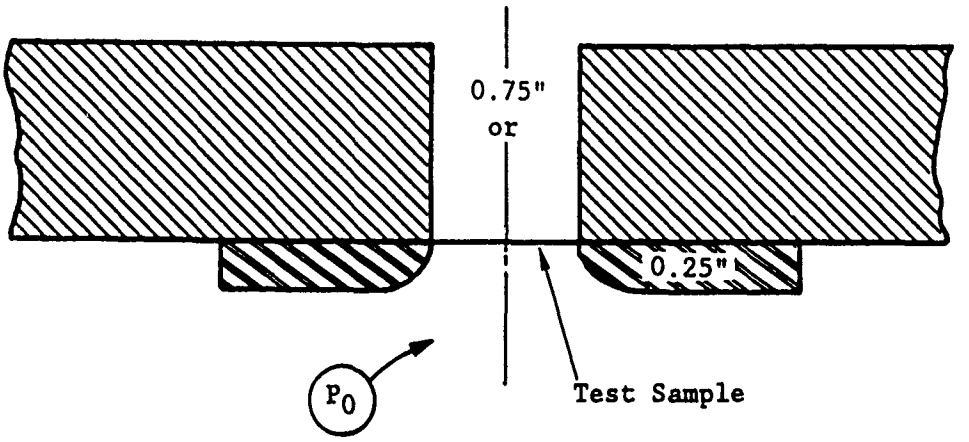

Figure 3-5. Static loading measurement configuration and rupture pattern.

Table 3-2. Summary of Surrogate Static Bursting Pressure Measurements.

Sample Number	Diameter	P0 (psi)
	Static Test	
B-2	0.75	24.0
E-1	0.75	24.0
E-2	0.75	23.0
E-3	0.75	21.0
F-1	0.75	24.5
F-4	0.75	25.0
G-1	0.75	31.0
		Average = 24.6 $\pm$ 3.09
A-2	1.50	12.0
C-2	1.50	13.0
D-4	1.50	17.0
F-2	1.50	11.5
F-3	1.50	12.0
G-2	1.50	14.5
		Average = 13.3 $\pm$ 2.09

STATIC TEST SAMPLE "F"

F-4 0.75" dia. 25.0 psi	F-2 1.50" dia. 11.5 psi
F-3 1.50" dia. 12.0 psi	F-1 0.75" dia. 24.5 psi

Figure 3-6. Typical sample data.

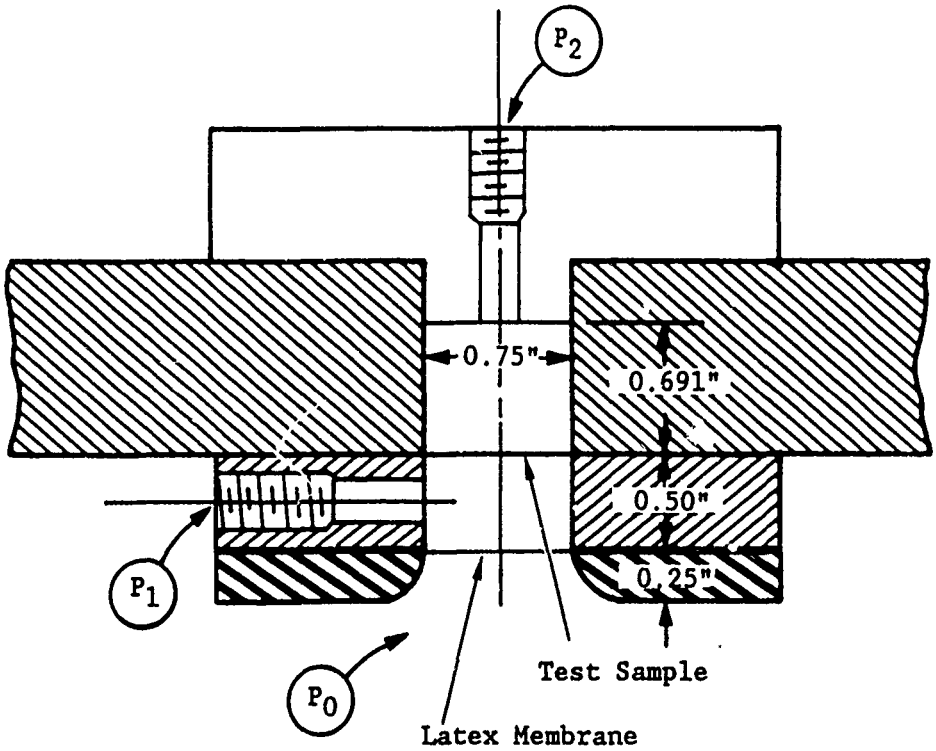

Figure 3-7. Test sample dynamic loading measurement configuration.

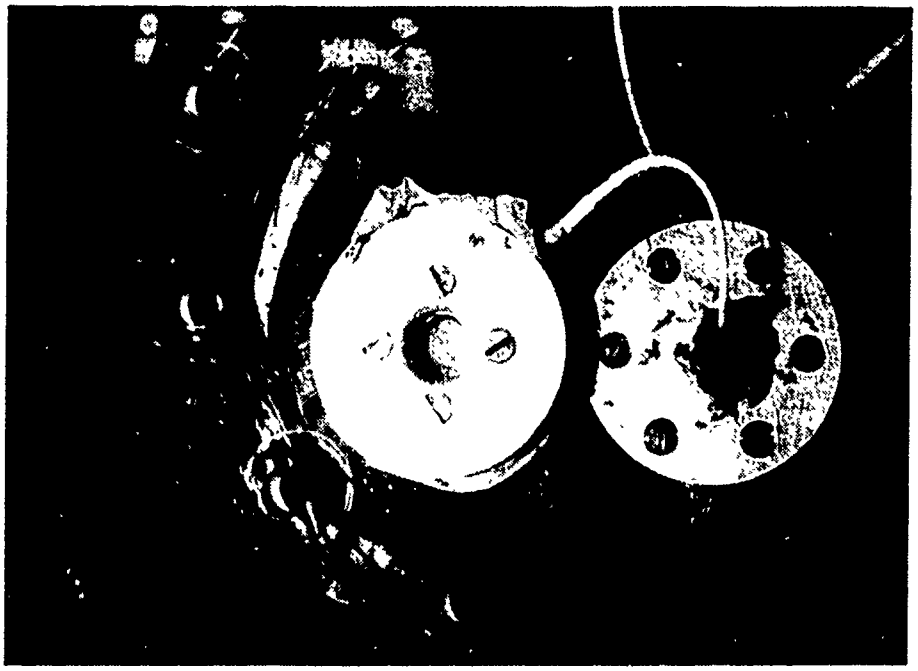

(a) Dynamic test sample installation

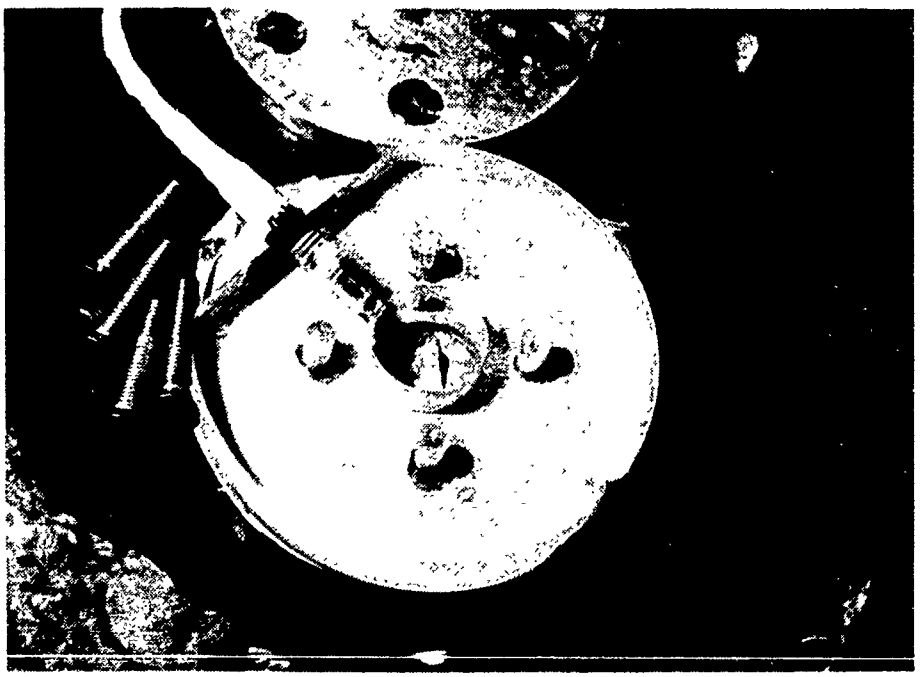

(b) Ruptured lambskin

Figure 3-8. Surrogate dynamic burst test setup.

Mounting the transducer on the side wall also prevented it being hit by the membrane. By using different test cavity radius fixtures, the effect of radius of curvature on membrane stress was also determined.

Figures 3-9 and 3-10 are examples of pressure signals from 0.75" diameter (5 cc) and 1.50" diameter (20 cc) tests. Figure 3-9 shows clearly how P_2 changes slowly until rupture occurs. Table 3-3 summarizes the results of this dynamic test series. Again, the difference in cavity radius results in the same properties of rupture strength (Eq. 1).

Comparison of Tables 3-2 and 3-3 indicated some interesting results. The measured differential pressures at rupture were approximately twice as great during rapid loading as in the static loading case.

A different dynamic test using the "wet" setup similar to the static setup in Figure 3-5 was used to confirm this result. Typical pressure signals from this test are shown in Figure 3-11 and the data is summarized in Table 3-3. Again, the test results indicate that the peak pressure differential at rupture appears greater under dynamic loading.

A series of different loading rate tests were carried out. We found that as the pressure rise time decreases the burst pressure increases. For 3 min., 1 sec, 374 ms, and 2.04 ms rise times, the peak burst pressures are 25, 27.2, 32.8, and 50.3 psi, respectively.

The larger differential pressure at rupture for the dynamic loading is probably the result of the slow response of the test membrane. A higher dynamic loading would be required when applied for a short period of time to produce the same critical stretching of the membrane. Therefore, loading rate, peak pressure and duration of the loading determine the critical strain for tissue injury. Since bubble pressure is an indication of how much the membrane wall has distorted to change bubble volume and if the rise time and "A"-duration of the input signal are kept constant, the peak bubble internal pressure, P_{in}, could be used as the correlate of bubble dynamics during blast.

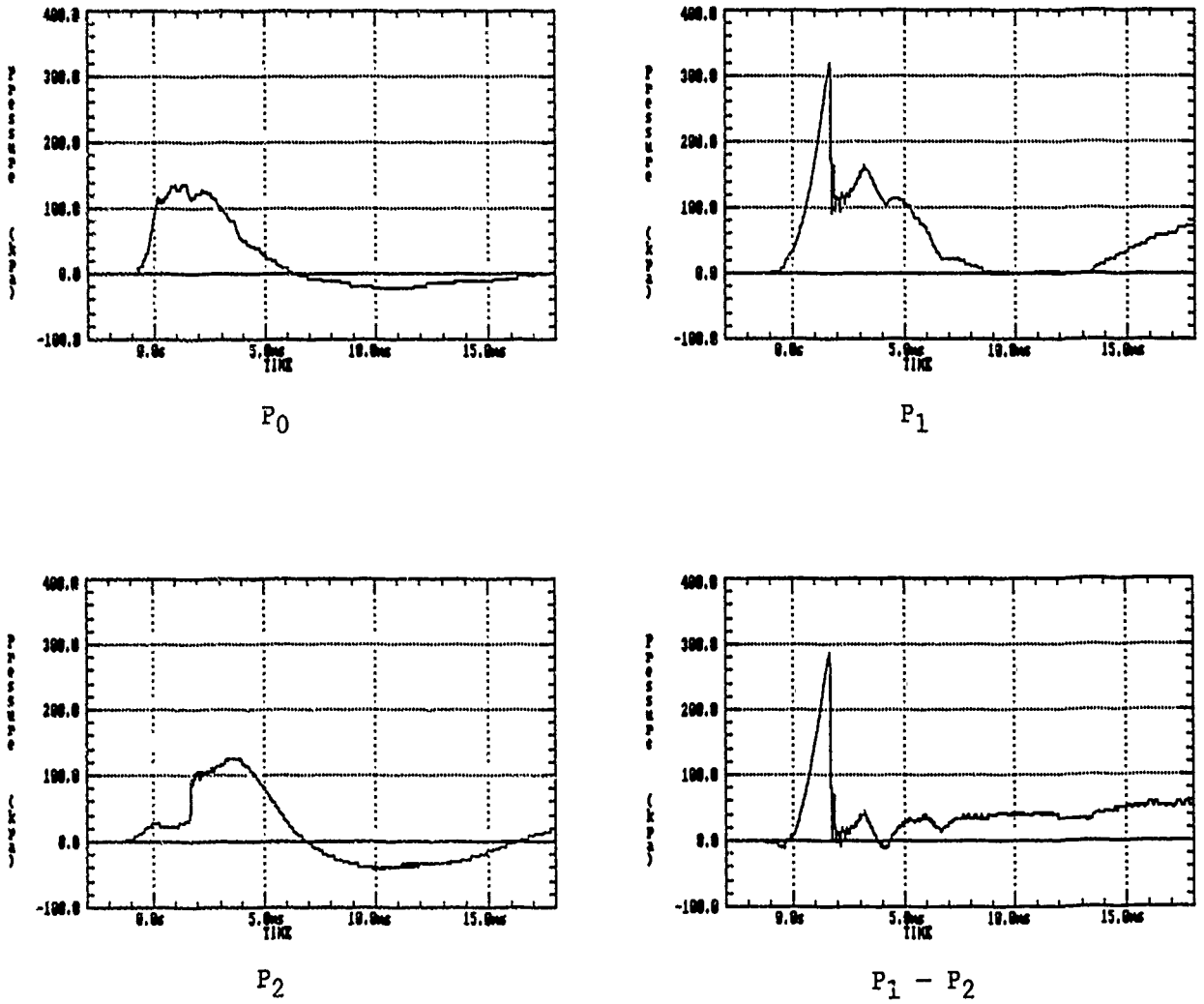

Figure 3-9. Typical dynamic burst pressure signals of a 0.75" diameter lambskin under air DP.

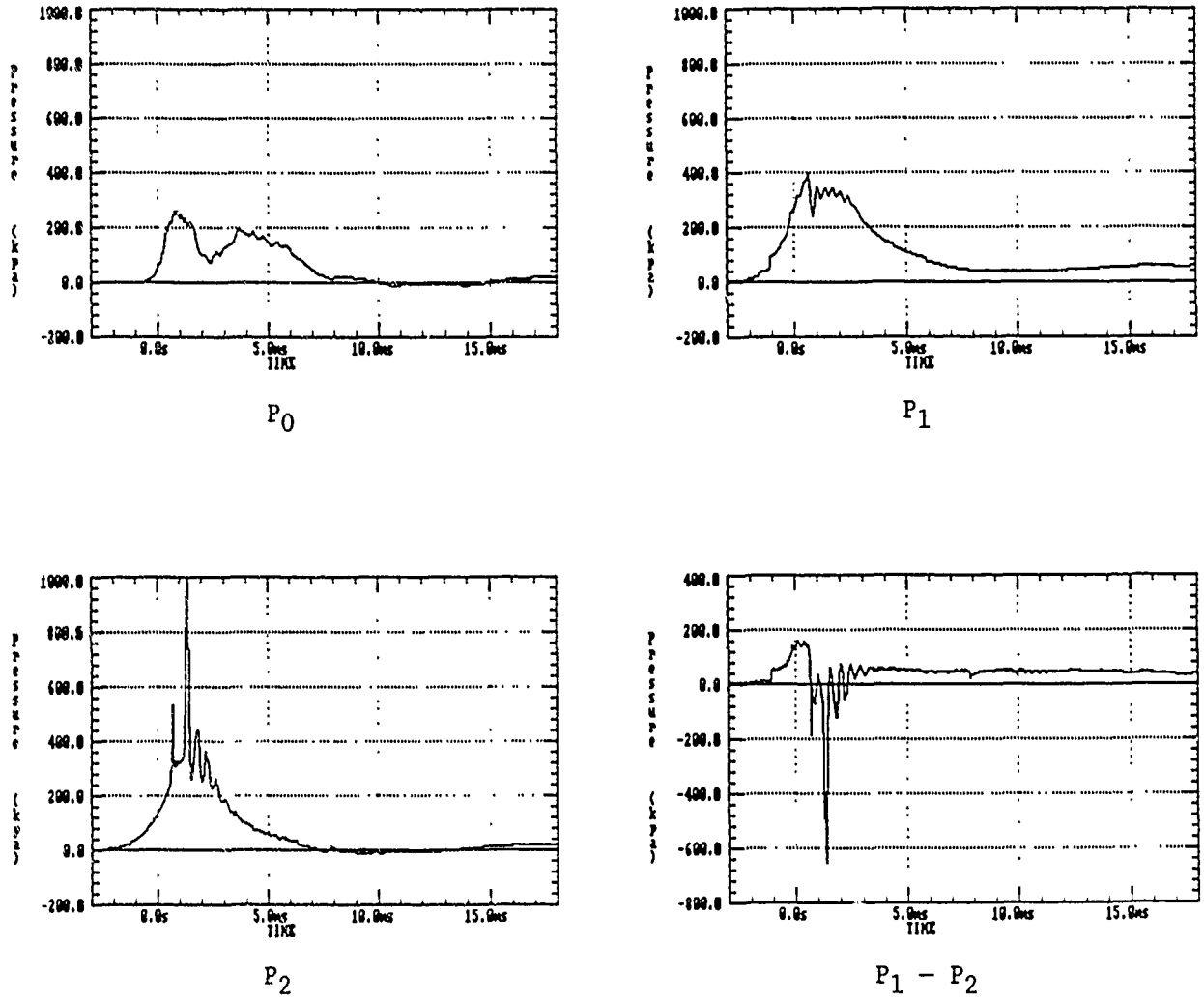

Figure 3-10. Typical dynamic burst pressure signals of a 1.50" diameter lambskin under air DP.

Table 3-3. Summary of Bursting Pressure Measurements.

Sample Number	Diameter	P0 (psi)	P1 (psi)	P2 (psi)	P1-P2 (psi)
			Dynamic Air Test		
0-1	0.75	----	51.8	5.50	46.3
A-1	0.75	19.7	46.3	5.00	41.3
B-1	0.75	33.4	60.1	16.6	43.5
B-3	0.75	36.2	62.3	11.1	51.2
C-1	0.75	27.4	66.1	11.0	55.1
H-1	0.75	40.6	62.8	12.1	50.7
					Average = 48.0 ± 5.21
D-2	1.50	37.3	57.3	34.2	23.1
G-4	1.50	37.3	43.0	22.6	20.4
H-2	1.50	40.6	40.8	16.6	24.2
					Average = 22.6 ± 1.96
			Dynamic Wet Test		
O-2	0.75	41.7	46.3		
H-3	0.75	41.7	48.0		

Po

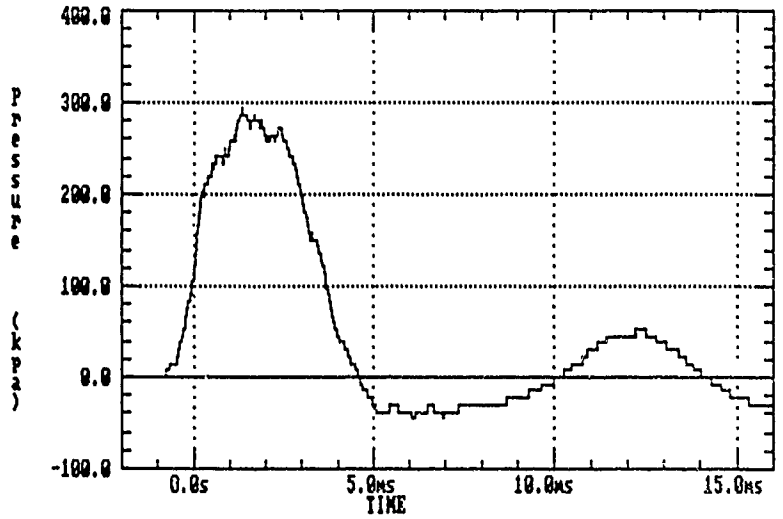

P1

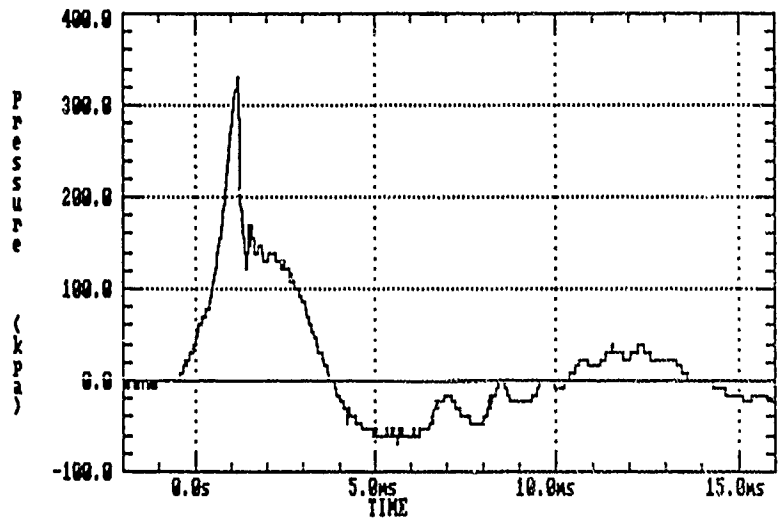

Figure 3-11. Typical 0.75" diameter wet dynamic burst test pressure signals.

4. SURROGATE BUBBLE DYNAMICS EXPERIMENTS

In order to compare injury conditions observed for small animals with those of sheep and man, it is necessary to have a mechanistic concept of the injury process and the controlling factors involved. Understanding these controlling factors will allow the development of an analytical model to predict G.I. injury thresholds. As shown earlier, injury is associated with local membrane distortion due to blast. The local dynamics produce stress (σ)which causes membrane distortion and, if it exceeds the material strength of the tissue, will inflict injury. Since local pressure is the only quantity that can be practically measured, we seek to relate the injury process to this quantity.

The local pressure can be expressed as either the local differential pressure across the membrane wall, $(P_{in} - P_{out}) = DP_w$; the differential pressure referenced to the chamber pressure, $(P_{in} - P_{chamber}) = DP$; or simply the internal bubble pressure (P_{in}). We used the differential pressure across the membrane wall (DP_w) as the gastrointestinal tract correlate in our earlier effort [4]; however, because DP_w is difficult to measure and the presence of the probe outside the bubble might disturb the bubble flow field, and because the internal bubble pressure P_{in} and DP do indicate the bubble response to blast, we chose peak P_{in} and DP as the test parameters. The evolution of the experimental approaches are summarized in the following.

4.1 DIFFERENTIAL PRESSURE MEASUREMENTS

Reference [4] details the rationale and test results of perfused rabbit gastrointestinal tract tests. Figures 4-1 and 4-2 illustrate a sample signal and the corresponding bubble oscillation at the bubble site for a given blast loading.

This bubble oscillation and associated wall deformation is a result of the rapid compression rate of the loading signal. The bubble is compressed by the fluid just outside the membrane wall. The inertia of the moving fluid overcompresses the gas and bubble expansion begins. Recoil then occurs and the bubble oscillation cycle continues until the motion is dissipated. The bubble oscillations are therefore governed by the laws of gas dynamics, the flow of the surrounding fluid, and the material properties of the membrane wall.

Previous studies using latex surrogates, Figure 4-3, show that the differential pressure (DP) between the local blast loading and the bubble internal pressure shows the correlation between the amplitude and frequency of DP and the loading pressure. Figure 4-4 illustrates how two pressure transducers were used to measure DP_w, $(P_{in} - P_{out})$, across a balloon membrane and Figure 4-5 shows the corresponding pressure traces.

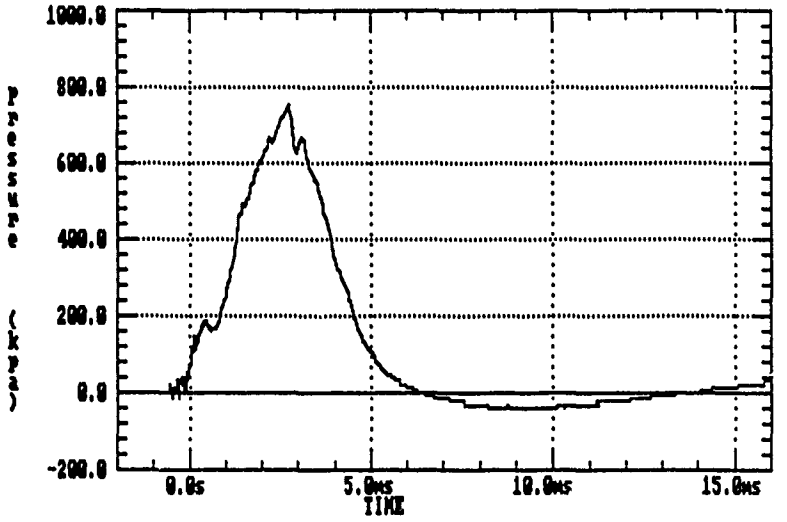

(a) Chamber pressure

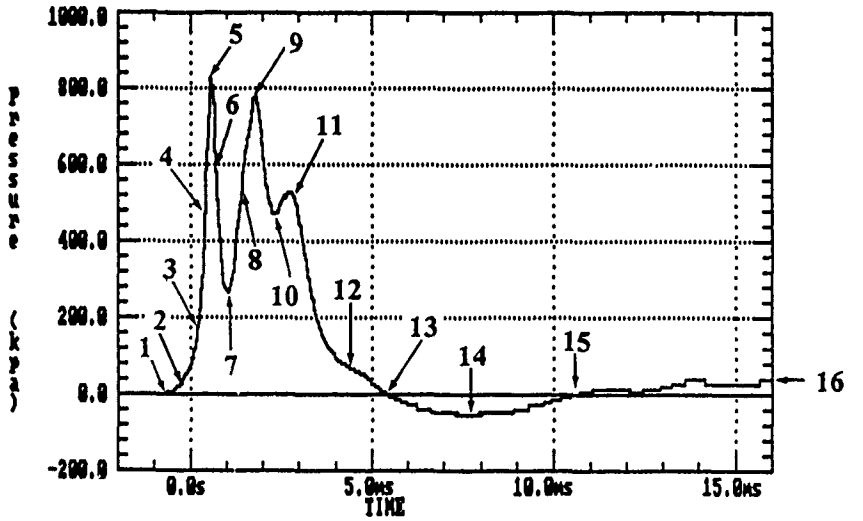

(b) Pressure inside caecum test bubble

Figure 4-1. Pressure signals during blast loading. Numbers shown correspond to the picture frames of Figure 4-2.

Figure 4-2. Surface deformation of air-filled caecum sections during blast loading.

Figure 4-2. (Cont'd).

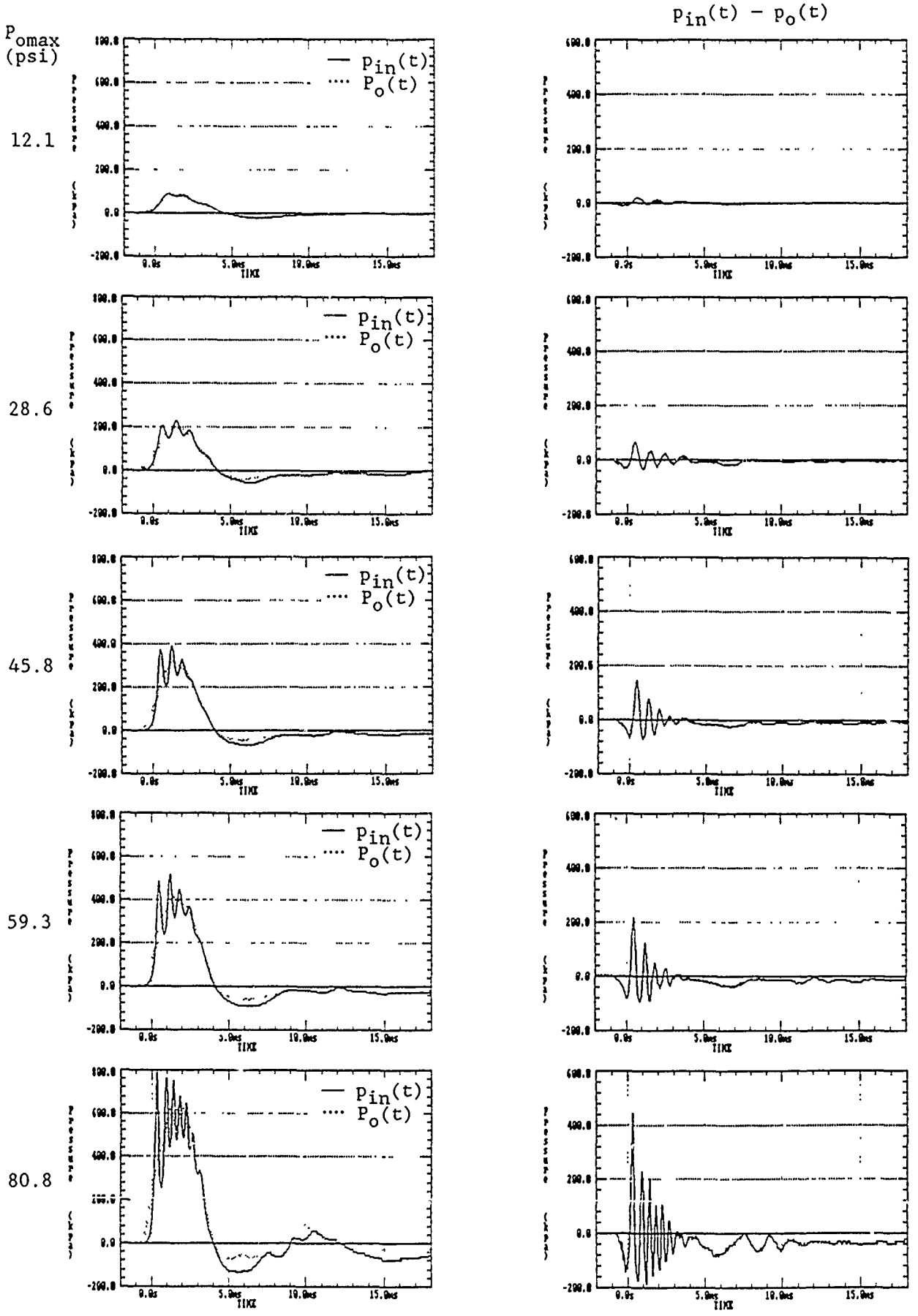

Figure 4-3. Pressure differentials between that of the test chamber and inside a balloon for different blast loadings.

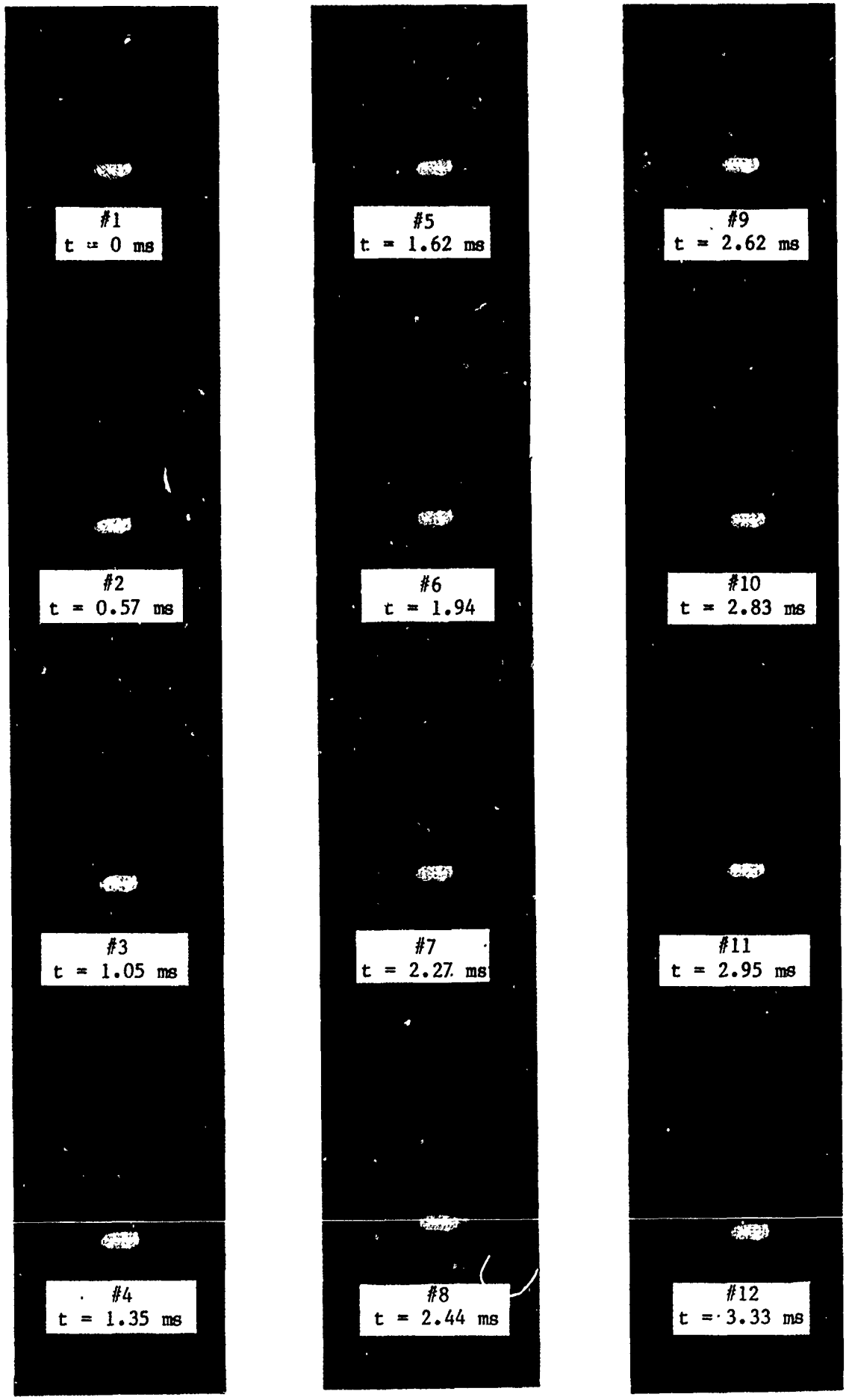

Figure 4-4. Surface deformation of a small balloon during blast loading.

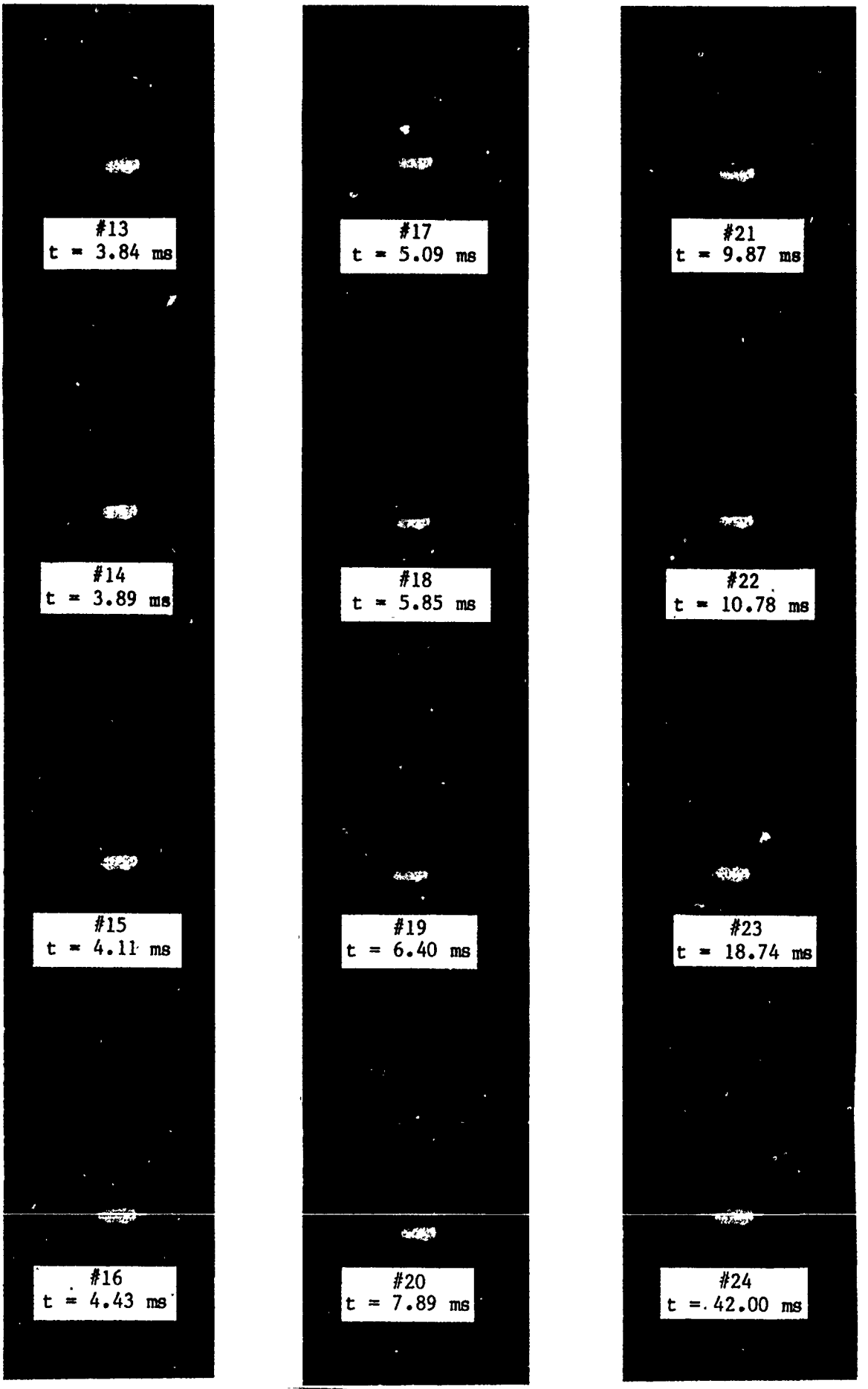

Figure 4-4. (Cont'd).

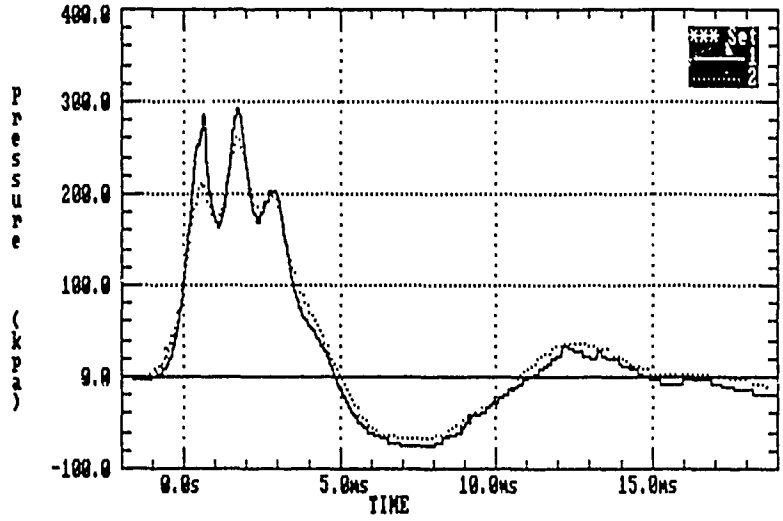

(a) Pressure signals inside, $p_{in}(t)$, and outside, $P_{out}(t)$, the balloon

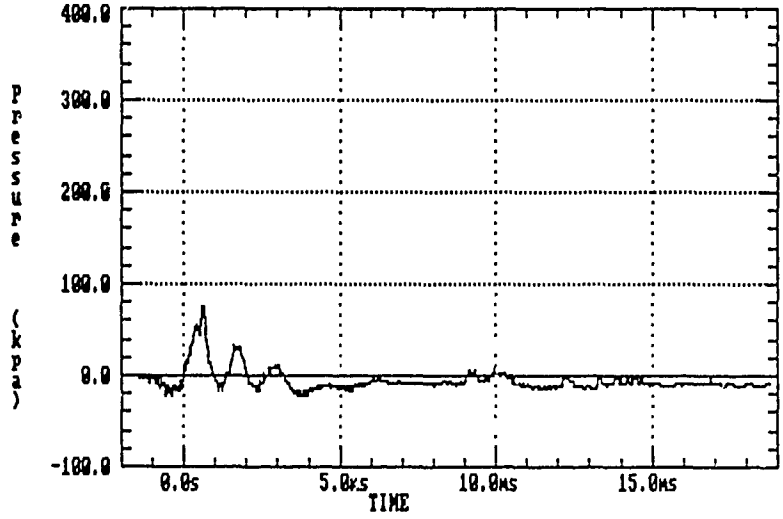

(b) Differential pressure, $p_{in}(t) - p_{out}(t)$

Figure 4-5. Pressure measurements across the balloon wall.

Figures 4-6 and 4-7 show that this differential pressure across the wall (DP_W) only exists at air bubble locations. The results from perfused G.I. tests, shown in Figures 4-8 and 4-9, appear to indicate the threshold level of DP_W with rabbit caecum injury. The difficulty of measuring DP_W using two transducers across the membrane shown in Figure 4-10 indicated that a more reliable DP_W measurement arrangement was required.

A "tubal fixture" (Fig. 4-11) was fabricated to measure DP_W across a surrogate material. The fixture allows a hole to be cut in the bottom of the surrogate to mount the internal pressure transducer. It is adjusted to be placed in the air bubble and looks "face-on" across the membrane to the external transducer. The membrane model was secured to the fixture with adhesive. The internal transducer passageway was sealed using teflon tape. The lambskin surrogate model was filled with water and a selected air bubble was injected. The model internal pressure was zeroed before each test. The test setup is shown in Figure 4-12.

Results for 5 cc and 10 cc air volumes are shown in Figure 4-13. The results agree with previous animal tests that larger radii of curvature associated with larger air volumes appear to produce a lower dynamic DP_W for a given chamber pressure.

4.1.1 Clamped Hemisphere Geometry

The clamped hemisphere fixture shown in Figure 4-14 was designed to independently test the effects on DP_W of bubble air volume and membrane wall radius of curvature. A lambskin caecum membrane section of a predetermined radius of curvature was placed in the fixture and O-ring sealed to the lower chamber. This allowed testing of a membrane that is uniform in all directions. It was a 2-D simplification of the previous tubal 3-D double curvature fixture.

The lower fixture chamber is secured to the upper fixture chamber with mounting bolts. The upper fixture chamber had flow ports to allow test chamber pressure conditions to exist at the outer surface of the membrane. The lower chamber was filled with water, than a predetermined air bubble volume was injected through the 3-way valve and the internal and external membrane wall transducers were adjusted to pretested stand-off distances. During the tests, the 3-way valve was used to adjust the internal pressure to the desired level. The results of the clamped hemisphere fixture tests are shown in Figures 4-15 through 4-24.

The effect of bubble volume for a constant radius of curvature (R_C = 0.75") was tested. Typical pressure signals for 5 cc and 10 cc test results are shown in Figures 4-16 and 4-17. The results of these tests indicated that if the radius of curvature is the same, then the air volume (within the limits tested) has no effect on DP_W.

For larger air volumes (25-40 cc) tested, lambskin tends to be damaged on contact with the transducers; the results are questionable.

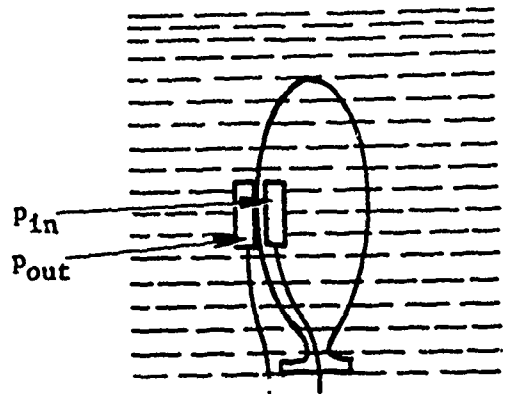

(a) Balloon filled with water

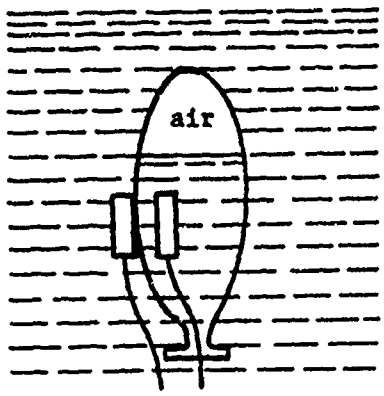

(b) Internal transducer under water

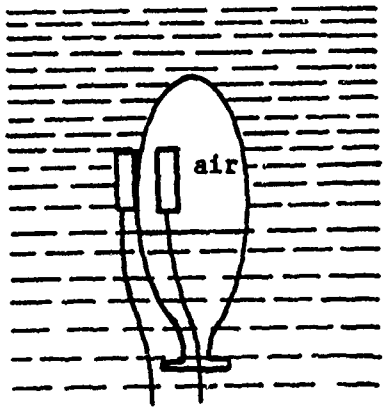

(c) Internal transducer in air

Figure 4-6. Test configuration for differential-pressure measurements across a small balloon.

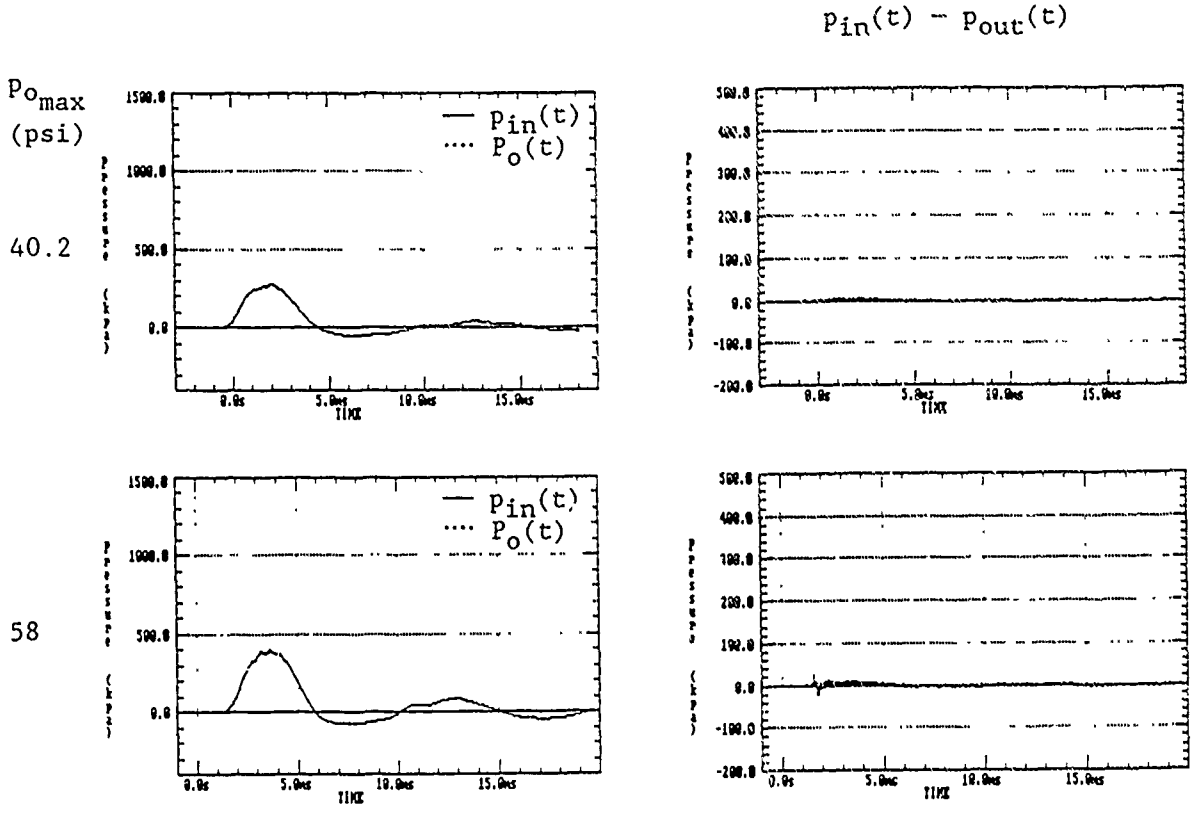

(a) Balloon filled with water $p_{in}(t)$ and $p_{out}(t)$

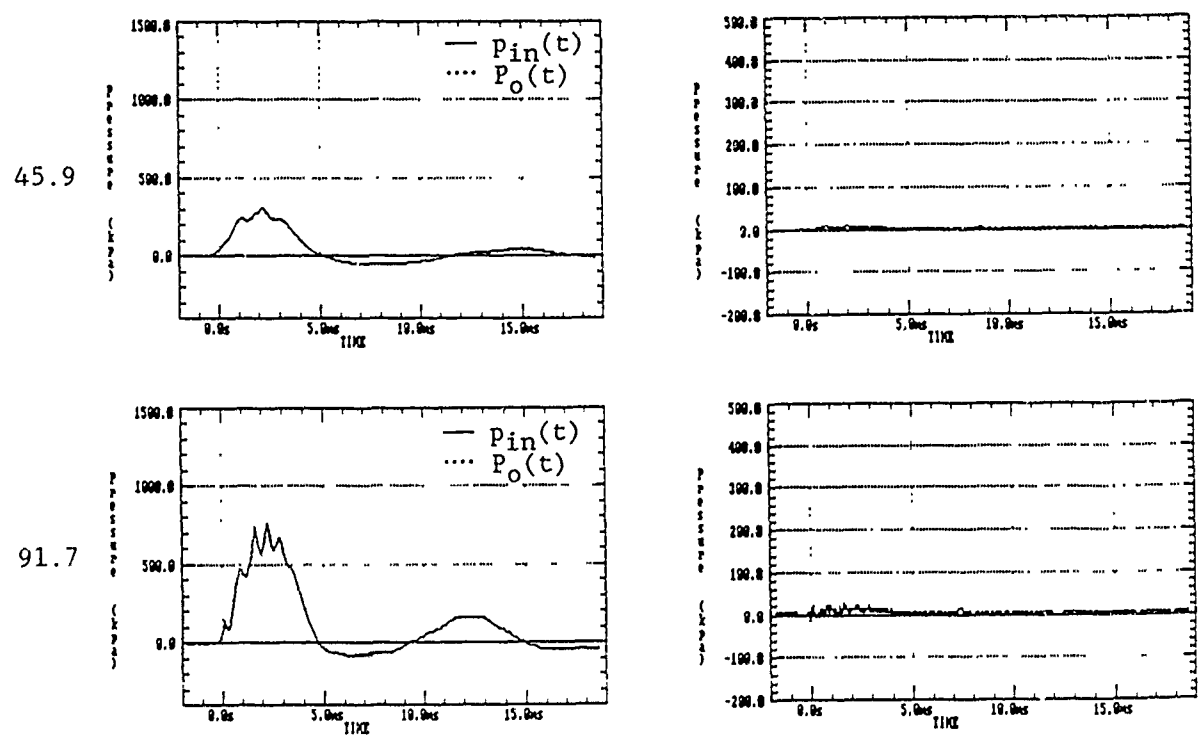

(b) Internal transducer under water $p_{in}(t) - p_{out}(t)$

Figure 4-7. Pressure pairs and their differences obtained from configurations shown in Figure 4-6.

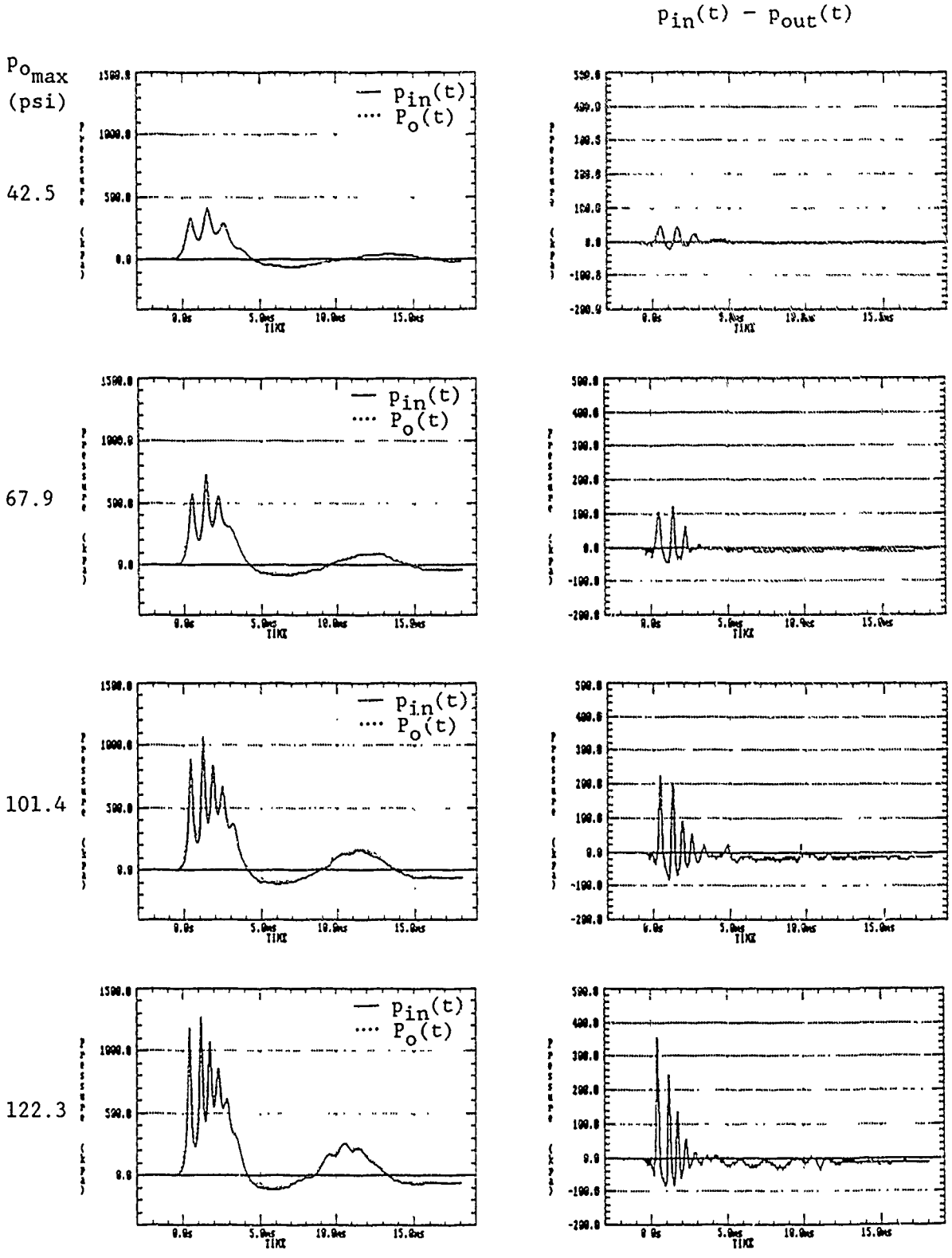

(c) Internal transducer in air

Figure 4-7. (Cont'd).

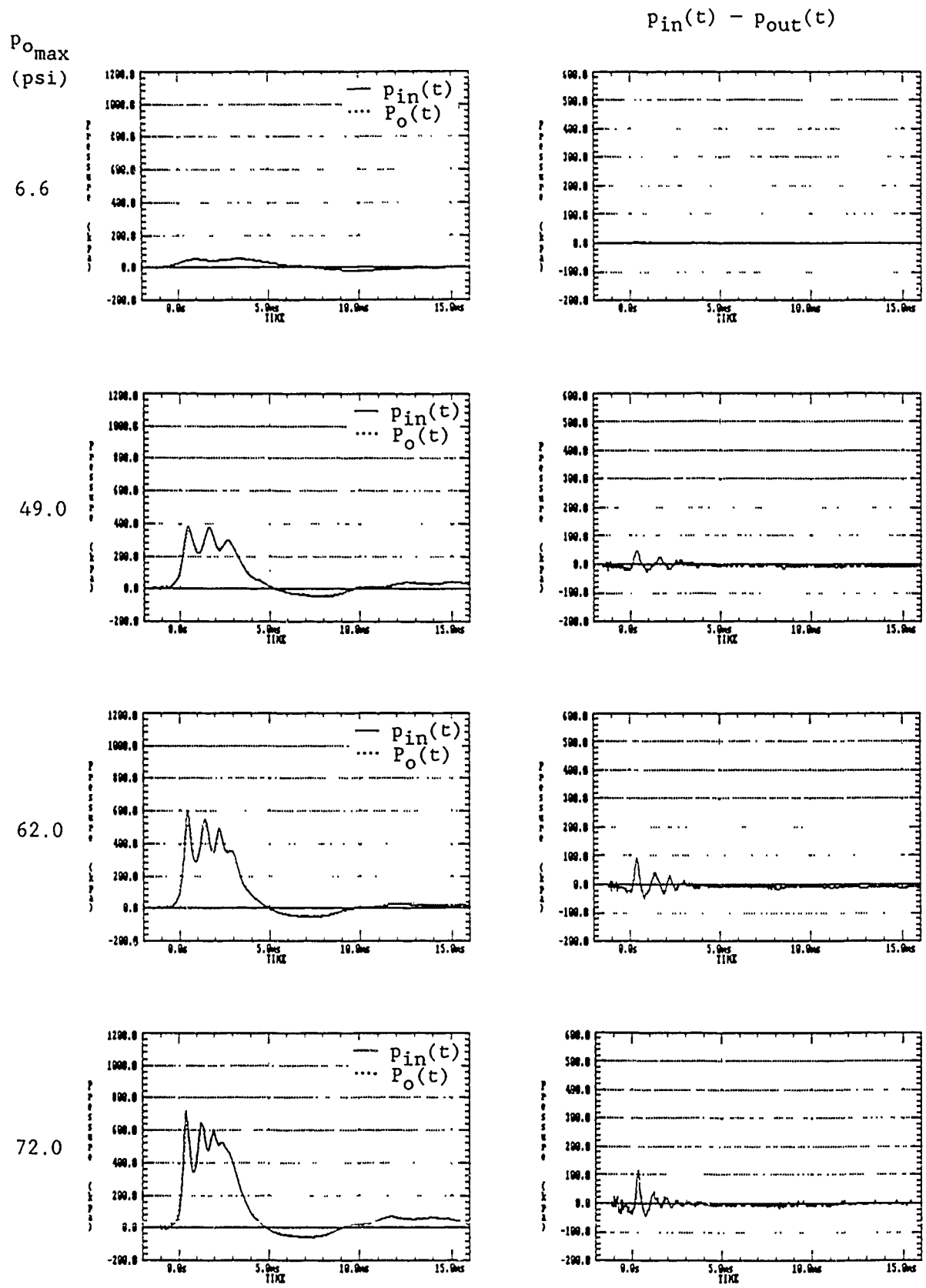

(a) Pressure signals across caecum wall (b) Pressure differentials

Figure 4-8. Pressure differential across a caecum wall for various blast pressures.

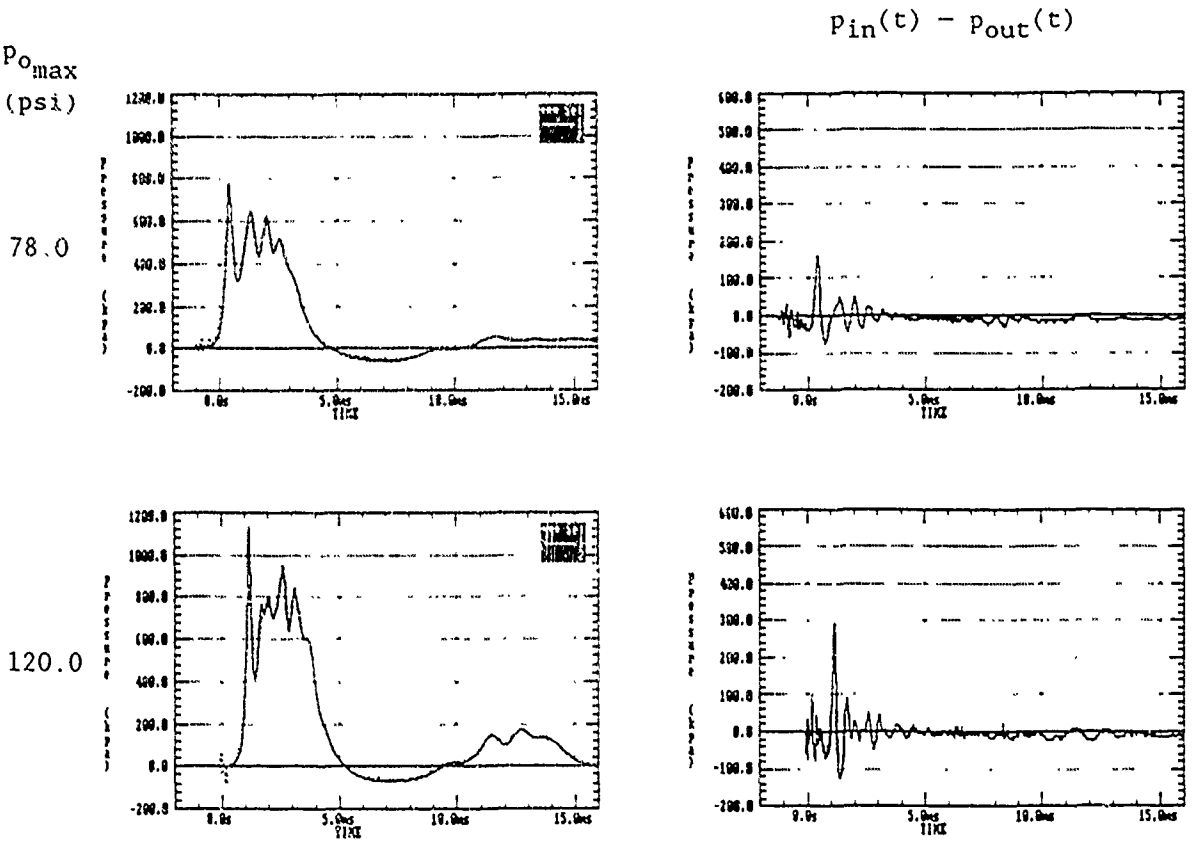

(a) Pressure signals across caecum wall (b) Pressure differentials

Figure 4-8. (Cont'd).

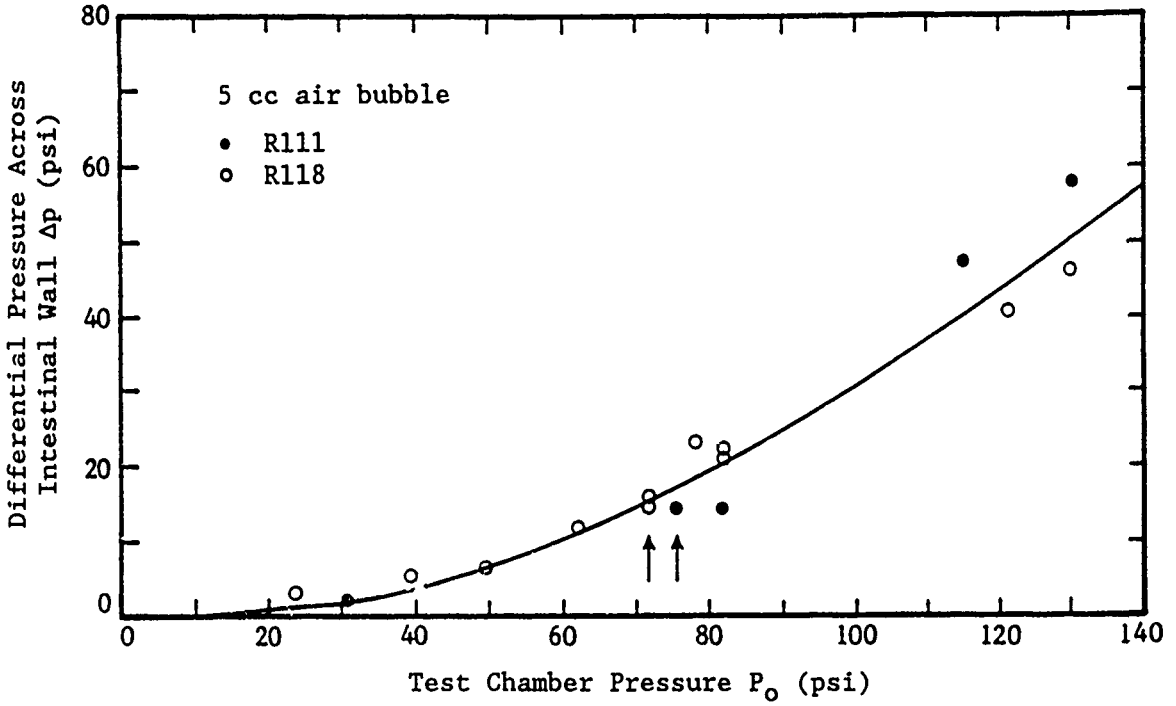

(a) 5 cc air bubble

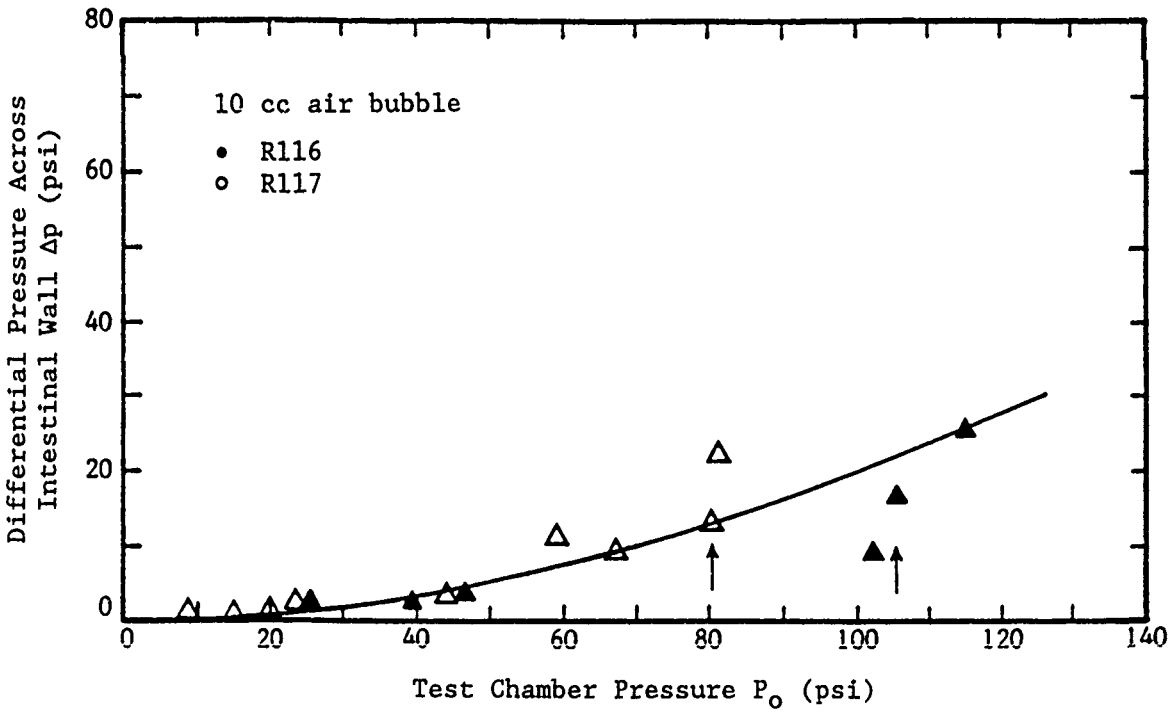

(b) 10 cc air bubble

Figure 4-9. Differential pressure across rabbit caecum wall versus test chamber pressure. Arrows indicate injury thresholds.

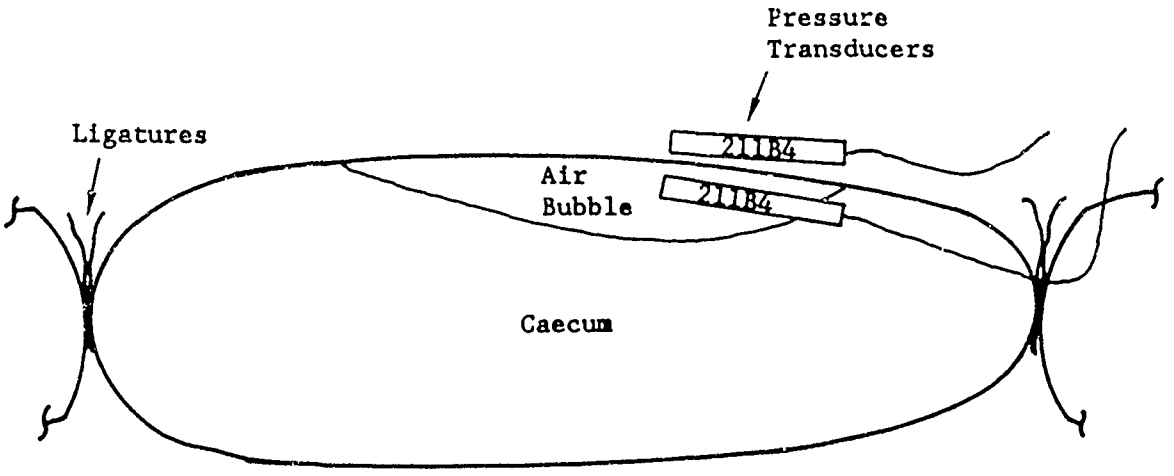

Figure 4-10. Caecum differential pressure measurement side-on transducer arrangement.

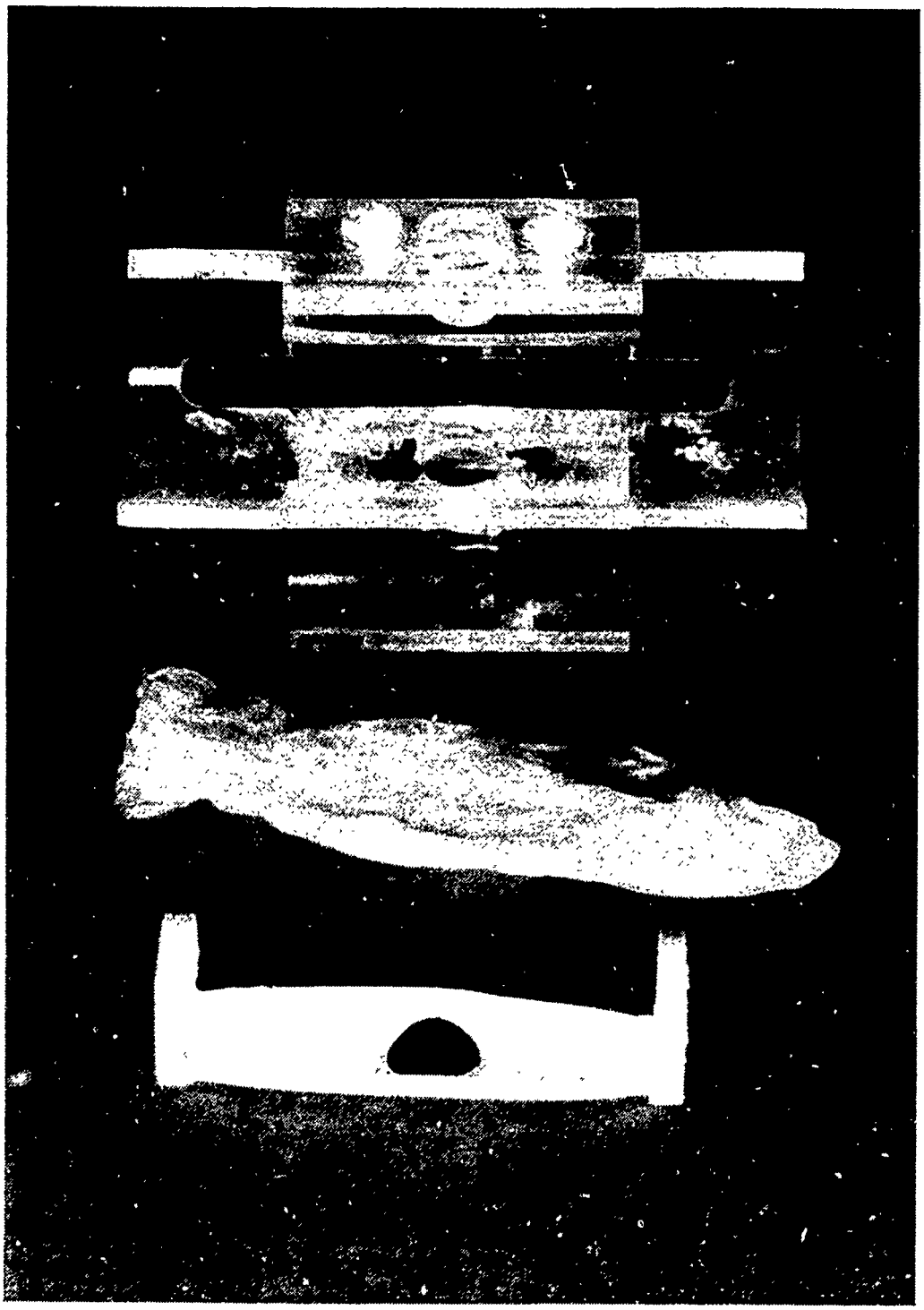

Figure 4-11. Double curvature test setup to measure differential pressure across the membrane wall (DP_w).

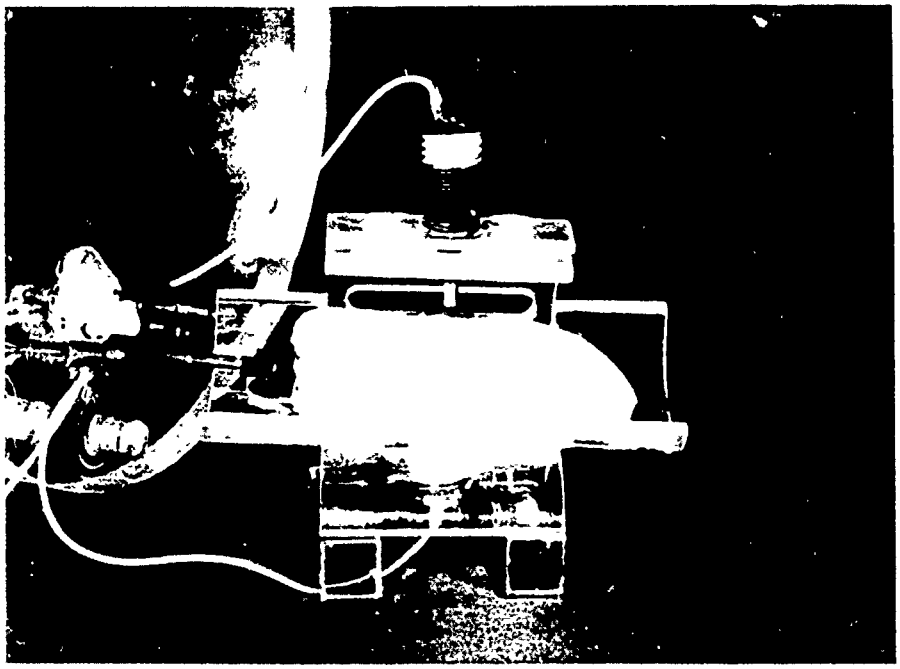

(a) R_L = 4.45 inch

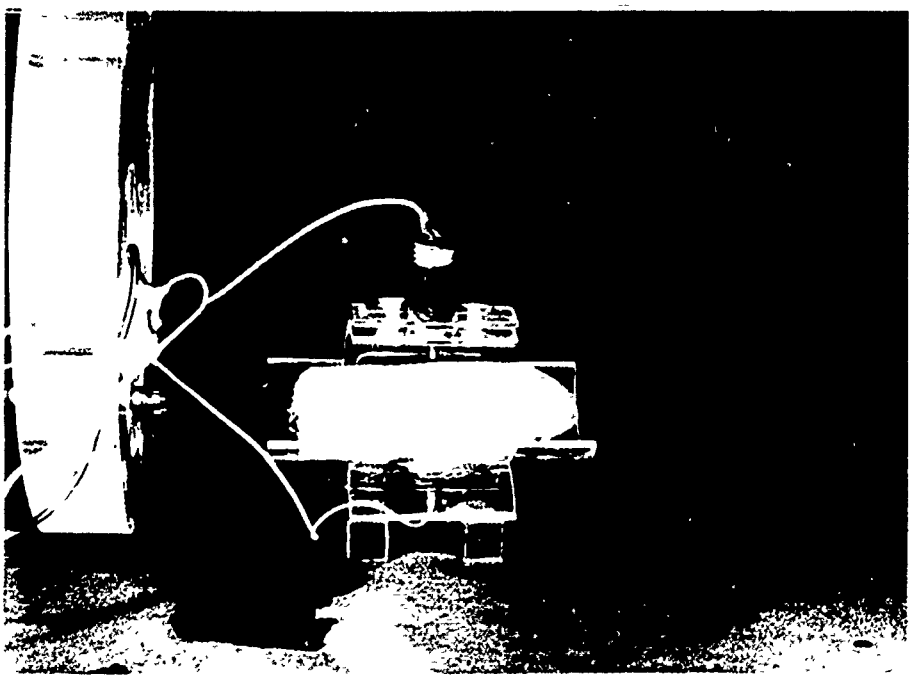

(b) R_L = ∞

Figure 4-12. Surrogate double curvature test fixture setup.

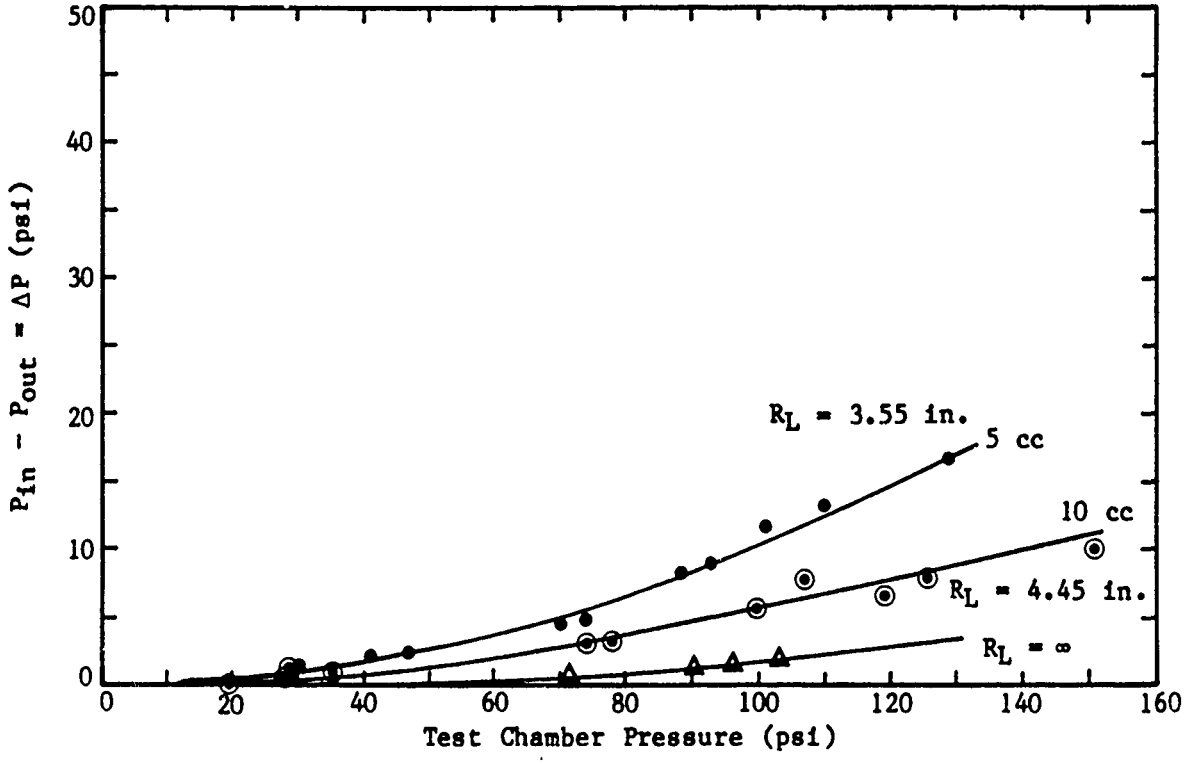

Figure 4-13. DP_w versus test chamber pressure across double curvature test samples. (R_r = 0.62 inch for all test samples.)

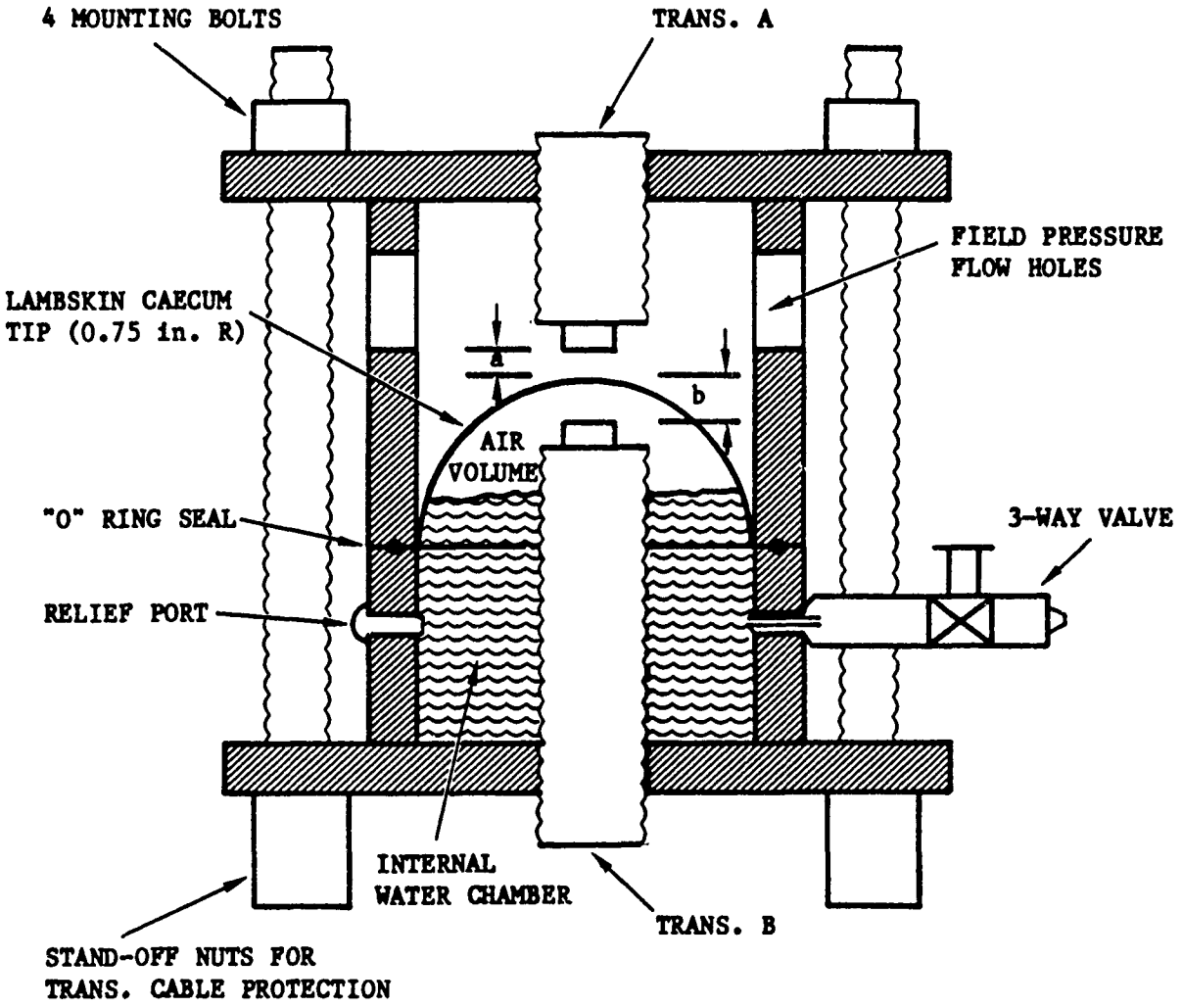

Figure 4-14. Schematic of single curvature membrane test fixture.

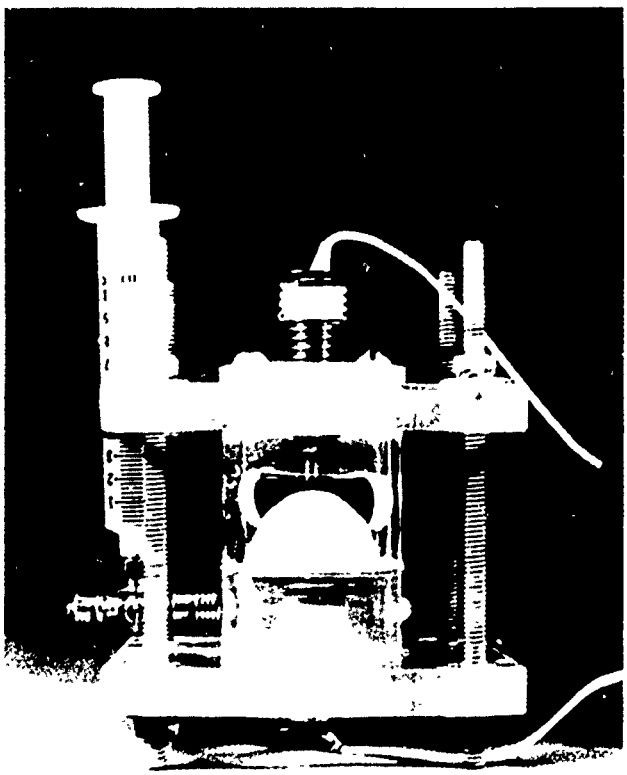

Figure 4-15. Single-curvature-membrane test fixture.

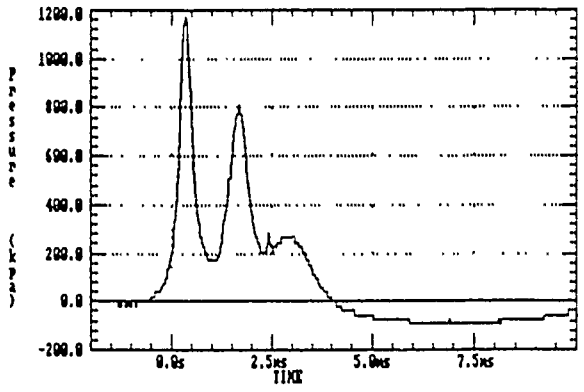

P_{in}

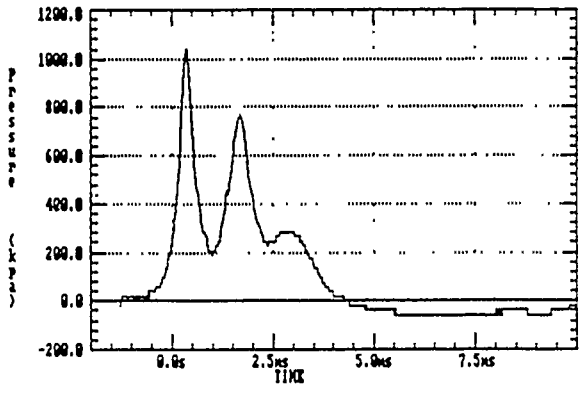

P_{out}

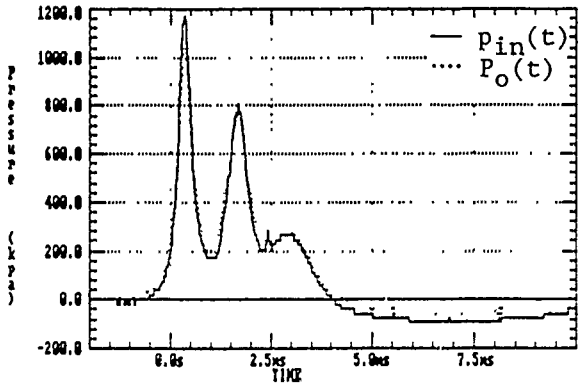

P_{in} and P_{out}

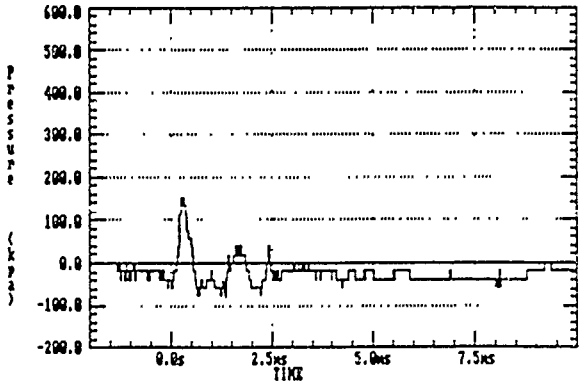

$P_{in} - P_{out}$

Figure 4-16. Pressure measurements across a R_c = 0.75 in. membrane with a 5 cc air bubble.

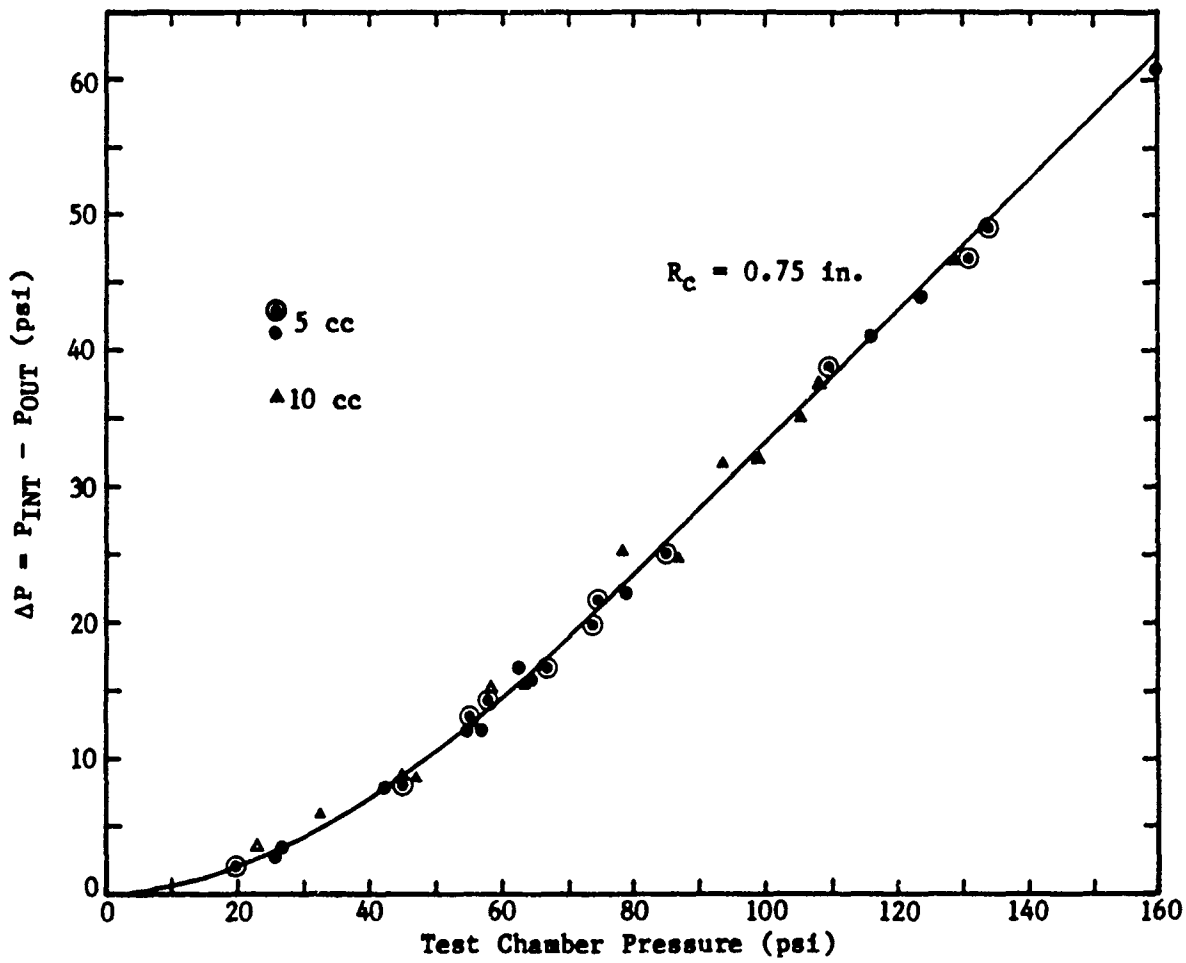

Figure 4-17. Differential pressure across bubble site membrane versus chamber pressure.

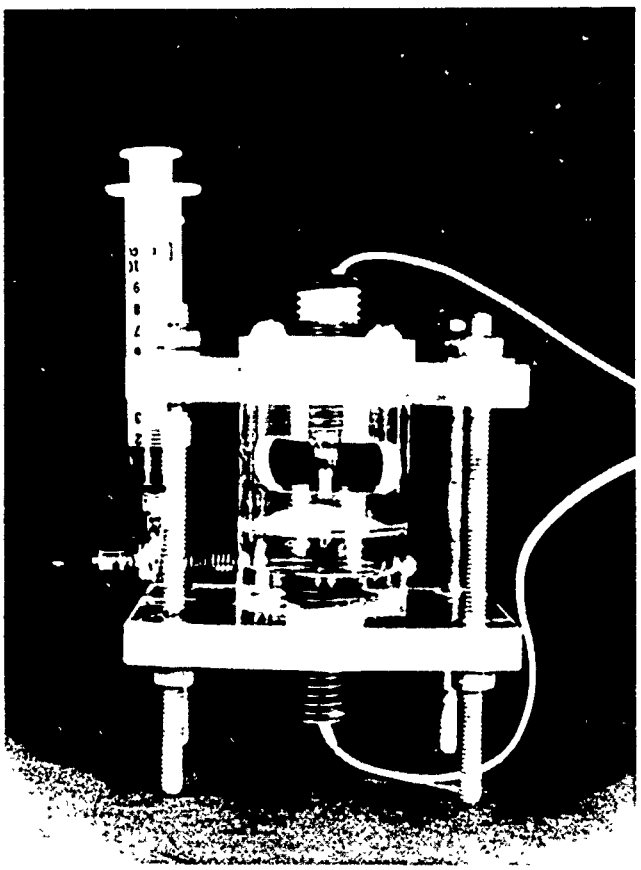

Figure 4-18. Large radius of curvature membrane, R_c = 4.24 in., test configuration.

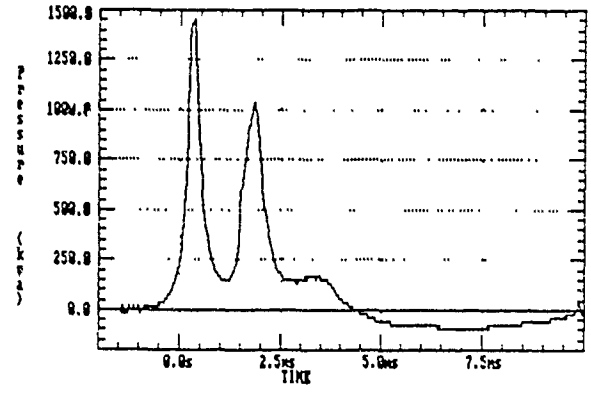

P_{in}

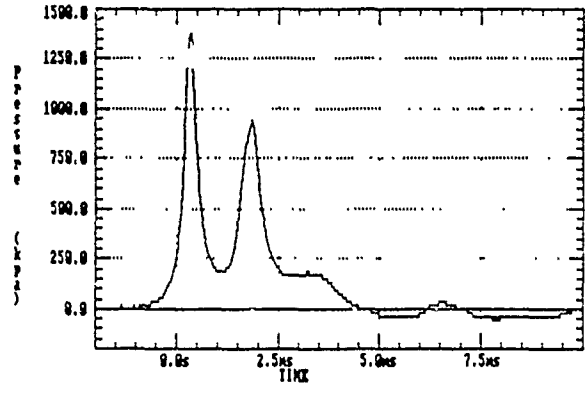

P_{out}

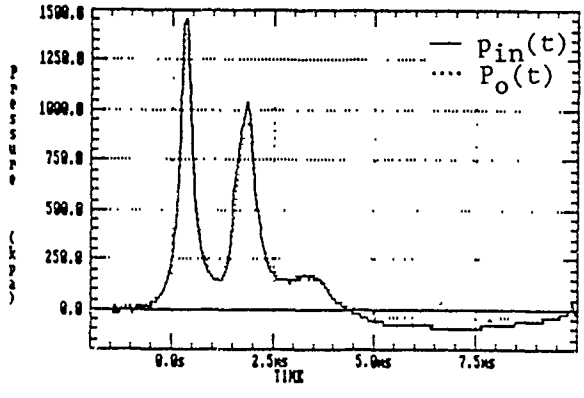

P_{in} and P_{out}

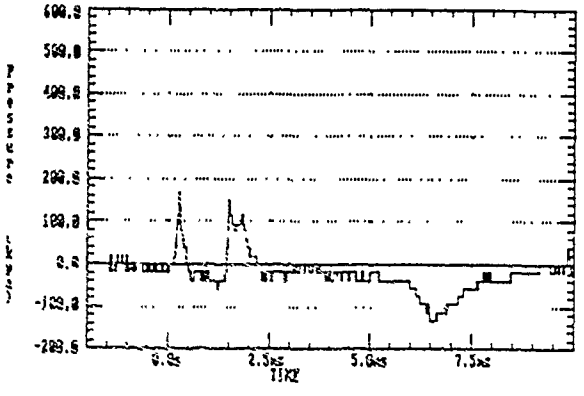

$P_{in} - P_{out}$

Figure 4-19. Pressure measurements across a R_c = 4.24 in. membrane with a 5 cc air bubble.

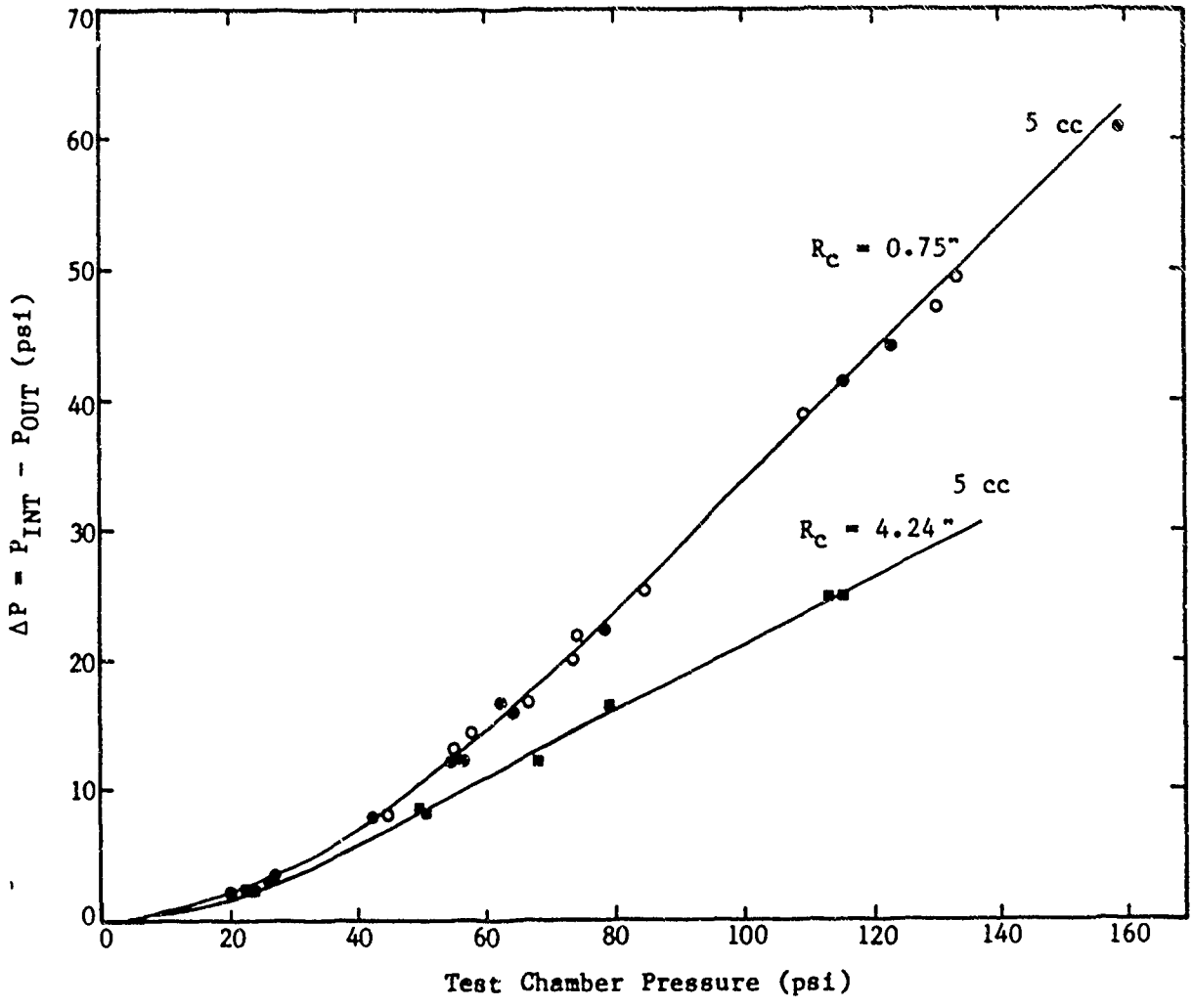

Figure 4-20. Effect of radius of curvature on DP across membrane wall.

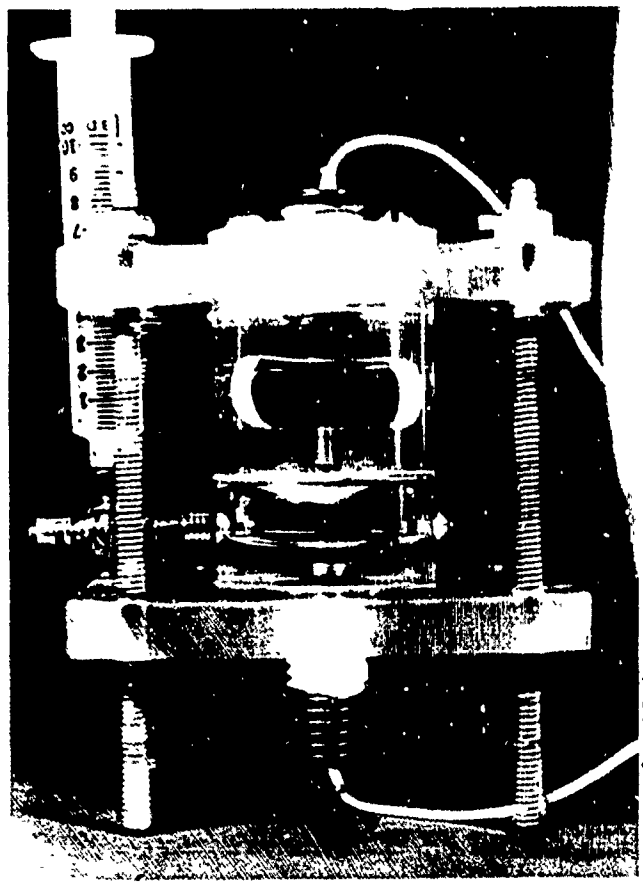

Figure 4-21. Negative radius of curvature test setup.

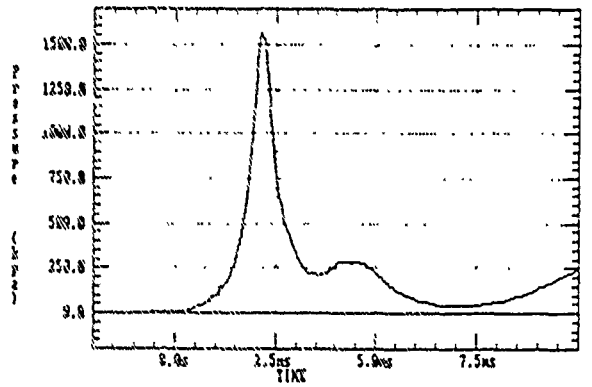

P_{in}

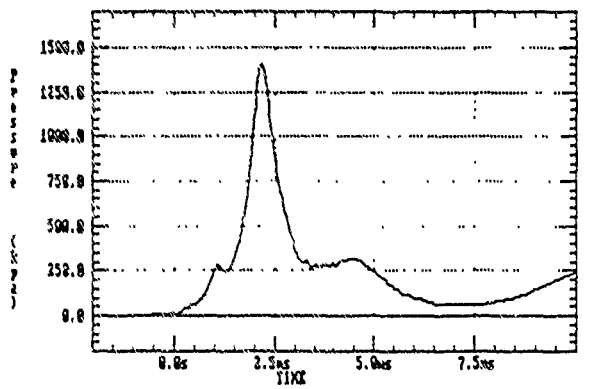

P_{out}

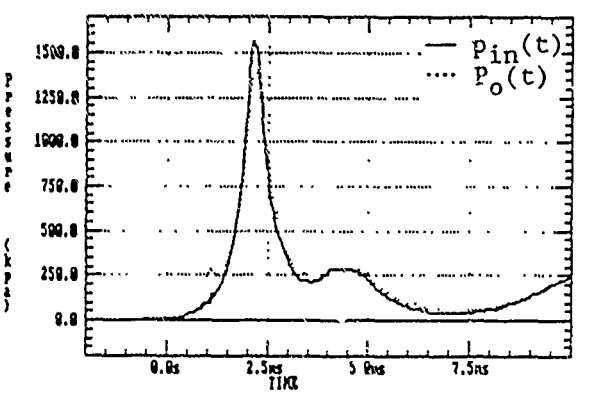

P_{in} and P_{out}

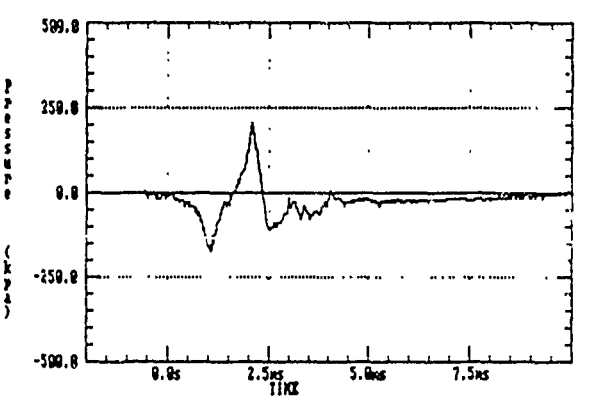

$P_{in} - P_{out}$

Figure 4-22. Pressure measurements across a negative curvature membrane.

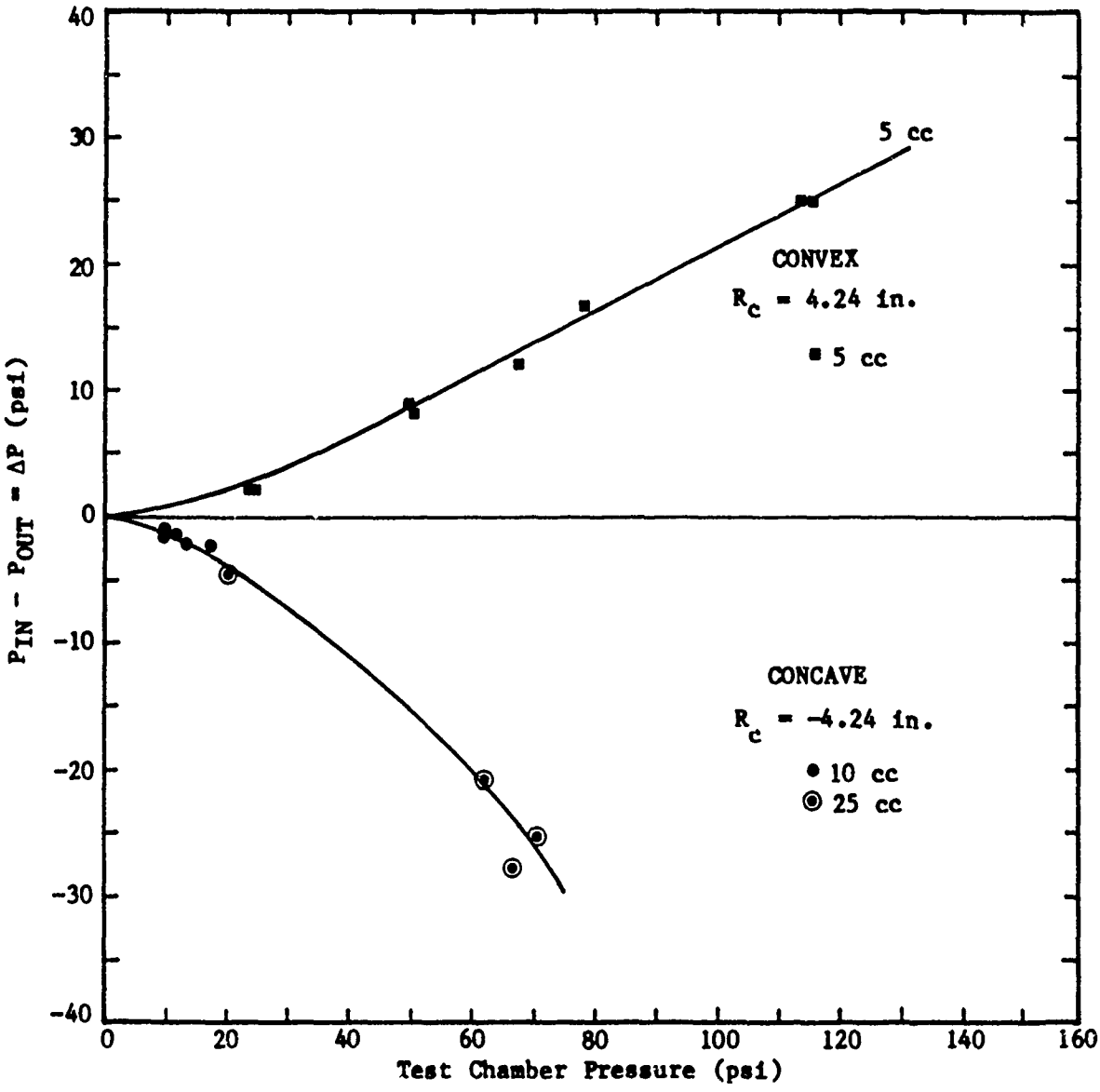

Figure 4-23. Comparison of DP across concave and convex curvature membranes.

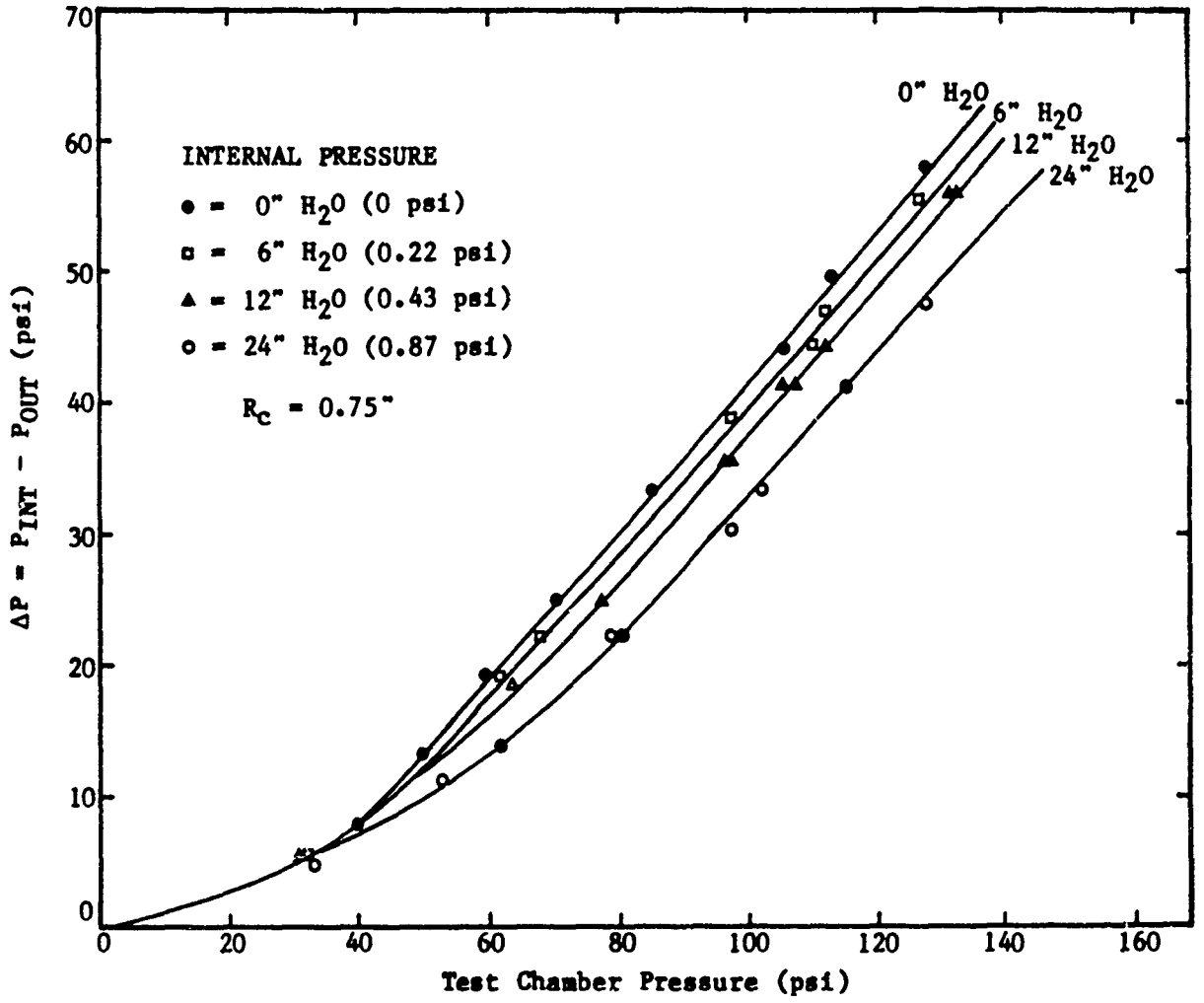

Figure 4-24. Effect of internal pressure on membrane wall DP.

Figure 4-18 shows the setup and Figure 4-19 a typical signal from a test using a "flat" section of lambskin caecum material with a radius of curvature of R_C = 4.24" and a 5 cc air bubble volume. The results of this larger radius is compared with R_C = 0.75" in Figure 4-20. As shown, for a given air volume a difference in DP_W could result for different radius of curvature membranes.

Figure 4-21 shows the setup for a negative radius of curvature test. It was set up two ways to test the effects of negative curvature. The first setup was as shown in Figure 4-21 with a 10 cc air bubble and face-on transducers with approximately 15 cc of water in the lower fixture chamber. The negative curvature was produced by removing a small amount of water from the fixture creating a slightly negative internal pressure in the lower fixture chamber and giving the membrane R_C = −4.24". This negative curvature condition was used to simulate the curvature at the folds of a caecum or in a kinked section of the G.I. tract.

One difficulty associated with this setup was that at test chamber pressures above 20 psi the membrane would move down during bubble compression and strike the internal transducer. The tests were limited to chamber pressure less than 20 psi.

For higher chamber pressure tests, water was removed from the lower fixture chamber leaving an air bubble volume of approximately 25 cc. The face-on transducer was replaced by a wall-mounted probe at the relief port shown in Figure 4-14. Since pressure is constant within the air volume, this transducer position will not affect the internal pressure measurement, and allowed higher test tank pressure tests. The external membrane wall transducer remained in the same face-on position as in the first setup.

Figure 4-22 shows typical transducer signals from this test. These negative radius of curvature signals show some characteristics that are unique to this particular setup. First, it can be seen that the internal pressure signal has a lower slope than external signal thus producing the negative sign on the DP_W measurement. As the test chamber pressure increases, the bubble volume begins to compress. But when the loading limits of the inverted membrane, which is under positive wall tension, is reached, it restricts the compression of the internal bubble volume. As the external pressure increases, the membrane absorbs the strain until bursting occurs, then the free bubble dynamics take over. The large negative DP_W pressure gradient quickly overcompresses the free bubble to very high magnitudes resulting in a positive DP_W until the test chamber pressure decreases and the bubble expands and breaks up.

The negative curvature experimental results are plotted in Figure 4-23 along with the results of the previous positive R_C = 4.24" test. As shown, despite the difference in sign, the magnitude is similar.

A final test was performed to determine the effects of internal pressure on the DP_W measurement. The setup used a 5 cc bubble and 6", 12" and 24" of water internal pressure. The internal pressure was preset by water column and locked in by using the three-way valve. The test results are shown in Figure 4-24. It appears that the higher the internal pressure the lower the magnitude of DP_W.

4.2 SURROGATE MODELS USED TO DEVELOP AND VERIFY THE BUBBLE CODE

A primary goal for G.I. injury study is to develop a prediction model for gastrointestinal injury from a free-field blast wave. This analytical tool is being developed based on principles of fluid mechanics, laboratory G.I. surrogate model measurements, and G.I. injury test

To this end, a mathematical model was developed to predict the pressure-time history of a bubble in a water-filled test chamber [5]. The predictions from this model agree well with surrogate experimental data for bubbles inside various hemispherical configurations, as shown in Figure 4-25.

This code uses the bubble volume, chamber pressure signal, and an estimated flow field pattern as the primary input parameters. The mathematical model for the dynamics of the air bubble and the elastic membrane is based on the energy integral for the liquid flow. This approach has been used successfully before for complex bubble motion problems. The three-dimensional nature of the flow is reduced to a single function that describes the flow area within the fluid. The final mathematical form is an ordinary differential equation for the motion of the interface coordinate. From this variable all other quantities, such as pressures, velocities, tensions, etc., can be calculated. The model is solved with a Runge-Kutta solution algorithm in FORTRAN on a personal computer. Graphical and tabular output are produced interactively [6].

4.2.1 Clamped Hemisphere Surrogate Model

Predictions of the BUBBLE code agreed well with data from the Clamped Hemisphere Surrogate Model after correct flow field assumptions were known.

Initial verification of the BUBBLE code used data gathered from the test fixture of Figures 4-26 and 4-27. This test fixture originally was designed to measure differential pressure, DPw, across the membrane wall. Because the test sample is hemispherical, the bubble is symmetrical and allows a simple one-dimensional description of volume change based upon change in bubble radius.

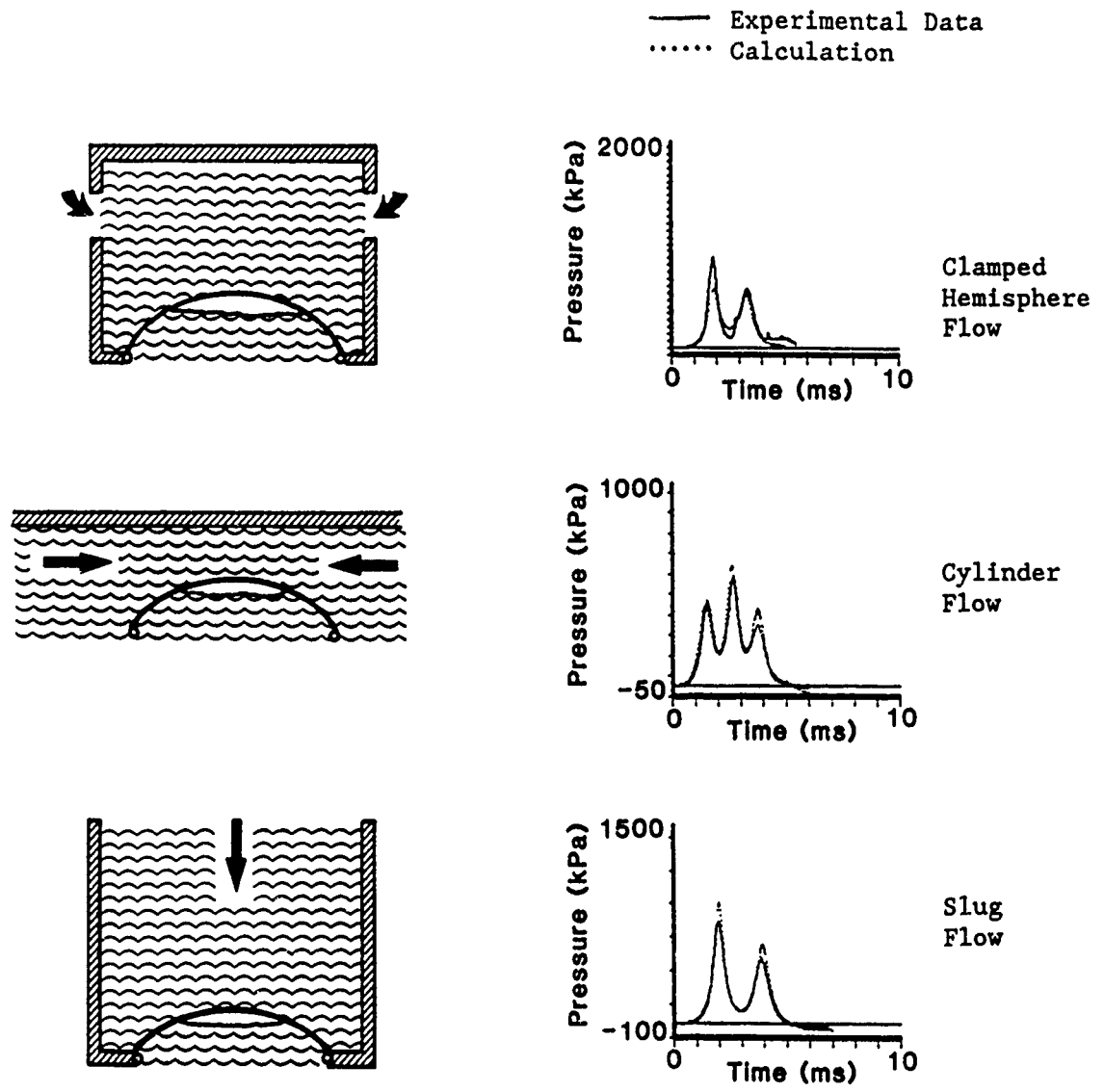

Figure 4-25. Surrogate tests and analytical modeling correlation.

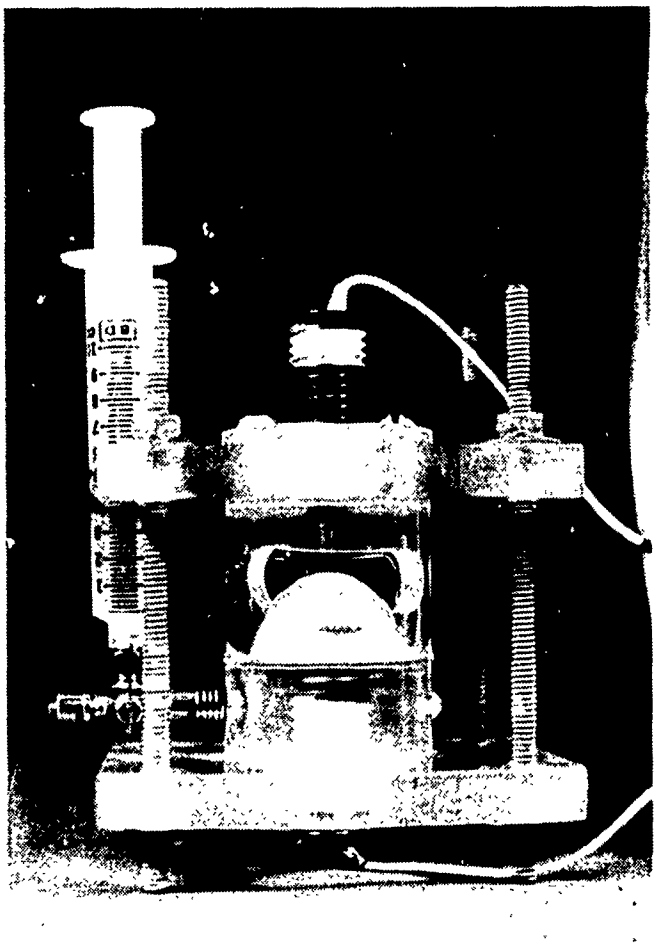

Figure 4-26. Clamped hemisphere single curvature surrogate fixture.

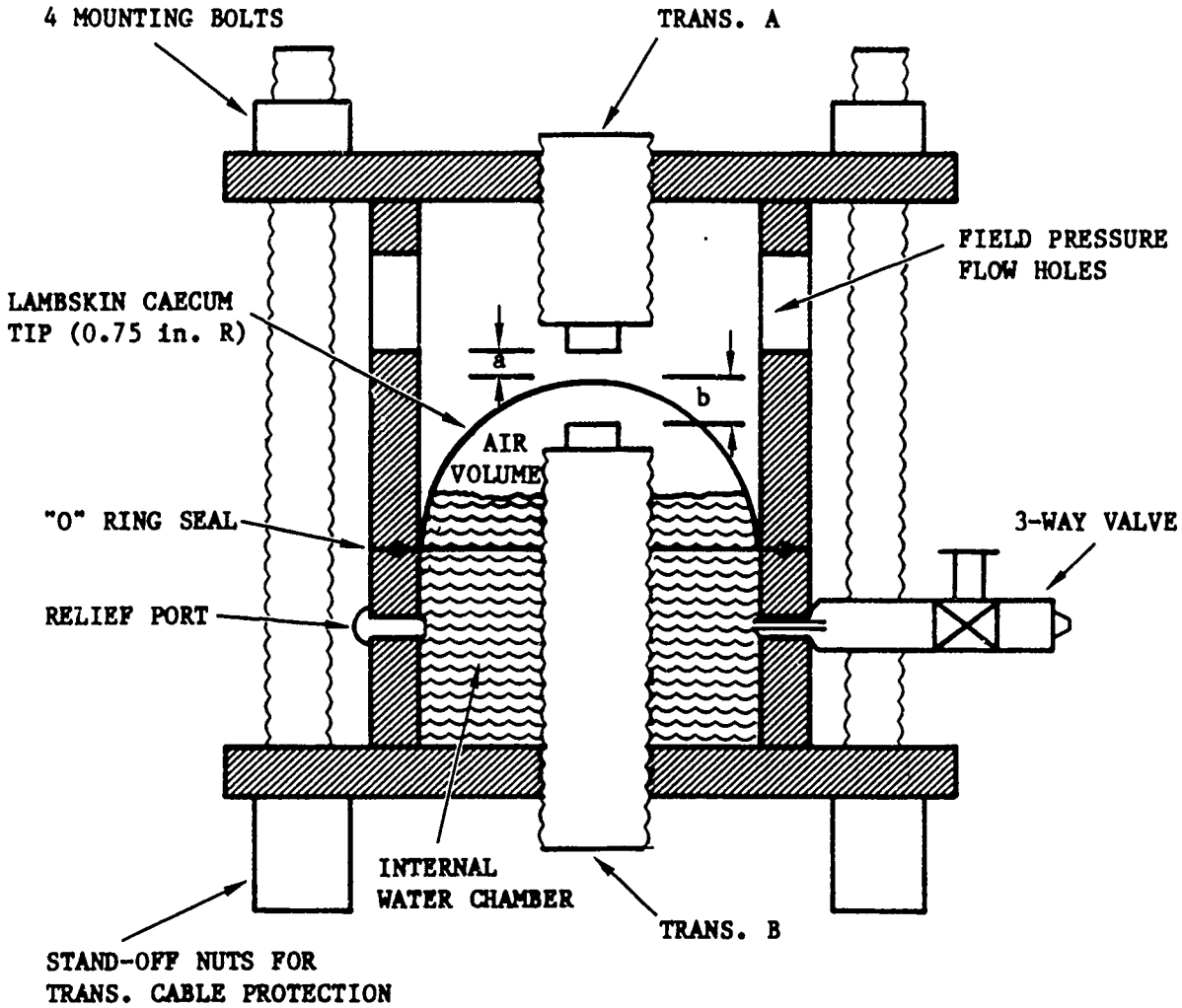

Figure 4-27. Schematic of single curvature clamped hemisphere surrogate test fixture.

These BUBBLE code predictions assume that the intestinal wall expands freely (i.e., no material properties effects). They also assume that there is water inside and outside the surrogate with no initial pressure differential. Primary inputs for the BUBBLE code are bubble air volume, actual loading chamber pressure signals and flow field boundary conditions.

Initial correlation of these predictions with the Clamped Hemisphere data did not show good agreement. The problem was traced to the flow field assumptions. Obviously the flow field for the surrogate configuration shown in Figure 4-26 is different from a free field bubble. The structural blockage restricted the flow to the collapsing bubble and resulted in a complex flow field.

This complex flow field was defined through additional surrogate experiments detailed in the next two sections. By using a combination of cylinder flow and slug flow boundary conditions, the BUBBLE code predictions were then correlated with the Clamped Hemisphere data. Even with this complex flow field, agreement was good in both magnitude and oscillation frequency throughout a range of chamber pressure signals, as shown in Figures 4-28 through 4-37.

4.2.2 Cylinder Flow Tests

A fixture was designed that allowed primarily side flow and restricted various amounts of top flow to the collapsing bubble (Fig. 4-38).

This setup is similar to the Clamped Hemisphere configuration except that the test sample has no upper chamber fixture to restrict the flow field around the collapsing bubble.

A 5 cc bubble was placed in this fixture and tested with a series of boundary conditions that restricted the top flow field but allowed a full side flow field. As seen in Figure 4-39, the mounting bolts on the figure were set at intervals to provide chamber lid-to-bubble distances (LX) of 1.90", 1.00", 0.25" and 0.0". The closer the bubble was to the lid, the more restricted the top flow field.

Results of this test series are summarized in Figures 4-40 and 4-41. Figure 4-40 shows that at LX values of 1.90" and 1.00" the first peak value for the bubble internal pressure signal as a function of chamber pressure is the same. In fact, an LX distance of 0.25" shows very little effect on the first peak value. At 0.0" or at actual lid contact, there is a significant change to the first peak value for P_{in}. Figure 4-41 illustrates that only at LX distances between 0.0" and 0.30" can a measurable effect on the first P_{in} peak be seen.

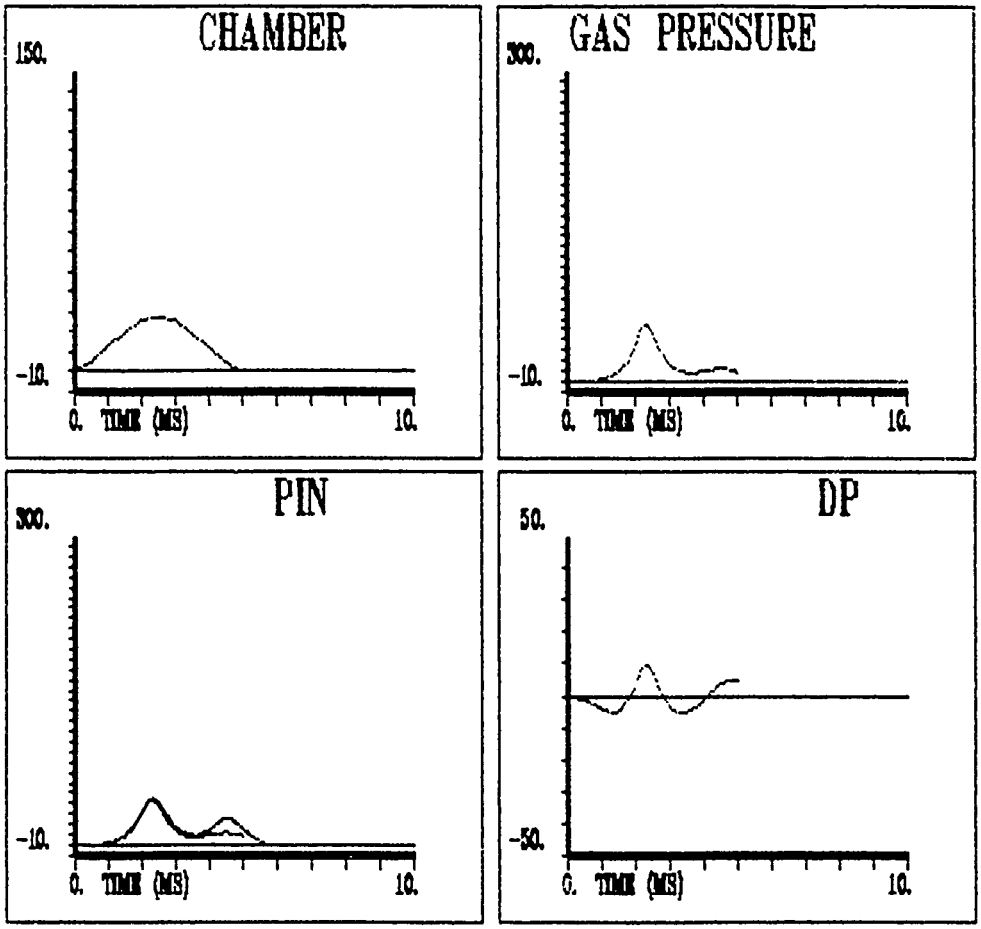

INPUT DATA:

Time step (ms) = .05

Initial pres(psi) = 14.7, Volume (cm3) = 5.0
Chamber press (psi) = 27.0, Dur (ms) = 4.94
Tank stiffness (psi/cm3) = 15.0 Damping (ms) = 5.0

Probe locations: In = .75 Out = 1.25
Starting position (cm) = 1.00

Geometry 1: Clamped hemisphere
Radius (cm) = 1.67
Outer boundary (cm) = 1.91

Figure 4-28. Clamped hemisphere correlation at chamber pressure of 27.0 psi.

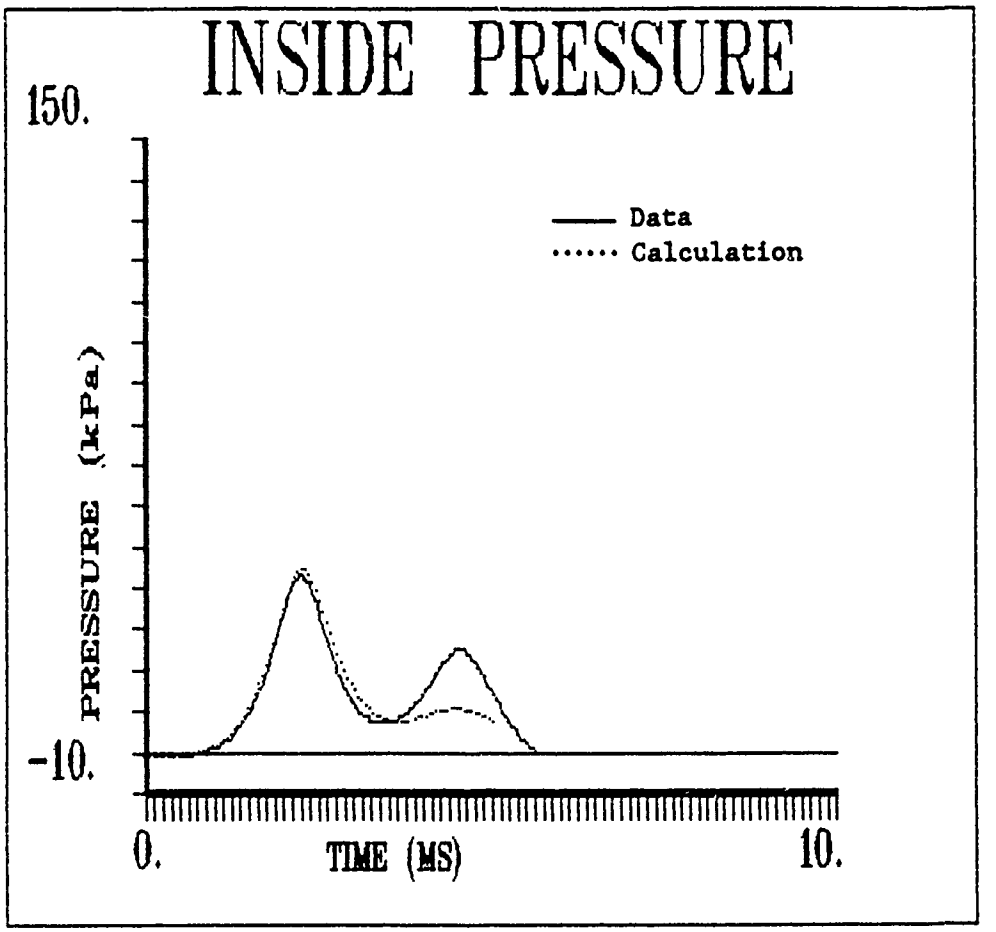

Figure 4-29. PIN correlation at chamber pressure of 27.0 psi.

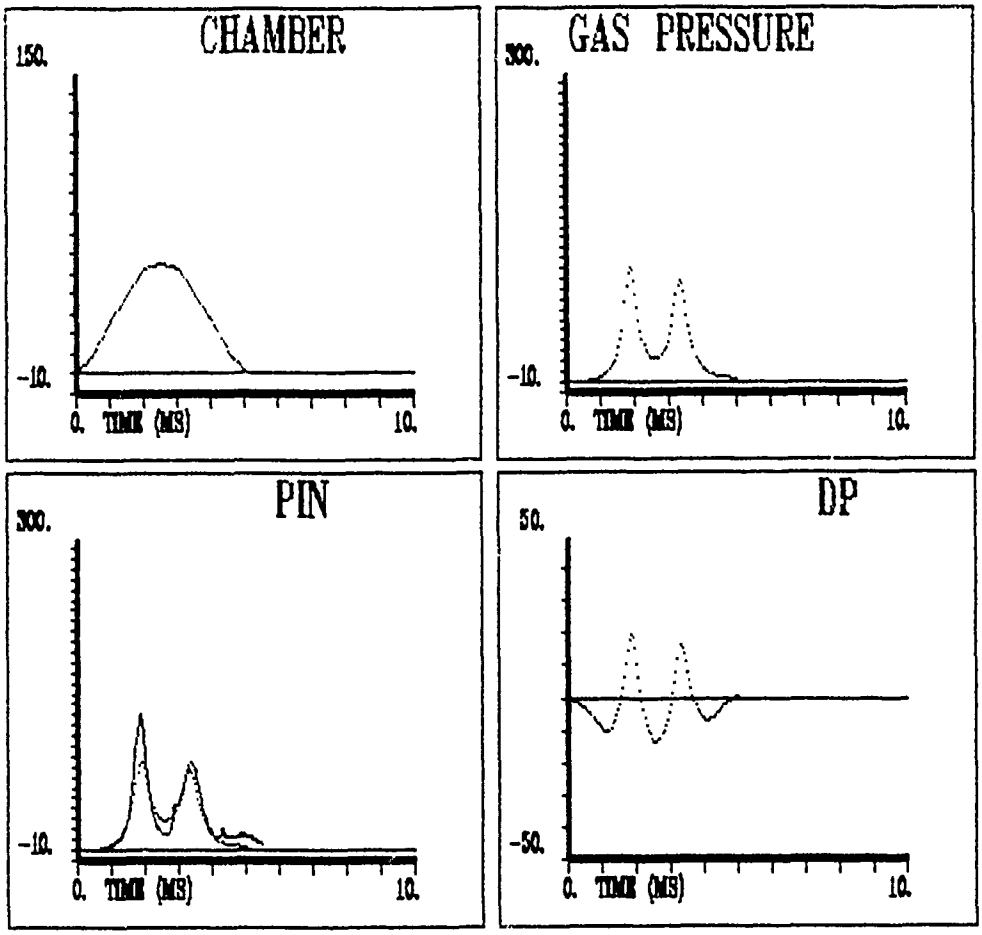

INPUT DATA:

Time step (ms) = .05

Initial pres(psi) = 14.7, Volume (cm3) = 5.0
Chamber press (psi) = 55.0, Dur (ms) = 5.06
Tank stiffness (psi/cm3) = 15.0 Damping (ms) = 5.0

Probe locations: In = .75 Out = 1.25
Starting position (cm) = 1.00

Geometry 1: Clamped hemisphere
Radius (cm) = 1.67
Outer boundary (cm) = 1.91

Figure 4-30. Clamped hemisphere correlation at chamber pressure of 55.0 psi.

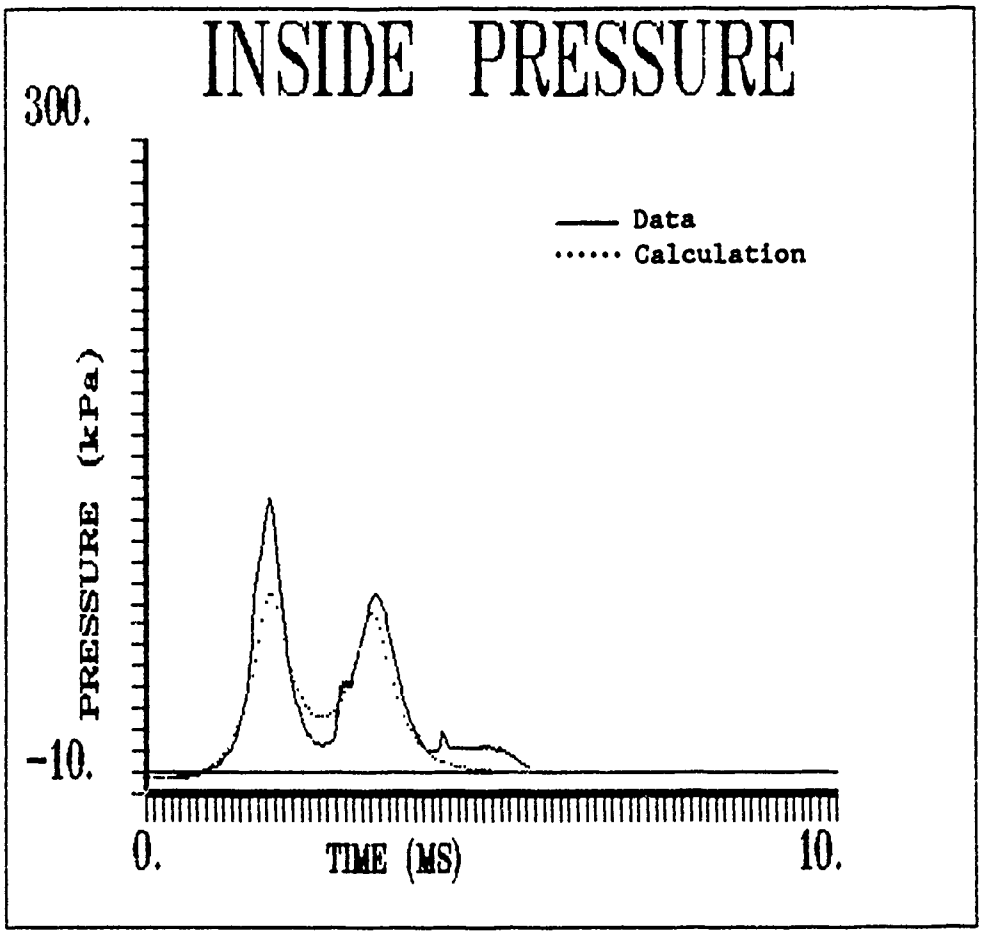

Figure 4-31. PIN correlation at chamber pressure of 55.0 psi.

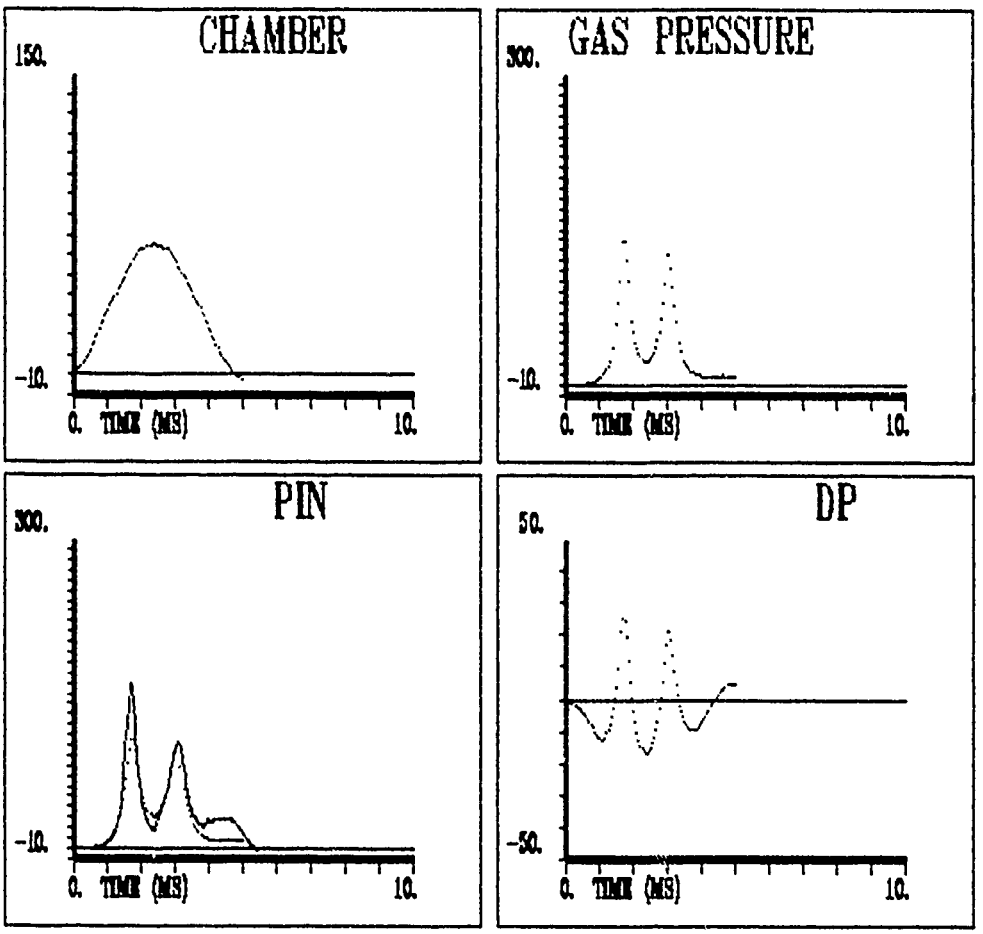

INPUT DATA:

Time step (ms) = .05

Initial pres(psi) = 14.7, Volume (cm3) = 5.0
Chamber press (psi) = 65.0, Dur (ms) = 4.76
Tank stiffness (psi/cm3) = 15.0 Damping (ms) = 5.0

Probe locations: In = .75 Out = 1.25
Starting position (cm) = 1.00

Geometry 1: Clamped hemisphere
Radius (cm) = 1.67
Outer boundary (cm) = 1.91

Figure 4-32. Clamped hemisphere correlation at a chamber pressure of 65.0 psi.

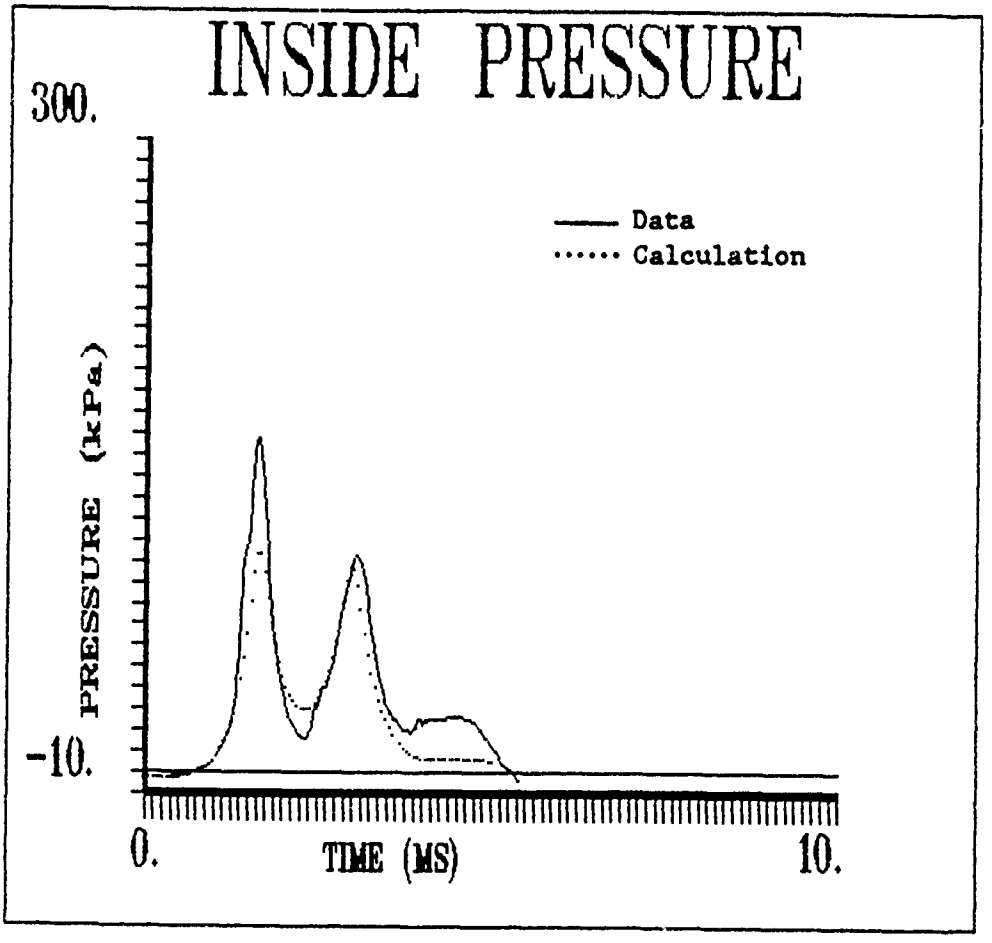

Figure 4-33. PIN correlation at a chamber pressure of 65.0 psi.

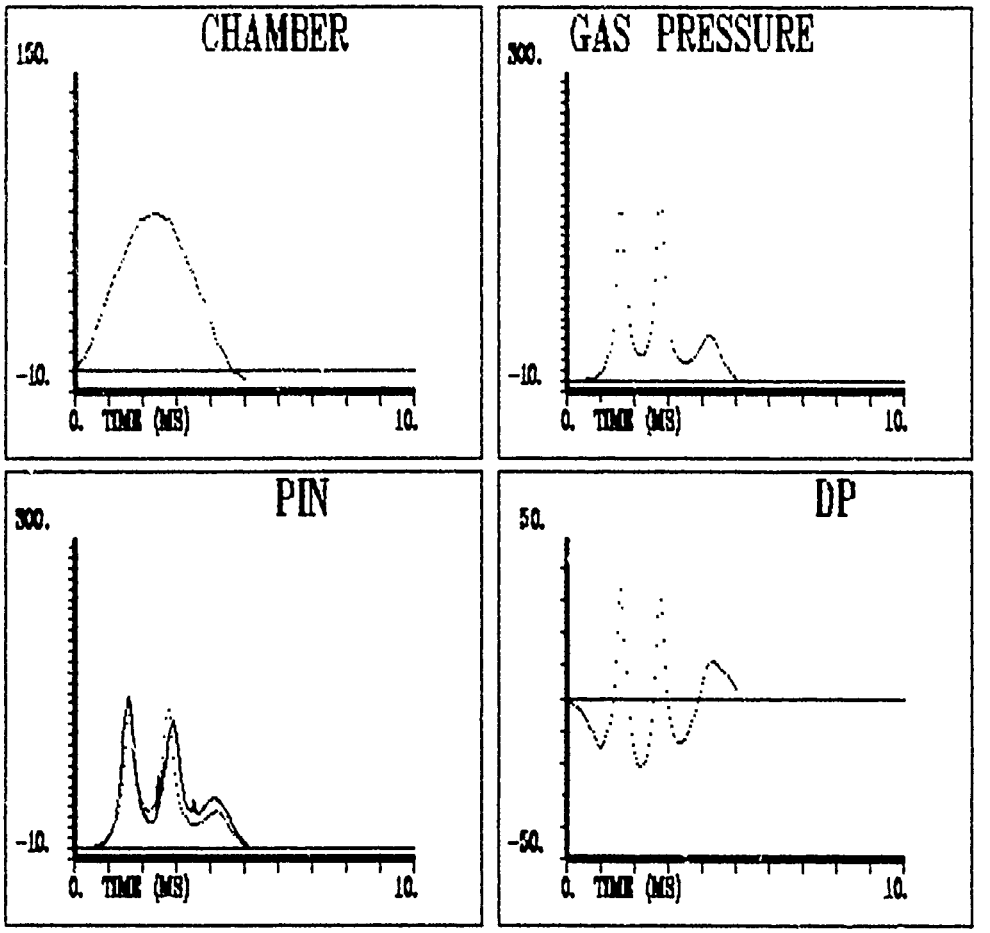

INPUT DATA:

Time step (ms) = .05

Initial pres(psi) = 14.7, Volume (cm3) = 5.0
Chamber press (psi) = 79.0, Dur (ms) = 4.66
Tank stiffness (psi/cm3) = 15.0 Damping (ms) = 5.0

Probe locations: In = .75 Out = 1.25
Starting position (cm) = 1.00

Geometry 1: Clamped hemisphere
Radius (cm) = 1.67
Outer boundary (cm) = 1.91

Figure 4-34. Clamped hemisphere correlation for a chamber pressure of 79.0 psi.

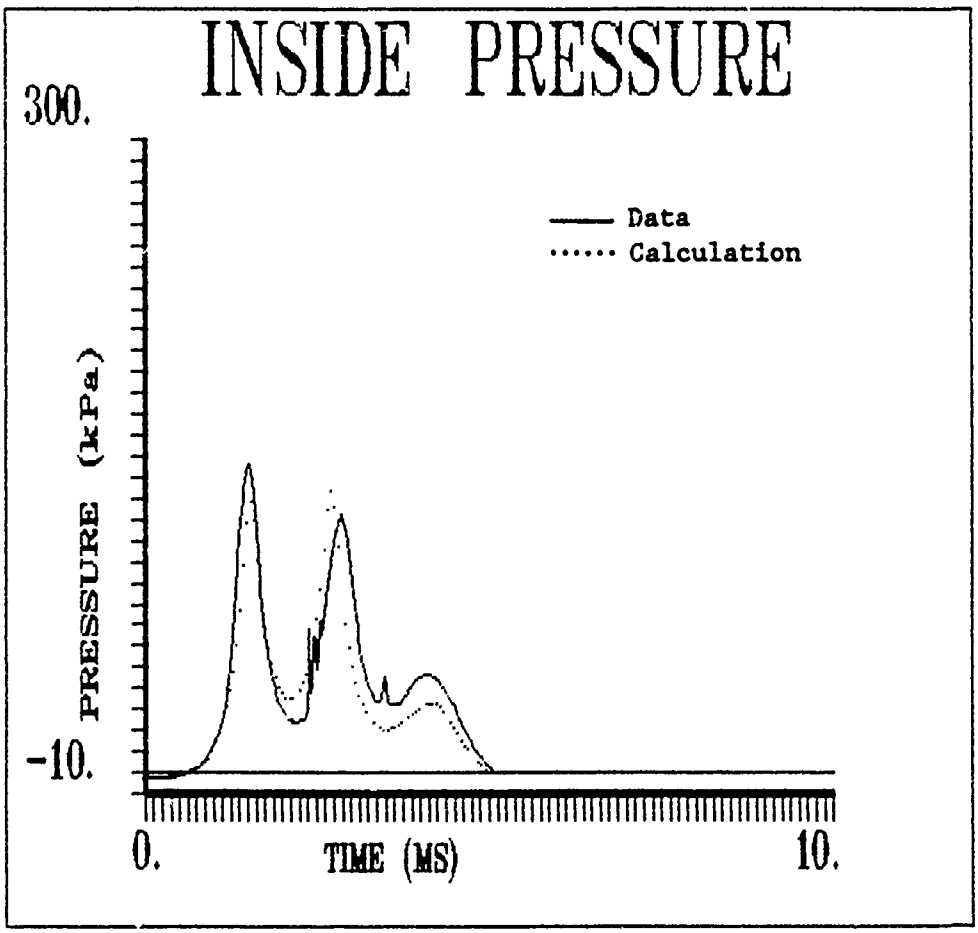

Figure 4-35. PIN correlation for a chamber pressure of 79.0 psi.

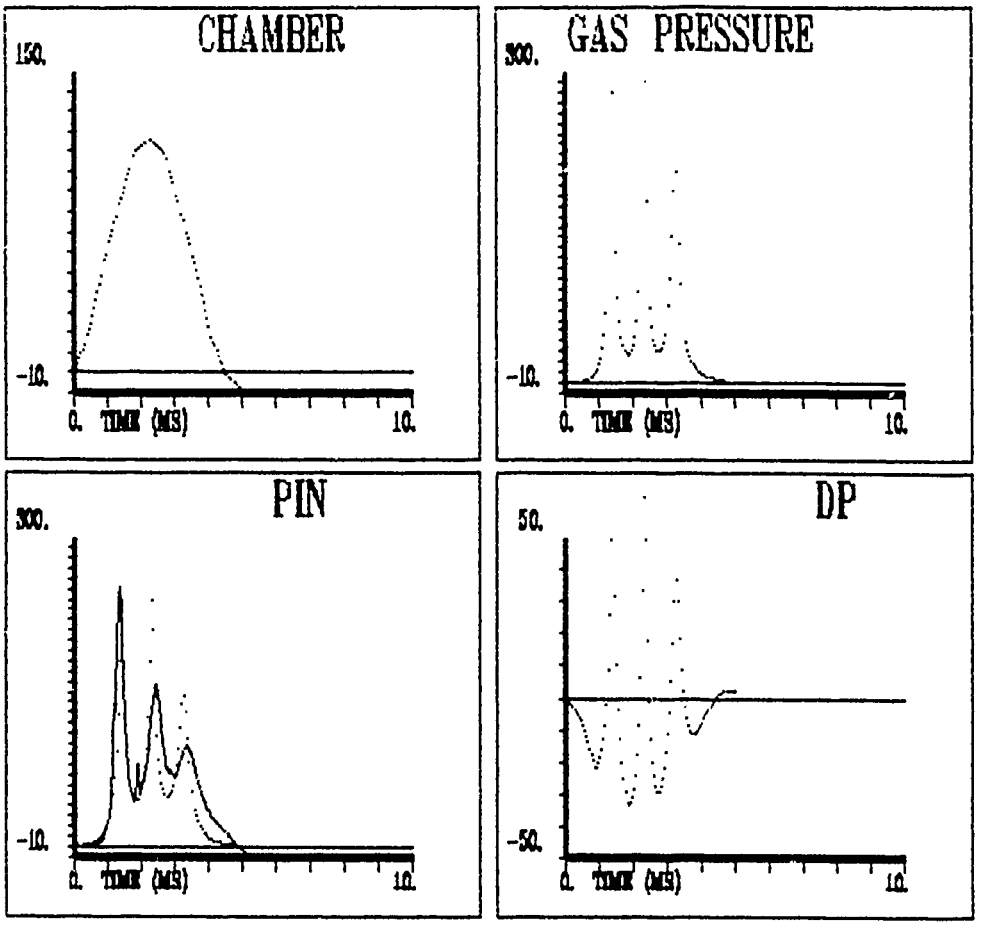

INPUT DATA:

Time step (ms) = .05

Initial pres(psi) = 14.7, Volume (cm3) = 5.0
Chamber press (psi) = 116.0, Dur (ms) = 4.48
Tank stiffness (psi/cm3) = 15.0 Damping (ms) = 5.0

Probe locations: In = .75 Out = 1.25
Starting position (cm) = 1.00

Geometry 1: Clamped hemisphere
Radius (cm) = 1.67
Outer boundary (cm) = 1.91

Figure 4-36. Clamped hemisphere correlation for a chamber pressure of 116.0 psi.

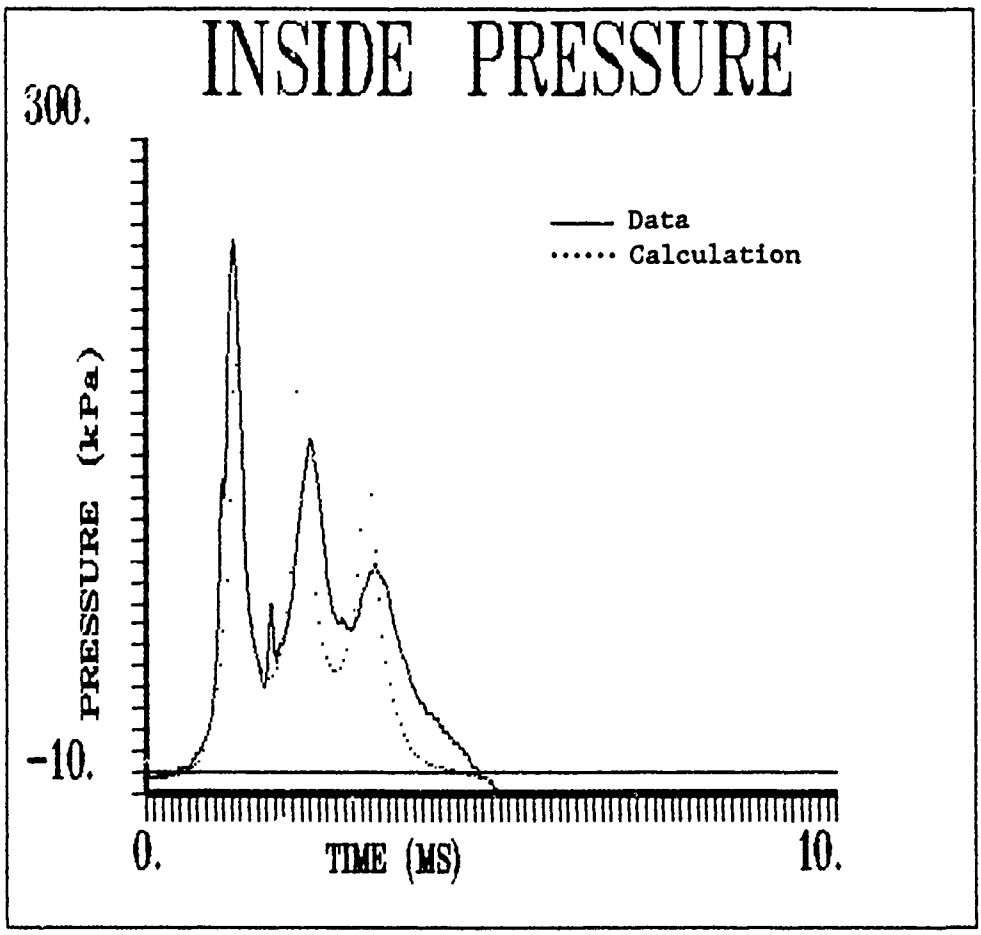

Figure 4-37. PIN correlation for a chamber pressure of 116.0 psi.

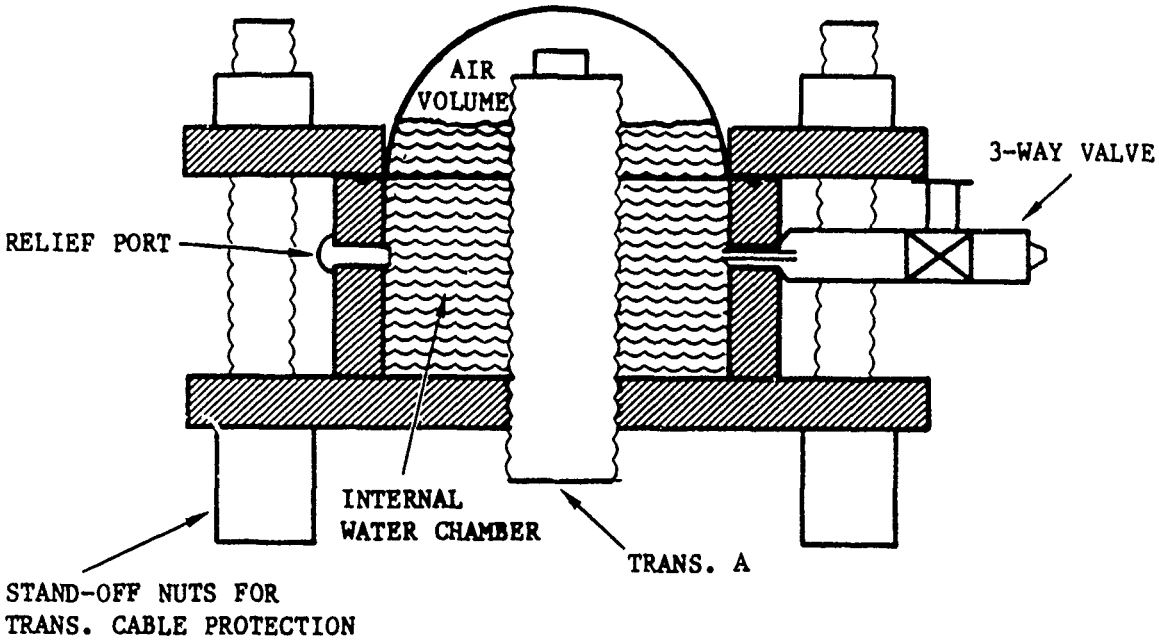

Figure 4-38. Cylinder Flow surrogate test setup schematic.

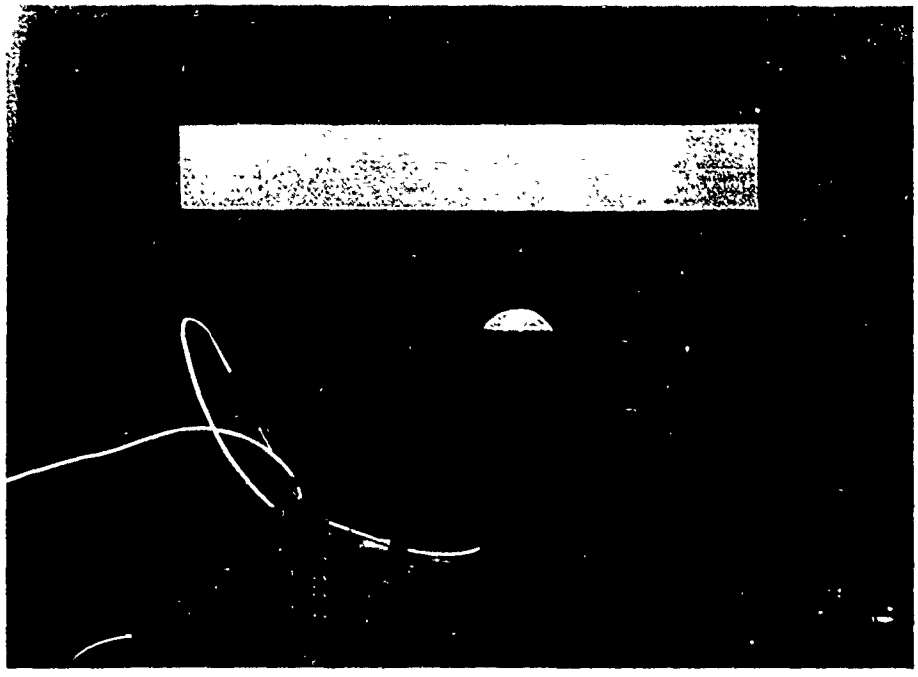

LX = 1.90"

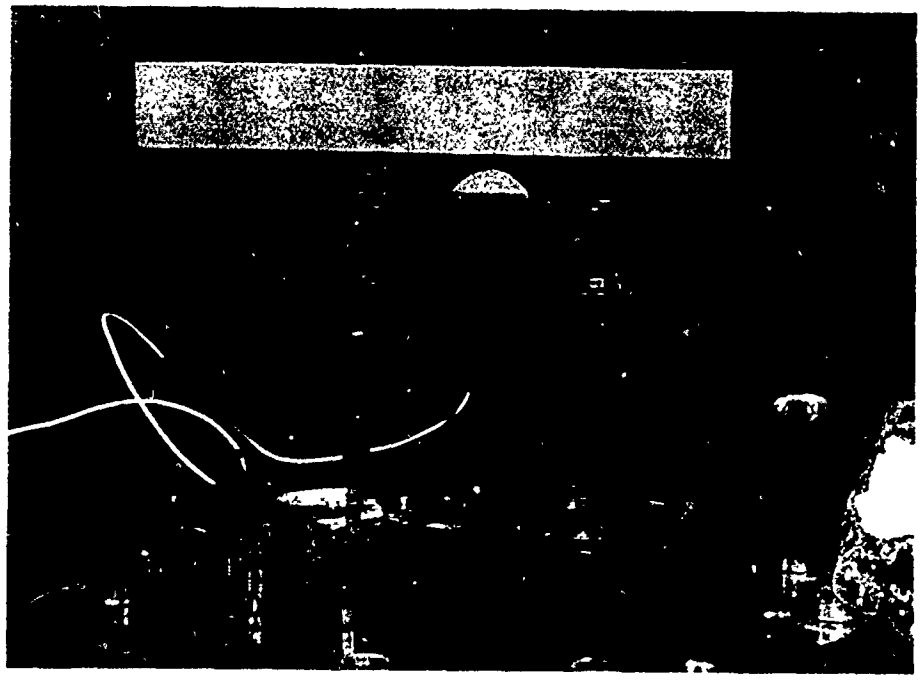

LX = 0.25"

Figure 4-39. Cylinder Flow surrogate test setup.

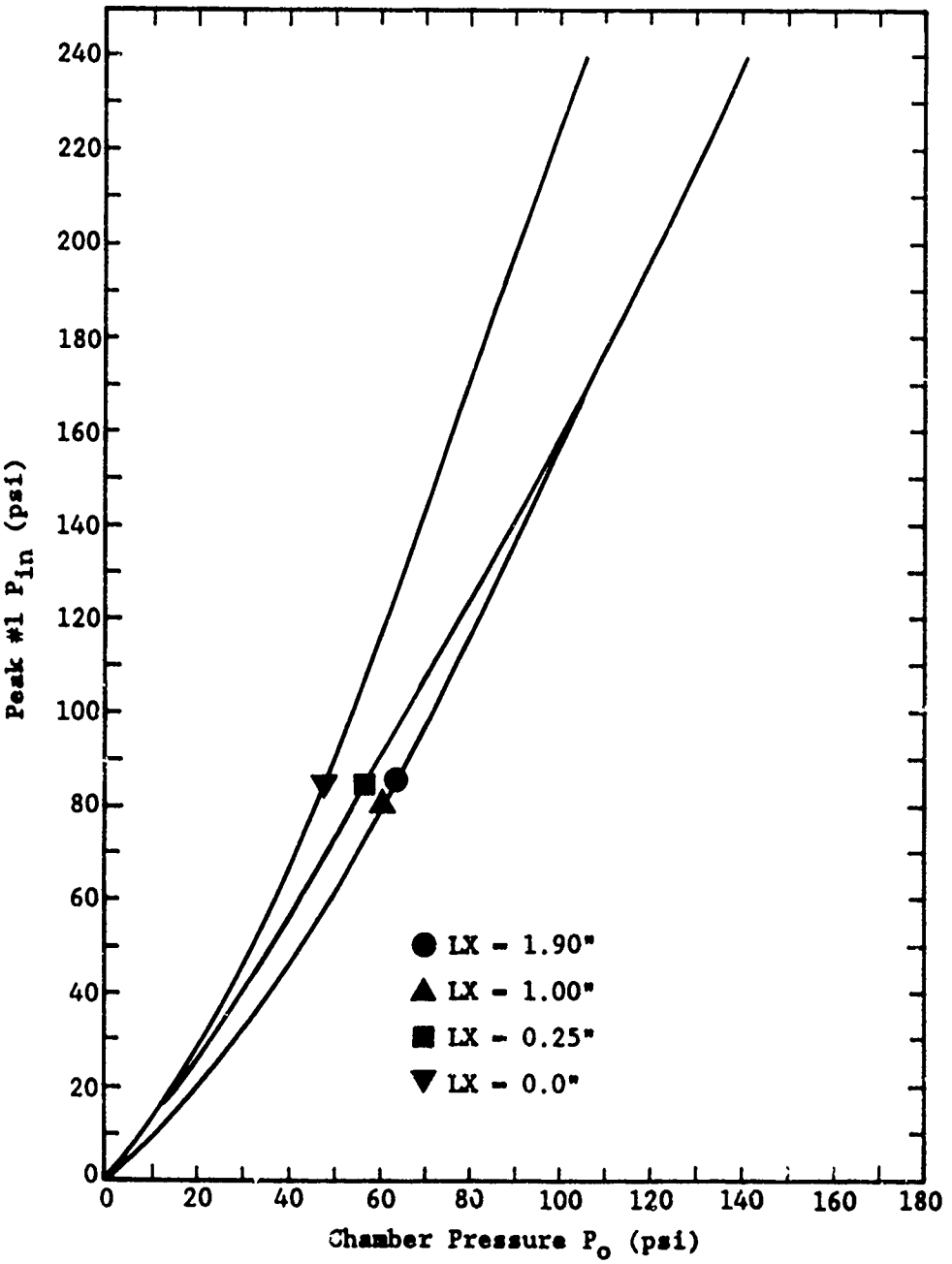

Figure 4-40. Effect of chamber lid distance (LX) on initial bubble internal pressure peak for Cylinder Flow field.

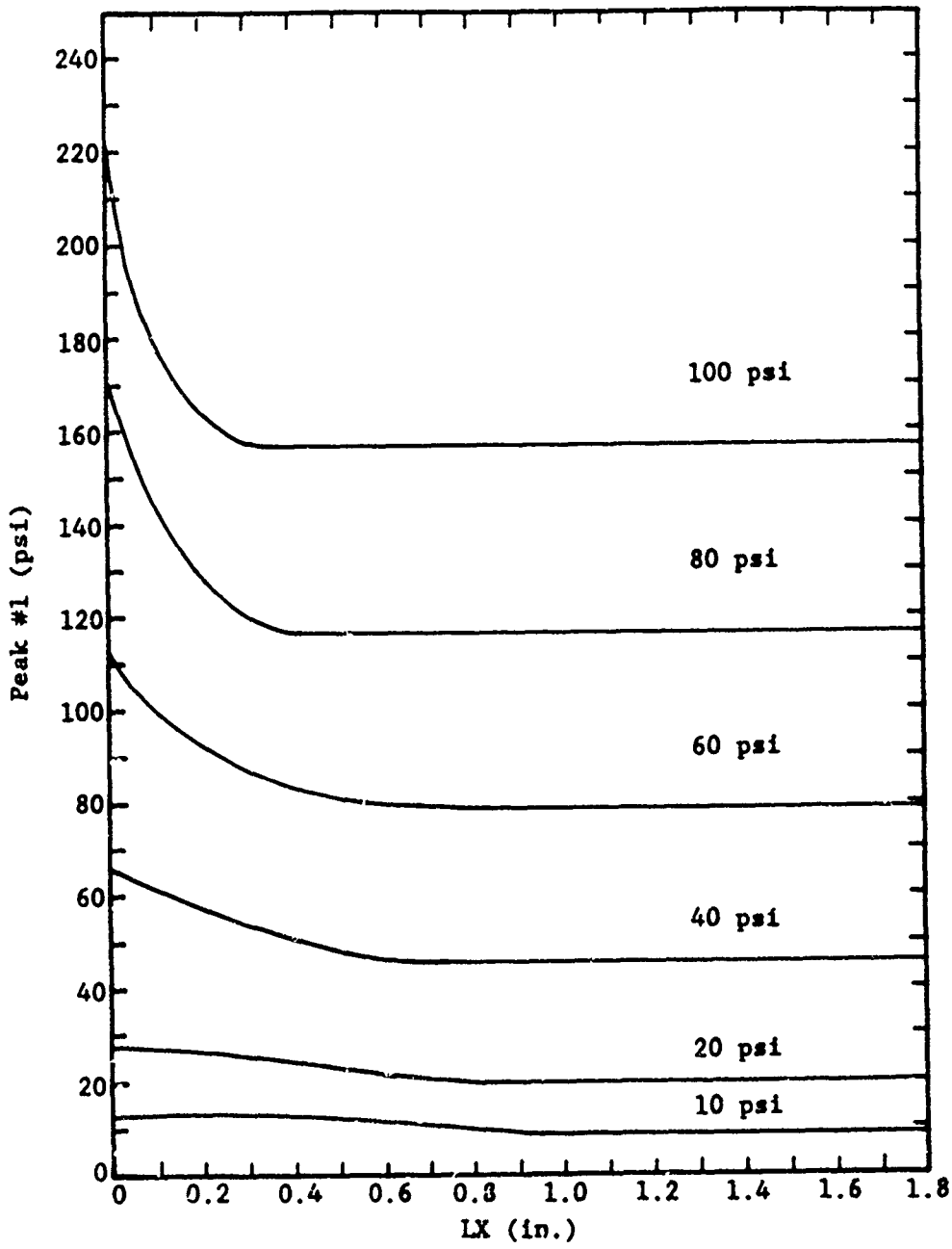

Figure 4-41. Initial internal bubble pressure peak versus chamber lid distance for Cylinder Flow field.

This test series therefore implies that for an unrestricted bubble within our test chamber, the primary flow field into the hemispherical bubble can be described as a cylindrical flow field with minimum top flow. A change in bubble volume due to increased chamber pressure would then be described mathematically by a reduction in the cylinder flow field radius. This concept is designated Cylinder Flow for our BUBBLE code and is illustrated in Figure 4-42.

Using this assumed Cylinder Flow field in the BUBBLE code resulted in the calculations and data correlations shown in Figures 4-43 through 4-45 for chamber pressures of 15.4, 48.3, and 74.6 psi, respectively. The BUBBLE code predictions agree well with the experimental data in both pressure magnitude and bubble oscillation frequency.

4.2.3 Slug Flow Tests

A fixture was designed that allowed primarily top or Slug Flow and restricted side flow to the collapsing bubble.

For these tests, a series of side flow restricting tubes were fabricated out of Plexiglas as shown in Figure 4-46. Figure 4-47 illustrates the installation of these tubes onto the basic hemispherical surrogate fixture used in the Cylinder Flow experiments described in Section 4.2.2. In the Slug Flow setup, the surrogate sample was placed in the pressure chamber at a bubble distance from the lid of 1.90". Then various tube lengths were added to prevent side flow and allow primarily top or slug flow into the collapsing bubble. The tube length subtracted from the standoff distance (LX) yields the chamber lid gap distance (GX).

Figure 4-48 illustrates how larger GX values (shorter tube lengths) restrict very little side flow. Therefore for short tube lengths (large GX) P_{in} are similar in frequency and magnitude to those of Cylinder Flow. However, as the GX values get smaller and the tube lengths get longer, the first P_{in} peak increases in magnitude and decreases in oscillation frequency as a function of chamber pressure. Therefore, as side flow is restricted the P_{in} values increase in magnitude. This observation is discussed further in Section 4.3.

The Slug Flow field was mathematically described and used as a flow geometry input in the BUBBLE code, Figure 4-49. Figures 4-50 through 4-52 show correlation of the BUBBLE code predictions with the slug flow experimental data for respective chamber pressures of 11.5, 50.4 and 76.7 psi. The agreement in Figures 4-50 and 4-51 is good, however Figure 4-52 shows that the BUBBLE code predicted two peaks, but with much higher peak values than seen in the laboratory. This discrepancy may be due to surrogate material property effects at these high chamber pressures. The current BUBBLE code does not account for these effects. These effects will be added after the BUBBLE code is further developed to accommodate nonsymmetrical BUBBLE flow fields.

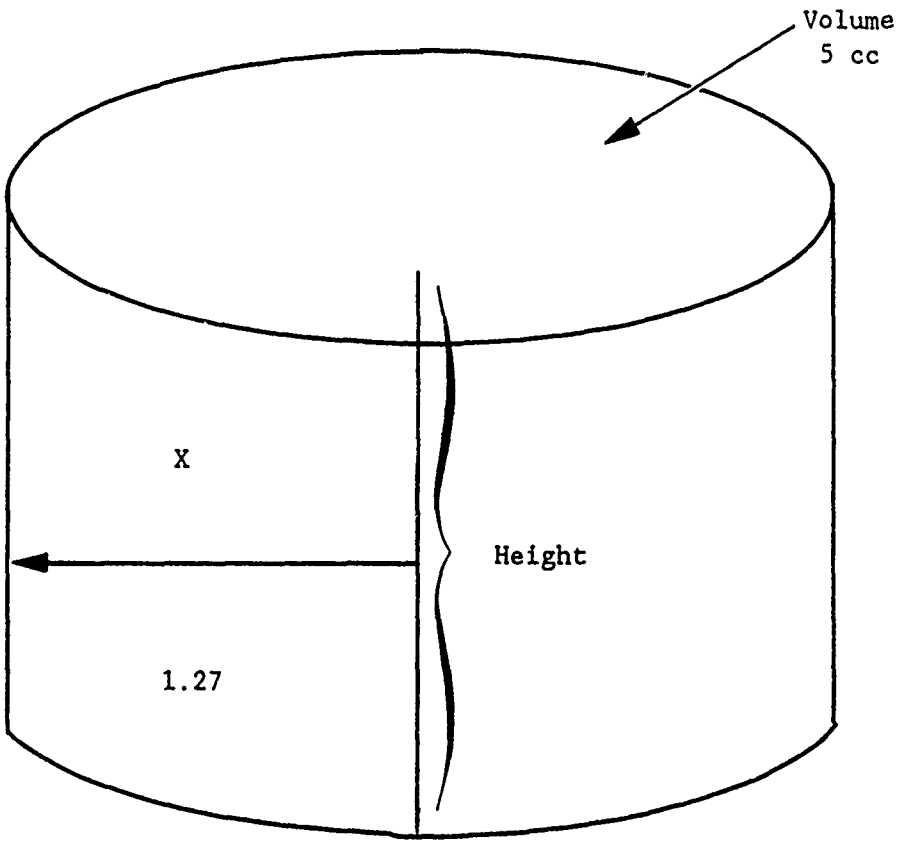

IGEOM = 7

Figure 4-42. Cylinder Flow field BUBBLE code input schematic.

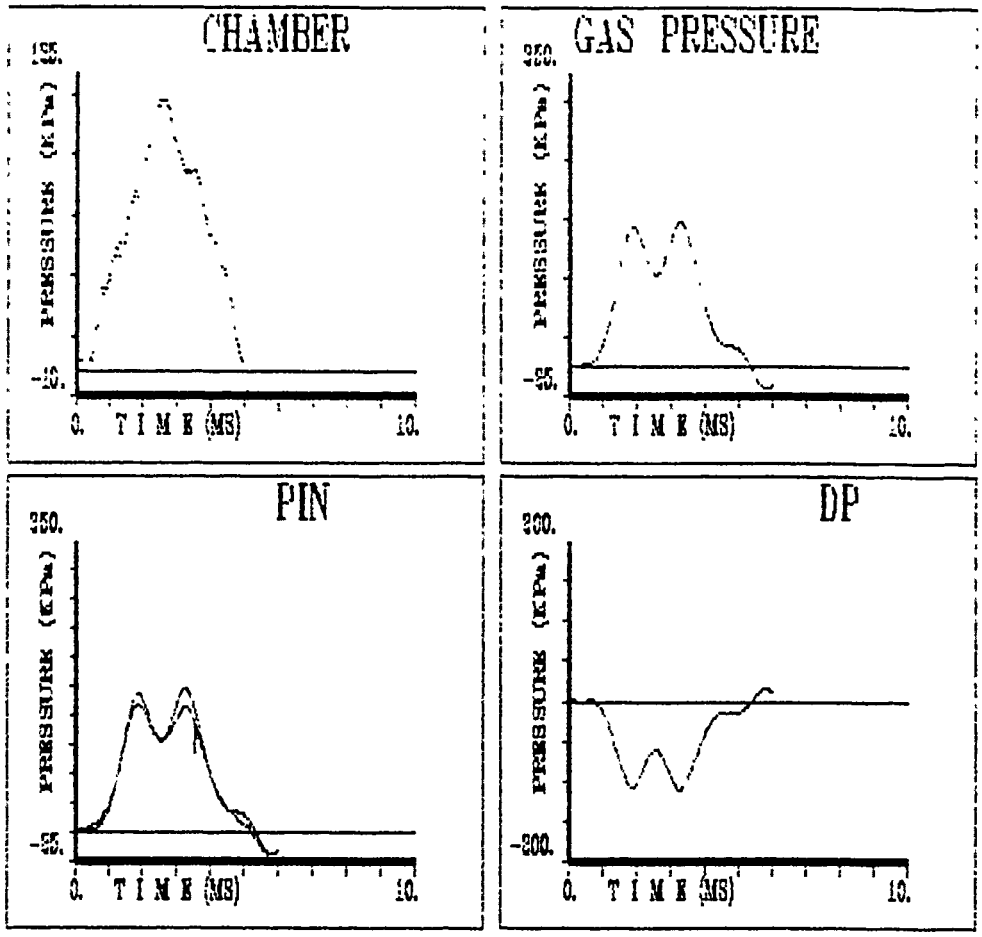

INPUT DATA:

Initial pres(KPa) = 100.0, Volume (cm3) = 5.0
Chamber press (KPa) = 104.8
Tank stiffness (KPa/cm3) = 102.0 Damping (ms) = 50.0

Probe locations: In = .25
Starting position (cm) = 1.27

Geometry 7: Cylinder
Radius (cm) = 1.27 Height (cm) = .39
Outer boundary (cm) = 1.92

Figure 4-43. Cylinder Flow correlation at a chamber pressure of 15.4 psi.

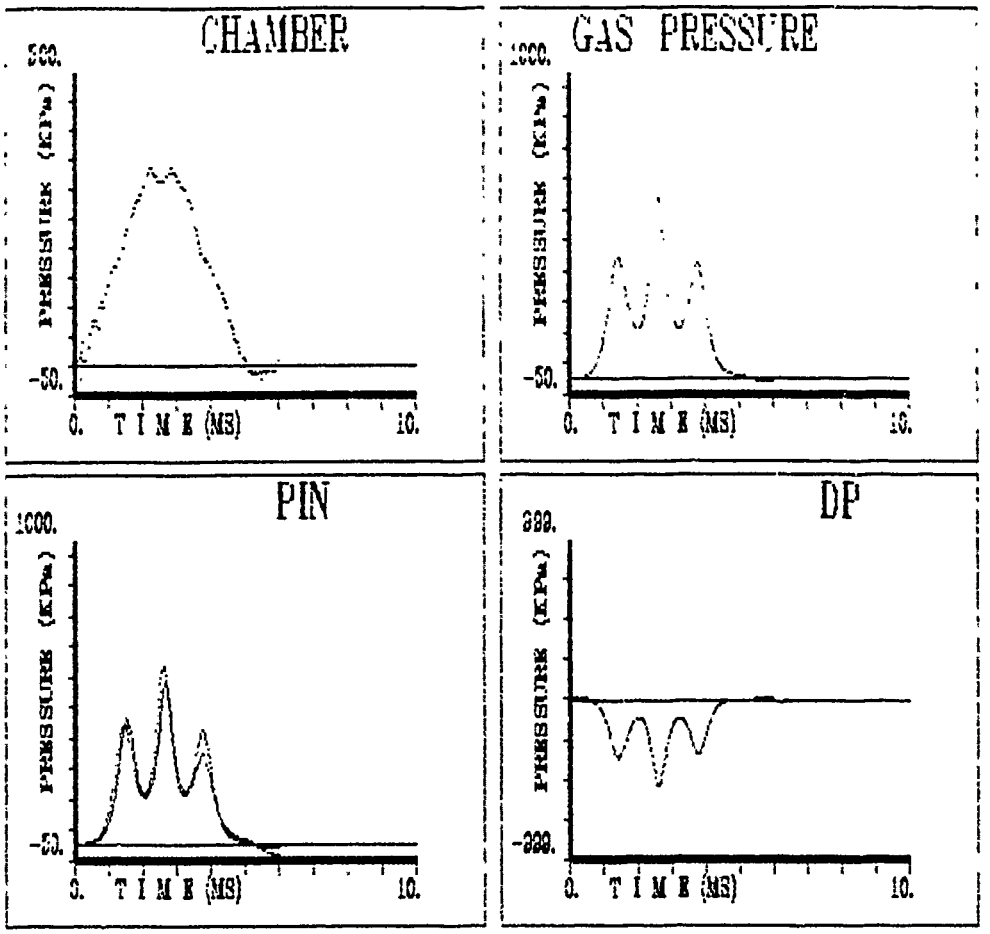

INPUT DATA:

Initial press(KPa) = 100.0, Volume (cm3) = 5.0
Chamber press (KPa) = 338.6
Tank stiffness (KPa/cm3) = 102.0 Damping (mc) = 50.0

Probe locations: In = .25
Starting position (cm) = 1.27

Geometry 7: Cylinder
Radius (cm) = 1.27 Height (cm) = .99
Outer boundary (cm) = 1.92

Figure 4-44. Cylinder Flow correlation at a chamber pressure of 48.3 psi.

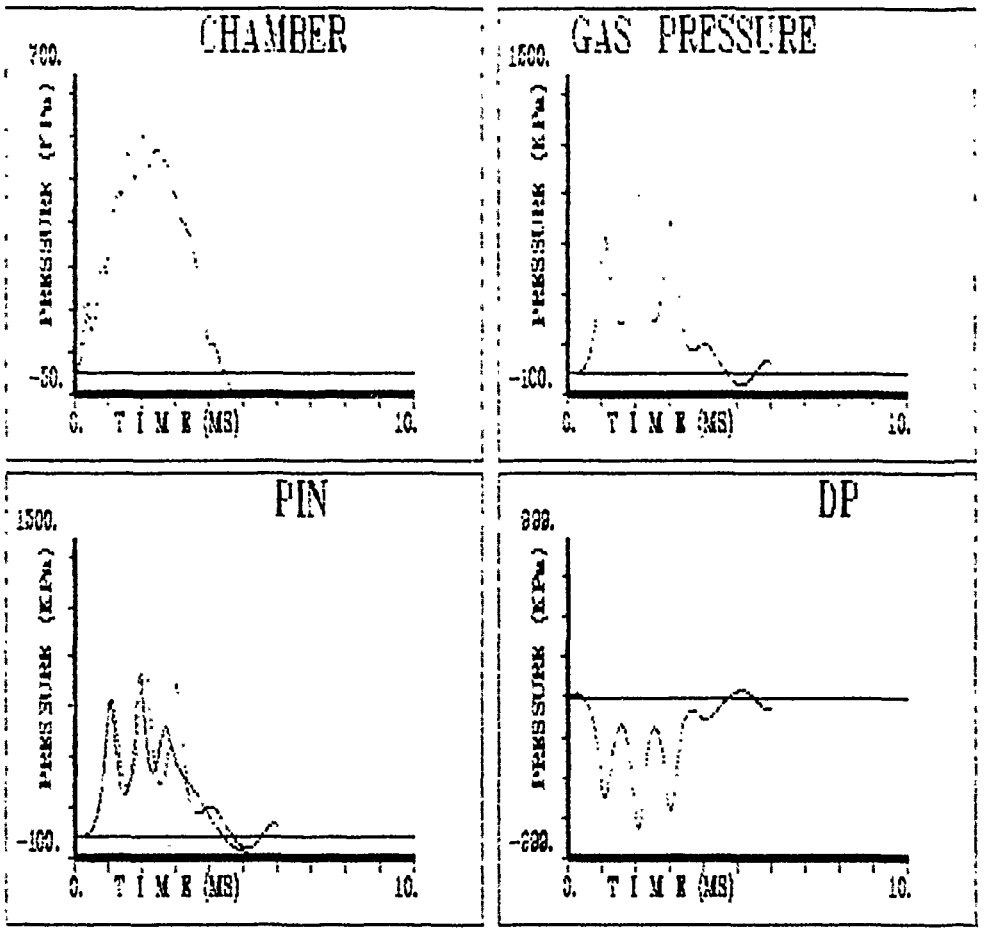

INPUT DATA:

Initial pres(KPa) = 100.0, Volume (cm3) = 5.9
Chamber press (KPa) = 507.5
Tank stiffness (KPa/cm3) = 102.0 Damping (ms) = 70.0

Probe location: In = .25
Starting position (cm) = 1.27

Geometry 7: Cylinder
Radius (cm) = 1.27 Height (cm) = .99
Outer boundary (cm) = 1.92

Figure 4-45. Cylinder Flow correlation at a chamber pressure of 74.6 psi.

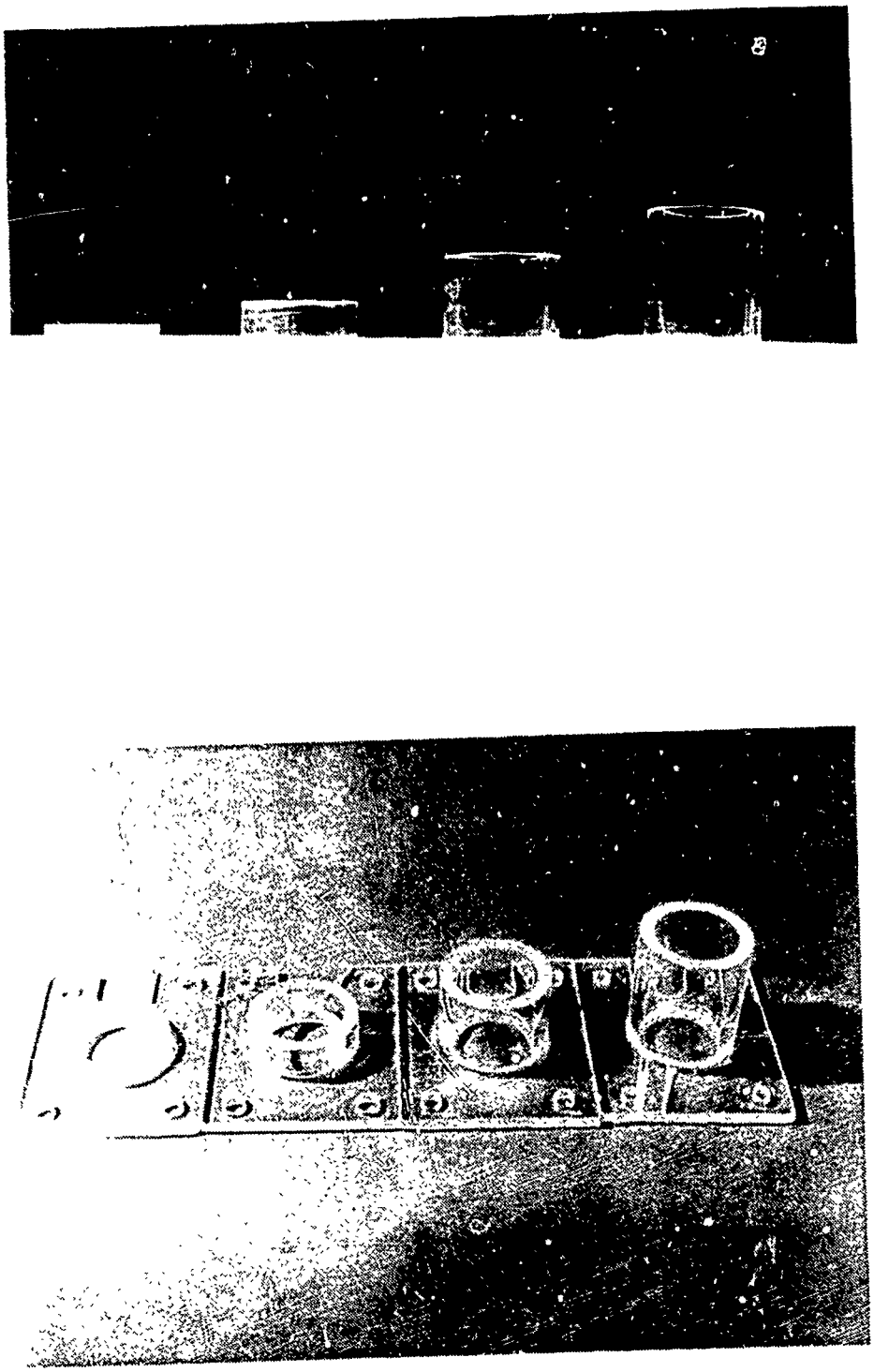

Figure 4-46. Slug Flow tube lengths.

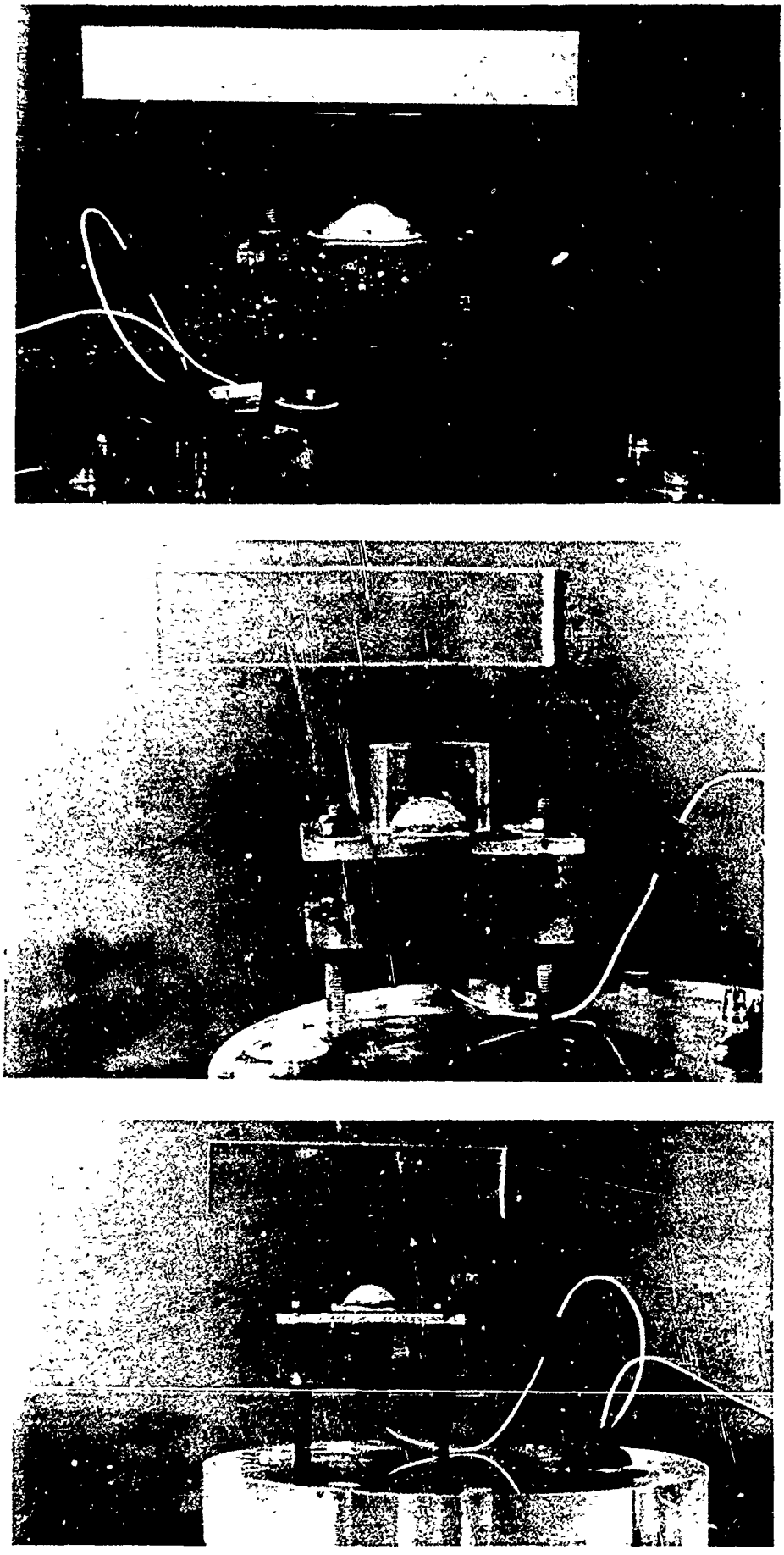

Figure 4-47. Slug Flow setups.

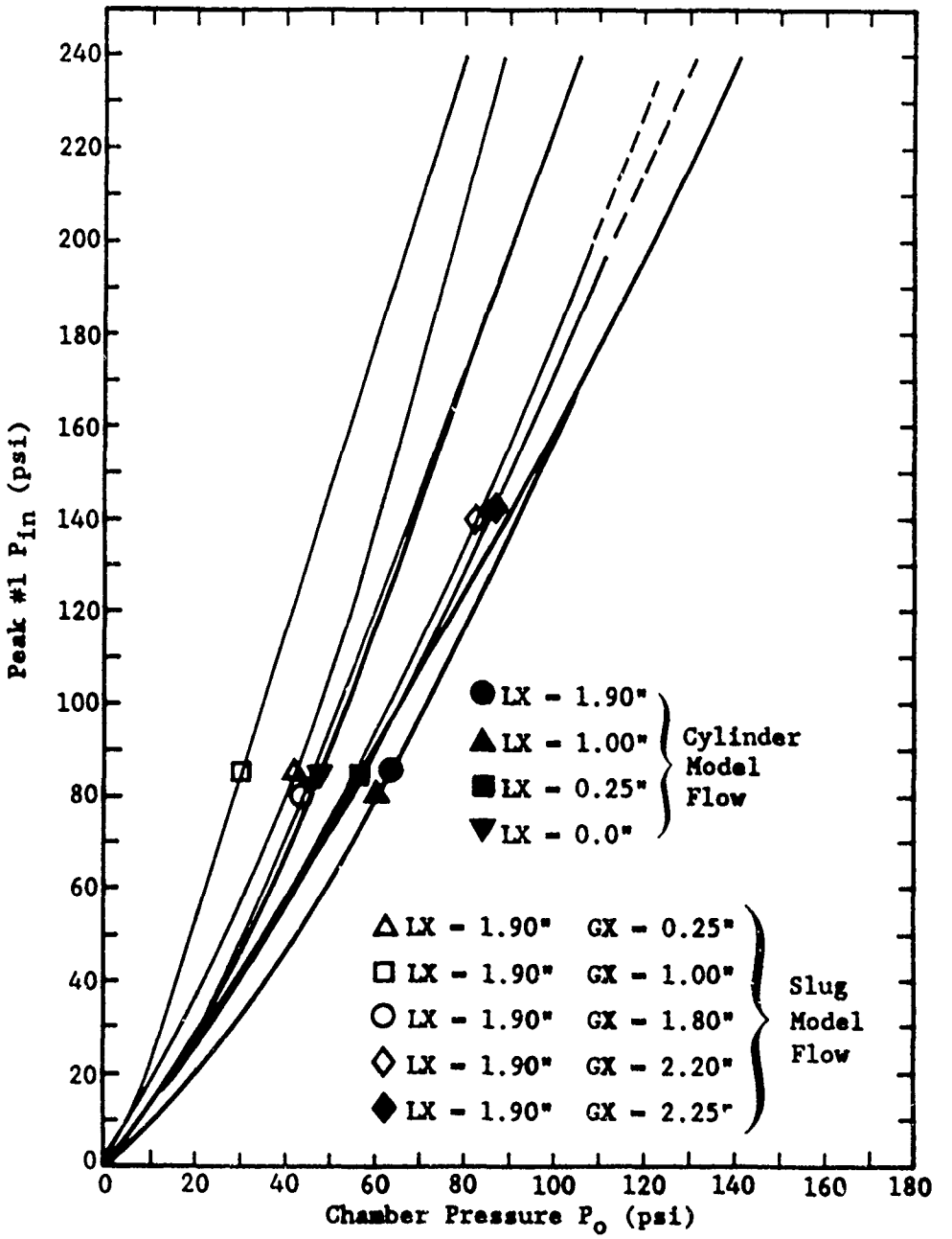

Figure 4-48. Comparison of bubble initial internal pressure peak as a function of chamber pressure for Cylinder Flow and Slug Flow field models.

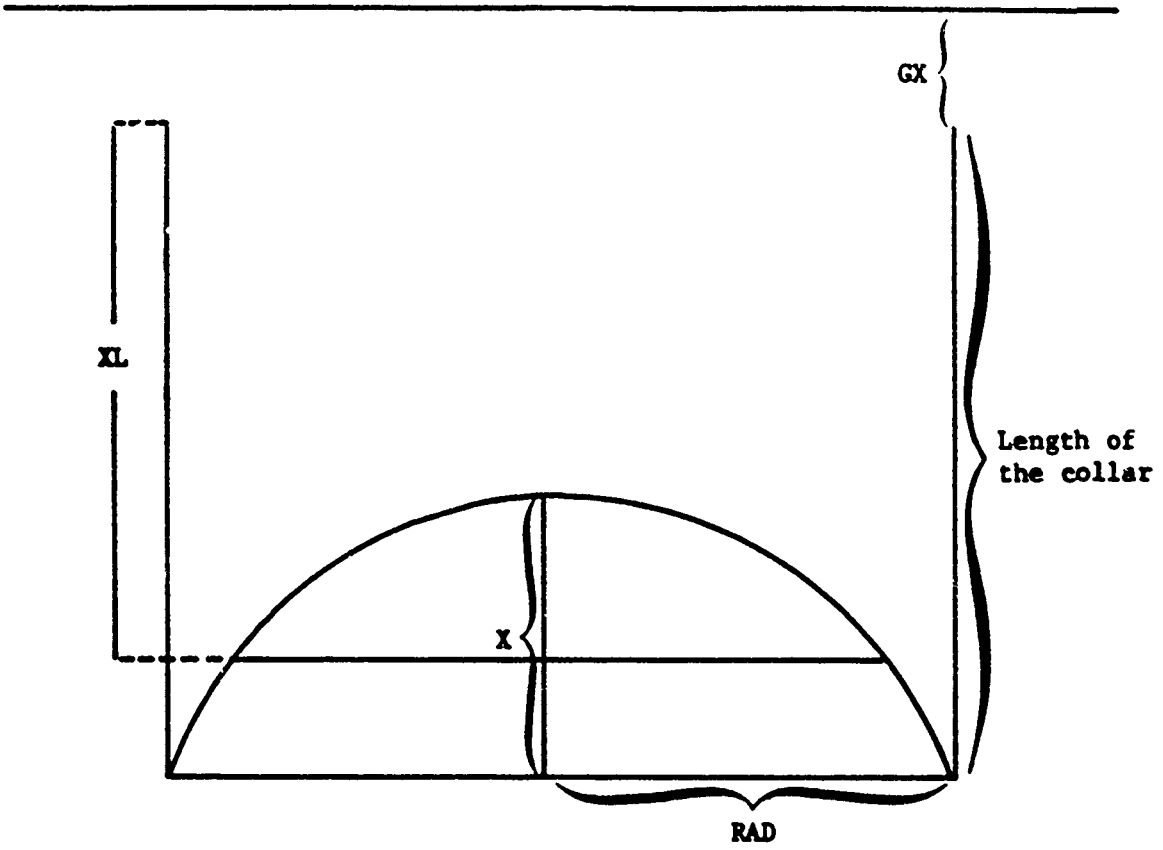

Figure 4-49. Slug Flow BUBBLE code input schematic.

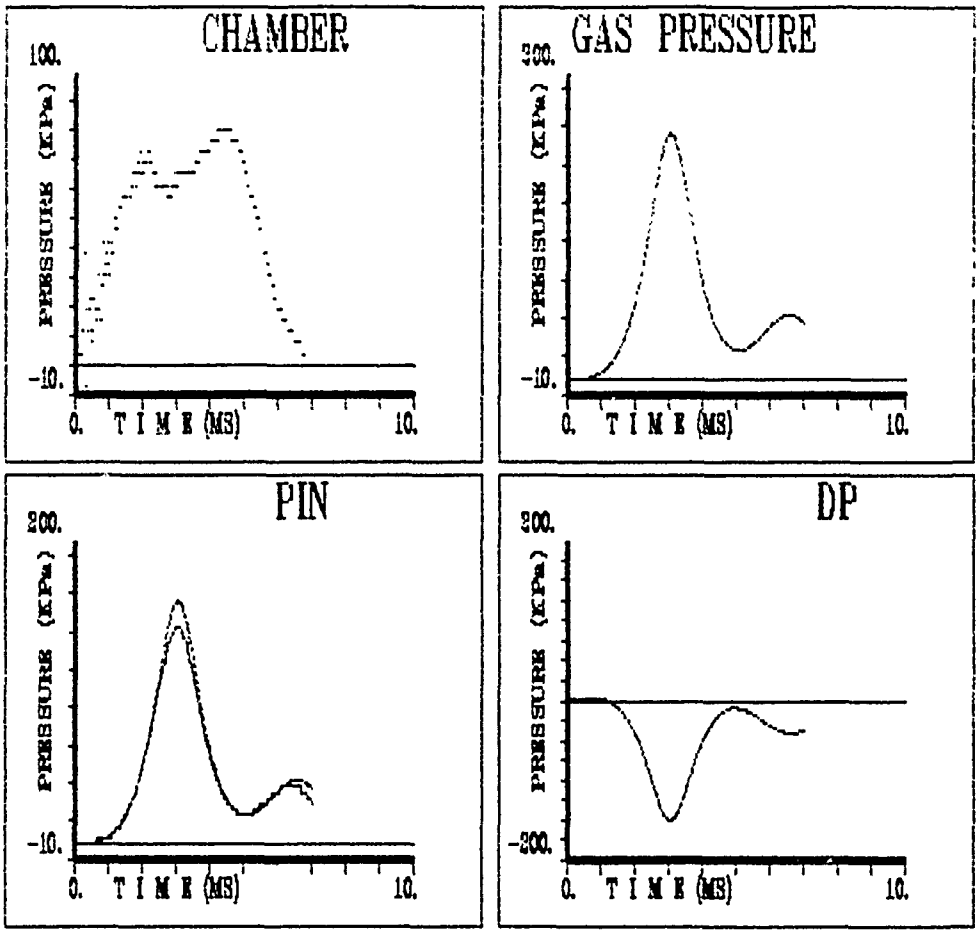

INPUT DATA:

Initial pres(KPa) = 100.0, Volume (cm3) = 5.0
Chamber press (KPa) = 78.2
Tank stiffness (KPa/cm3) = 102.0 Damping (ms) = 50.0

Probe locations: In = .89
Starting position (cm) = 1.91

Geometry 2: Water slug
Radius = 1.91 Length = 3.58

Figure 4-50. Slug Flow correlation at a chamber pressure of 11.5 psi.

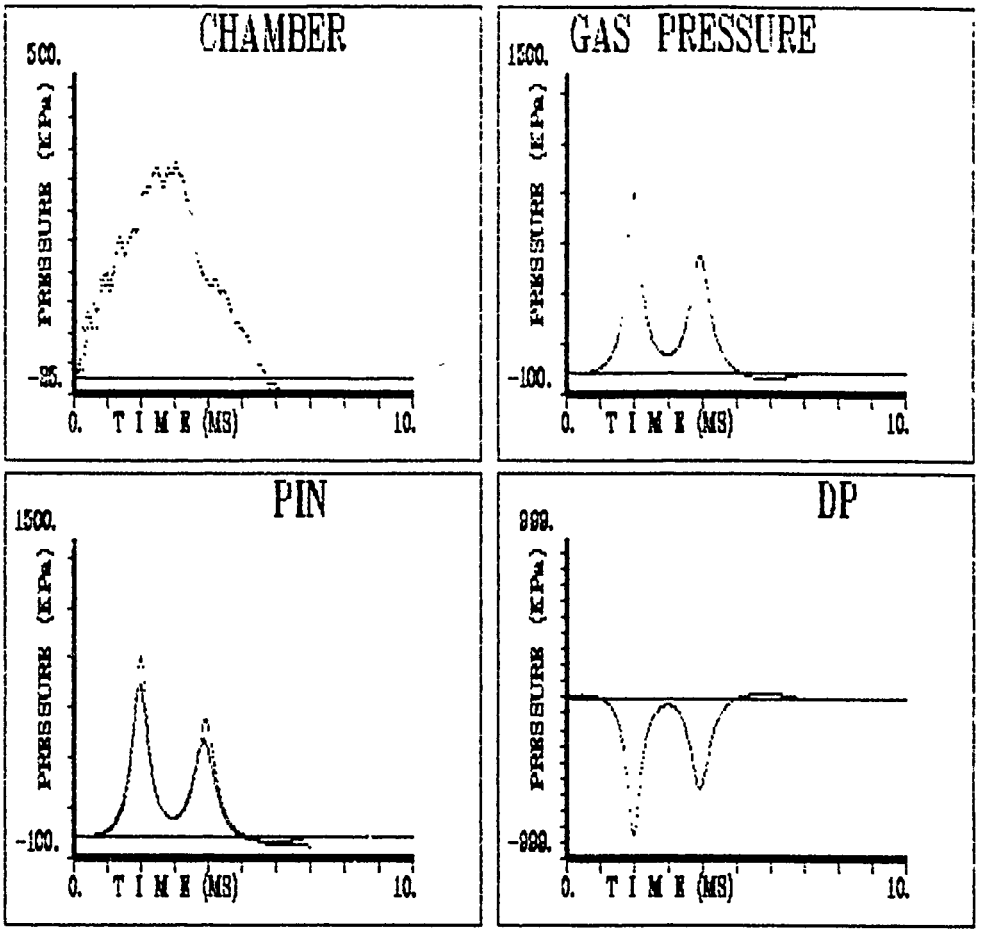

INPUT DATA:

Initial pres(KPa) = 100.0, Volume (cm3) = 5.0
Chamber press (KPa) = 342.9
Tank stiffness (KPa/cm3) = 102.0 Damping (ms) = 50.0

Probe locations: In = .89
Starting position (cm) = 1.91

Geometry 2: Water slug
Radius = 1.91 Length = 3.58

Figure 4-51. Slug Flow correlation at a chamber pressure of 50.4 psi.

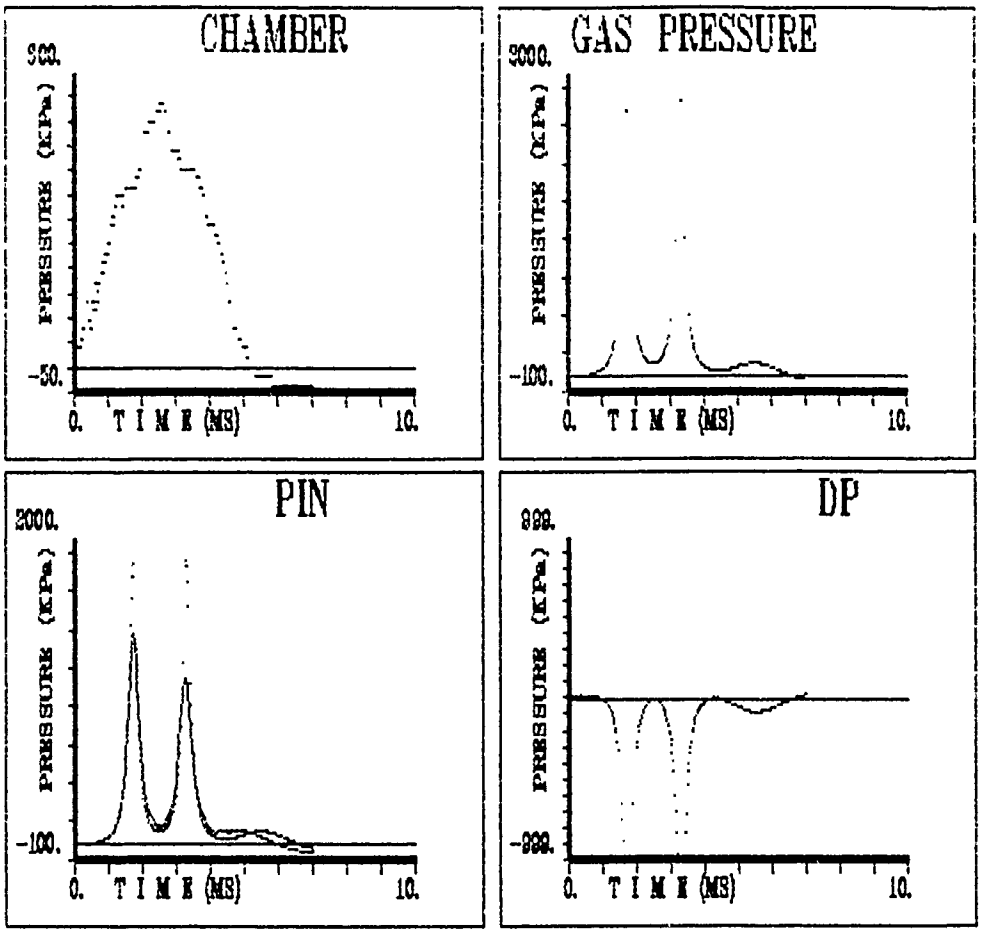

INPUT DATA:

Initial pres(KPa) = 100.0, Volume (cm3) = 5.0
Chamber press (KPa) = 521.8
Tank stiffness (KPa/cm3) = 102.0 Damping (ms) = 50.0

Probe locations: In = .89
Starting position (cm) = 1.91

Geometry 2: Water slug
Radius = 1.91 Length = 3.58

Figure 4-52. Slug Flow correlation at a chamber pressure of 76.7 psi.

Figures 4-53 and 4-54 illustrate that a prerequisite for a reasonable prediction of the bubble pressure is the flow field geometry. These figures show correlation of data at 68 psi chamber pressure using a setup with the shortest tube length 0.25". Previous observations, Figure 4-48, have indicated that this setup is Cylinder Flow. Figure 4-53 shows a BUBBLE code prediction using the Slug Flow geometry while Figure 4-54 shows a prediction using the Cylinder Flow geometry. Obviously knowing the correct flow field geometry is the key to good bubble response prediction. The surrogate models have been very useful in quickly defining these various flow fields, thus allowing good correlation of BUBBLE code predictions with laboratory data.

4.2.4 Double Curvature Surrogate Model Correlation with BUBBLE Code

The BUBBLE code has been developed to predict bubble pressures given the chamber pressure and an estimate of the allowed flow pattern. Simulations in previous symmetrical geometries have been quite successful using simple estimates of the flow patterns. The latest series of tests using a double curvature surrogate, Figure 4-55, have a more complex geometry. Nonetheless, previous flow models were used to make a series of calculations. The agreement is only qualitative, Figures 4-56 through 4-58, indicating that a more precise estimate of the flow pattern in long thin bubbles is required. Future surrogate model tests will be useful in determining this flow pattern for input into the BUBBLE code.

4.3 DOUBLE CURVATURE SURROGATE TESTS

A surrogate technique was developed to identify and measure the primary input variables needed to predict the collapse of a bubble in a 3-D tubular structure similar to the G.I. tract. Parameters found to affect the bubble internal pressure signal and thus the membrane wall stress were air bubble volume, bubble shape, and G.I. internal viscosity. Factors which may influence the bubble collapse flow field, but currently designed tests showed inconclusive results, are G.I. internal fill pressure and viscous neighboring bodies. Some surrogate test data was verified against previous animal tests and future tests are discussed.

4.3.1 Double Curvature Surrogate G.I. Test Fixture and Technique

A surrogate technique to measure internal bubble pressure (P_{in}) with minimum influence on the data was designed and verified for data accuracy.

Figure 4-59 shows the double curvature fixture developed for G.I. surrogate model tests. The test specimen was made from commercially prepared lamb caecum as described in Section 3.1. The O-ring and internal gasket design allows for securing the test specimen without glue or external ties that might induce unwanted membrane stress.

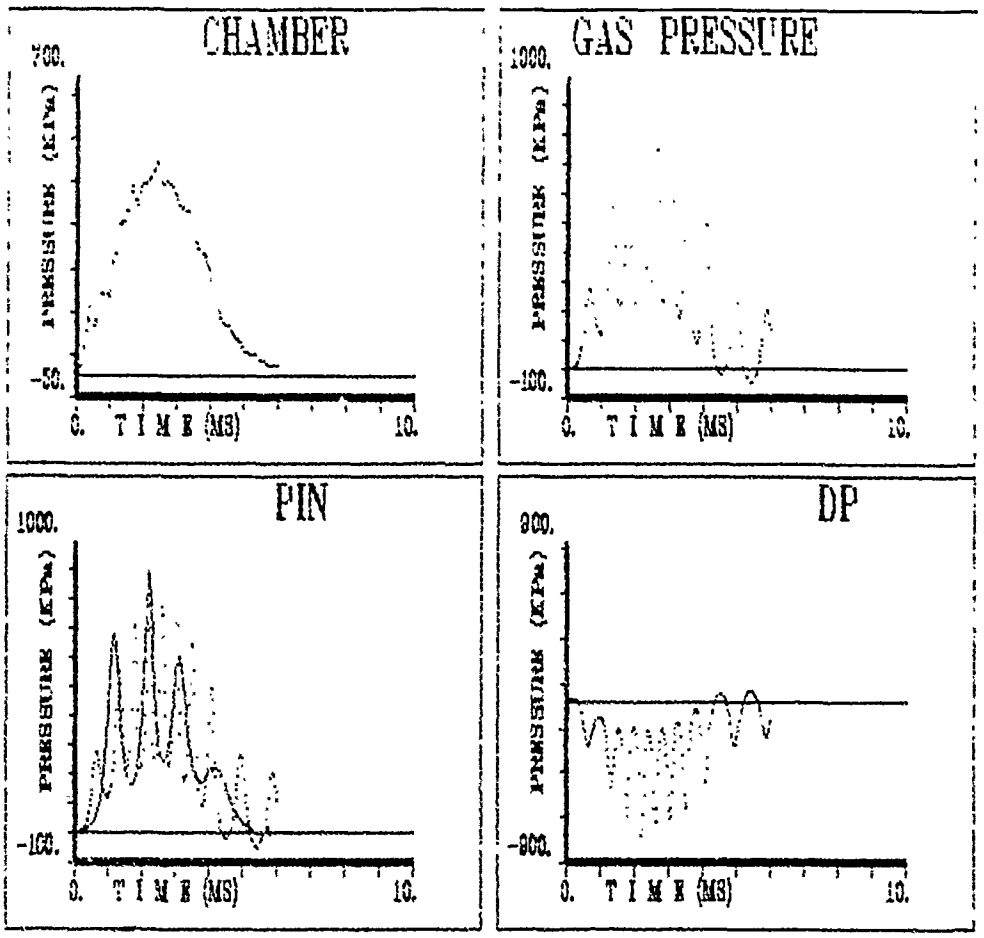

INPUT DATA:

Initial pres(KPa) = 100.0, Volume (cm3) = 5.9
Chamber press (KPa) = 462.6
Tank stiffness (KPa/cm3) = 102.0 Damping (ms) = 30.0

Probe locations: In = .89
Starting position (cm) = 1.91

Geometry 2: Water slug
Radius = 1.91 Length = .25

Figure 4-53. Slug flow correlation at a chamber pressure of 68.0 psi. Poor correlation is due to improper flow geometry assumption.

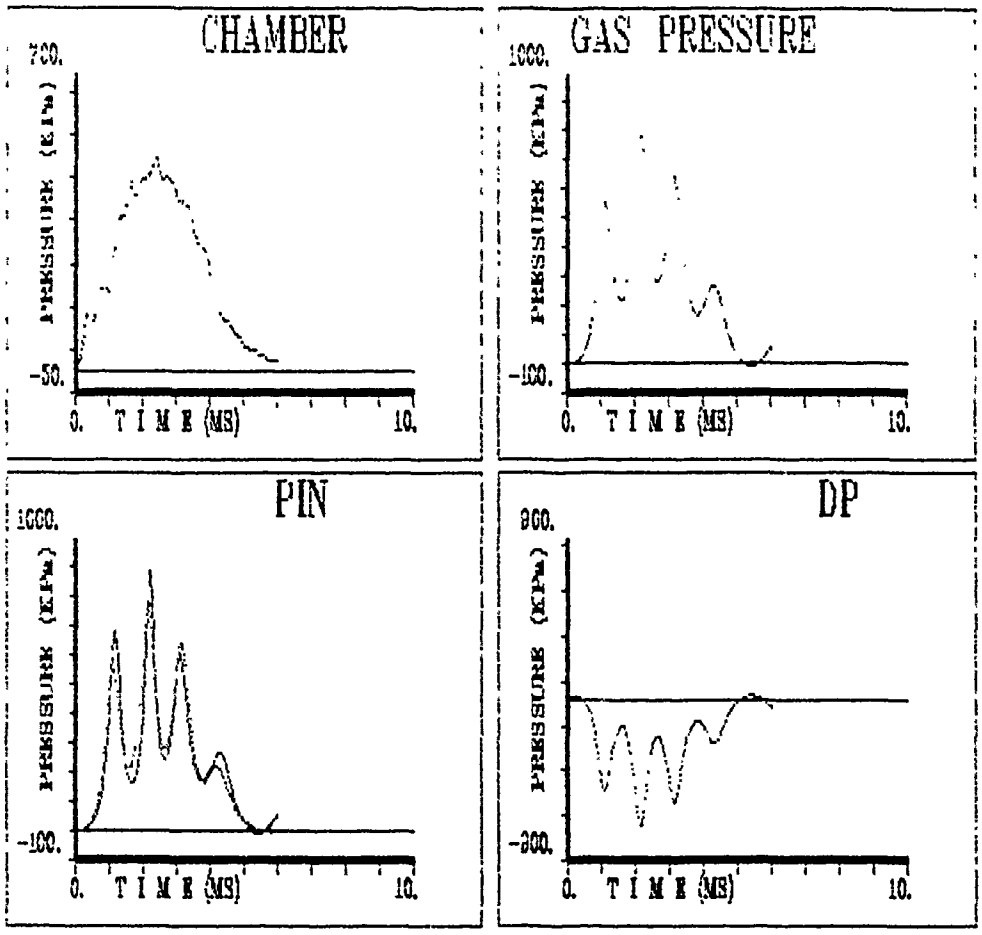

INPUT DATA:

Initial pres(kPa) = 100.0, Volume (cm3) = 5.0
Chamber press (KPa) = 462.9
Tank stiffness (KPa/cm3) = 102.0 Damping (ms) = 50.0

Probe locations: In = .25
Starting position (cm) = 1.27

Geometry 7: Cylinder
Radius (cm) = 1.27 Height (cm) = .99
Outer boundary (cm) = 1.92

Figure 4-54. Cylinder flow correlation at a chamber pressure of 68.0 psi. Good correlation is due to proper flow geometry assumption.

(a) Side view

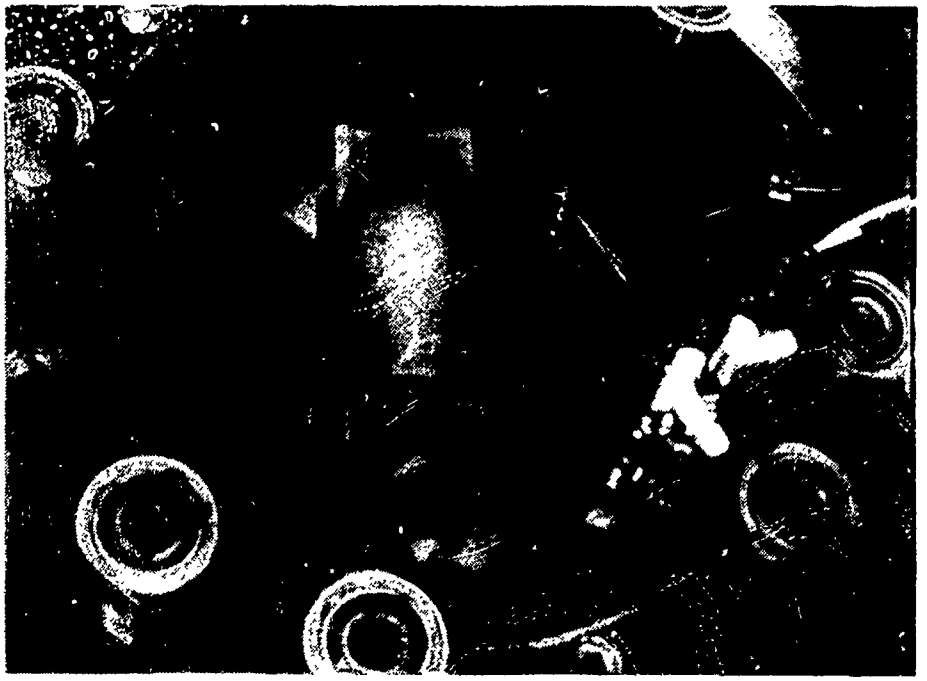

(b) Top view

Figure 4-55. Double curvature surrogate test fixture installation.

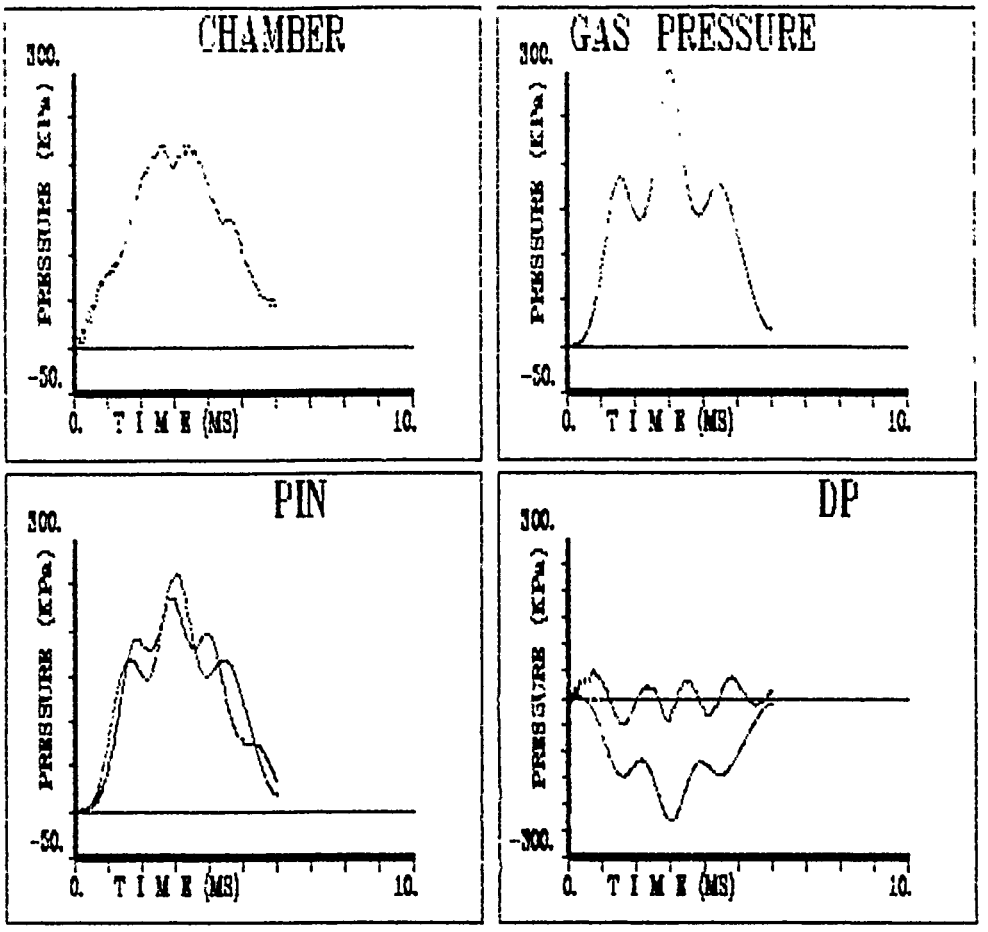

INPUT DATA:

Ambient press (KPa) = 100.0 Volume (cm3) = 10.0
Chamber press (KPa) = 212.2
Tank stiffness (KPa/cm3) = 102.0 Damping (ms) = 50.0

Probe locations: In = 1.72
Starting position (cm) = 2.03

Geometry 7: Cylinder
Radius (cm) = 2.54 Height (cm) = .77
Outer boundary (cm) = 2.24

Figure 4-56. Double curvature surrogate correlation at a chamber pressure of 31.2 psi.

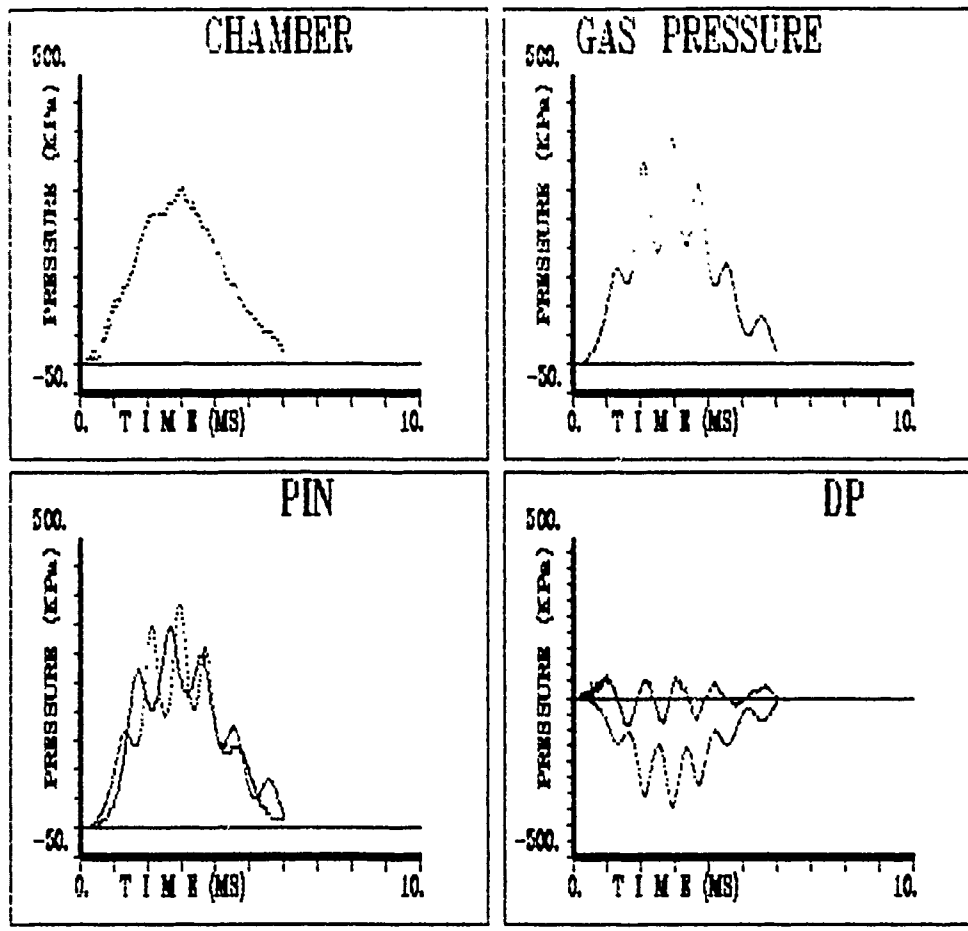

INPUT DATA:

Ambient press (KPa) = 100.0 Volume (cm3) = 5.0
Chamber press (KPa) = 298.0
Tank stiffness (KPa/cm3) = 102.0 Damping (ms) = 50.0

Probe locations: In = .71
Starting position (cm) = 1.02

Geometry 7: Cylinder
Radius (cm) = 2.54 Height (cm) = 1.54
Outer boundary (cm) = 1.12

Figure 4-57. Double curvature correlation at a chamber pressure of 43.8 psi.

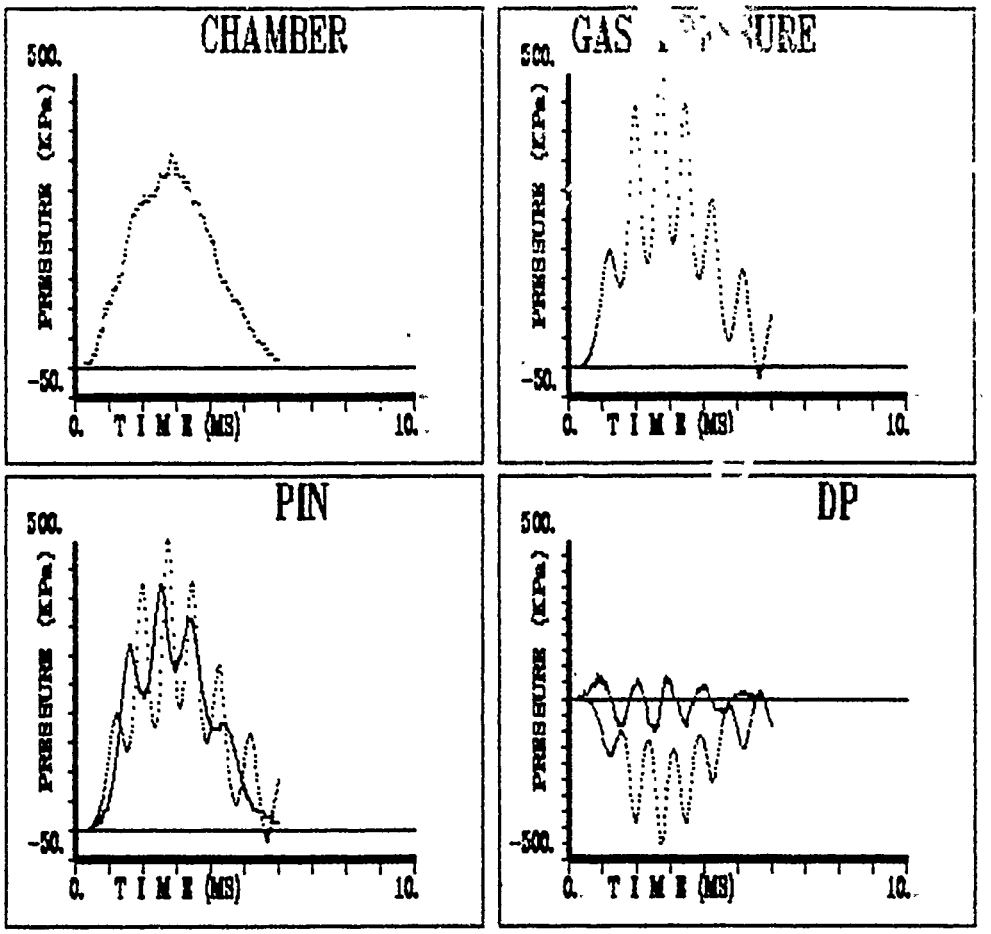

INPUT DATA:

Ambient press (KPa) = 100.0 Volume (cm3) = 5.0
Chamber press (KPa) = 350.3
Tank stiffness (KPa/cm3) = 102.0 Damping (ms) = 50.0

Probe locations: In = .71
Starting position (cm) = 1.02

Geometry 7: Cylinder
Radius (cm) = 2.54 Height (cm) = 1.54
Outer boundary (cm) = 1.12

Figure 4-58. Double curvature correlation at a chamber pressure of 51.5 psi.

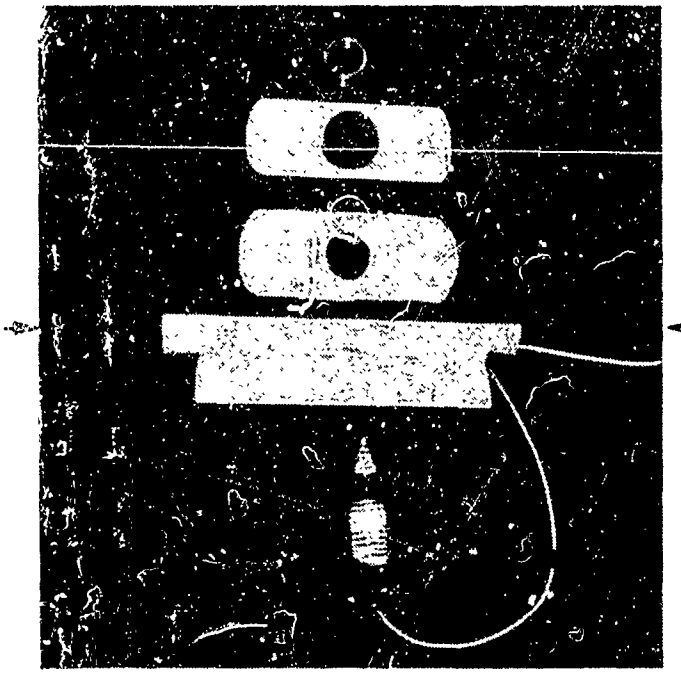

(a) Components

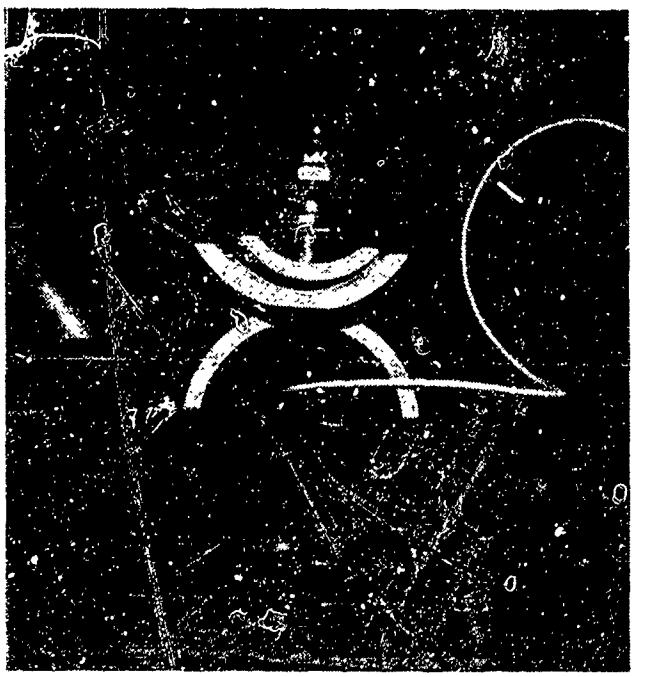

(b) Assembly

Figure 4-59. Surrogate test fixture with O-ring/gasket seal.

Assembly involved cutting a hole in the bottom of the surrogate to allow the transducer mount entry into the model and placement of the transducer tip into the bubble. The surrogate was sealed and secured to the fixture by the internal gasket, lock plate, O-ring and locknuts on the threaded transducer mount. A catheter was inserted and tied to the test surrogate to allow injection of air. A typical surrogate assembly is shown in Figure 4-60.

A Kistler vertically mounted Model 211B4 pressure transducer was used for bubble pressure measurement (P_{in}). High speed movies have shown that the pressure transducer tip usually remains in the long thin air bubble during collapse. However, to ensure accurate P_{in} measurements, a test was conducted to determine the effect of transducer distances from the air bubble. Figure 4-61 illustrates that for a 5 cc bubble the DP versus chamber pressure data is consistent as long as the transducer remains within any part of the air bubble. Maximum DP is the peak pressure value when subtracting the chamber wall pressure signal (Pc) from the bubble internal pressure signal (P_{in}). At transducer distances outside the bubble, greater than 0.18" at bubble center, the DP values show a marked shift downward. This data also indicates that the flow field for water filled surrogates involves an internal fluid flow boundary of at least 0.25" from the bubble.

4.3.2 Data Repeatability

In order to have confidence in the surrogate test technique, a series of tests was conducted to verify data repeatability from shot-to-shot and surrogate sample-to-sample. The surrogate test results showed good data repeatability.

Figure 4-62 illustrates the effect of multiple shots on a single surrogate sample. The sample was filled with water and contained a 5 cc air bubble. It was subjected to repeated shots in random order for test chamber pressure levels from 10 to 60 psi. Internal bubble pressure and chamber wall pressure signals were used to calculate DP. The maximum DP versus peak chamber pressure was plotted. The result shows that repeated test shots did not appear to affect the material properties of the surrogate.

Figure 4-63 shows calibration tests for a 5 cc bubble. The 5 cc setup was tested using a series of different surrogate samples. The result shows good surrogate sample-to-sample repeatability.

4.3.3 Bubble Volume Effect

Air bubble volume was investigated and found to be one of the controlling parameters for the bubble internal pressure signal and hence the membrane wall stress. The bubble oscillation frequency, which may be related to membrane wall fatigue, is inversely proportional to the bubble volume.

(a) Fixture

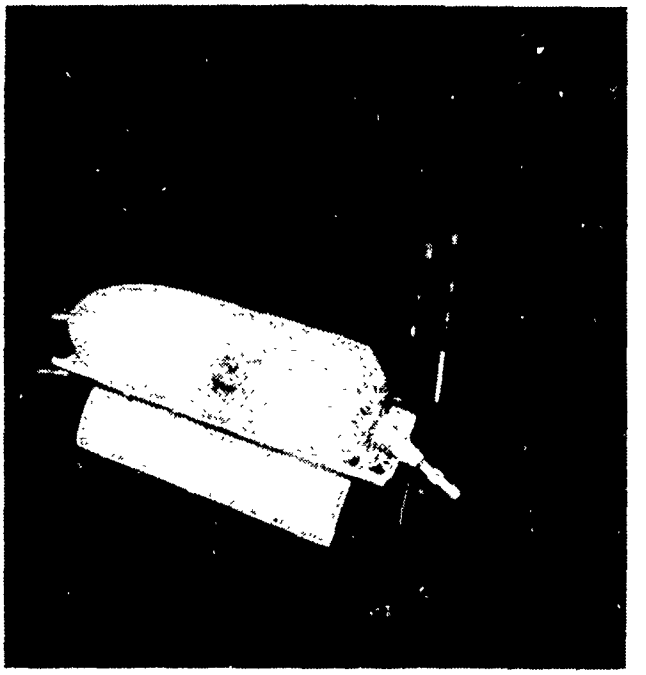

(b) Surrogate

Figure 4-60. Typical surrogate test unit.

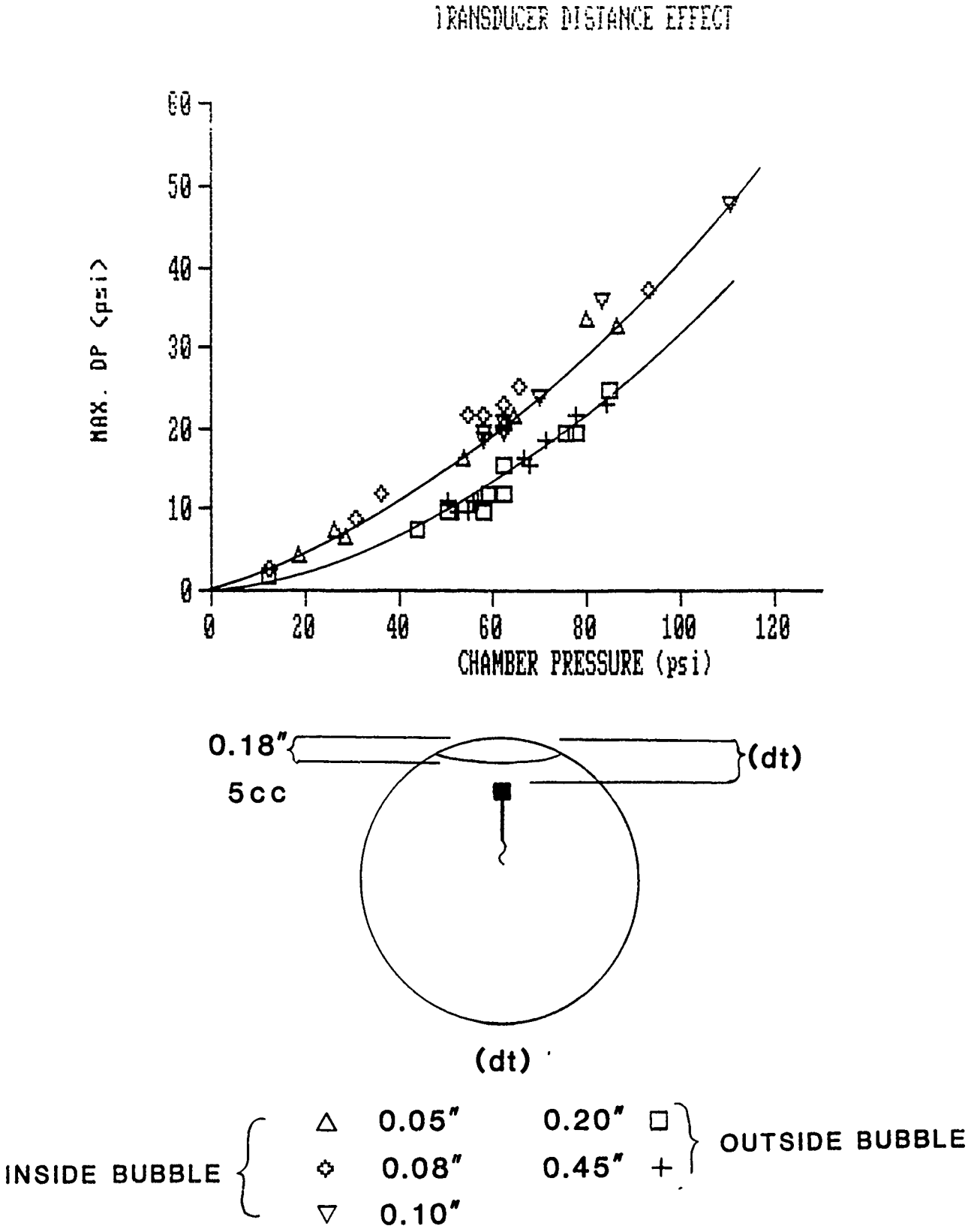

Figure 4-61. Effect of transducer distance from bubble surface.

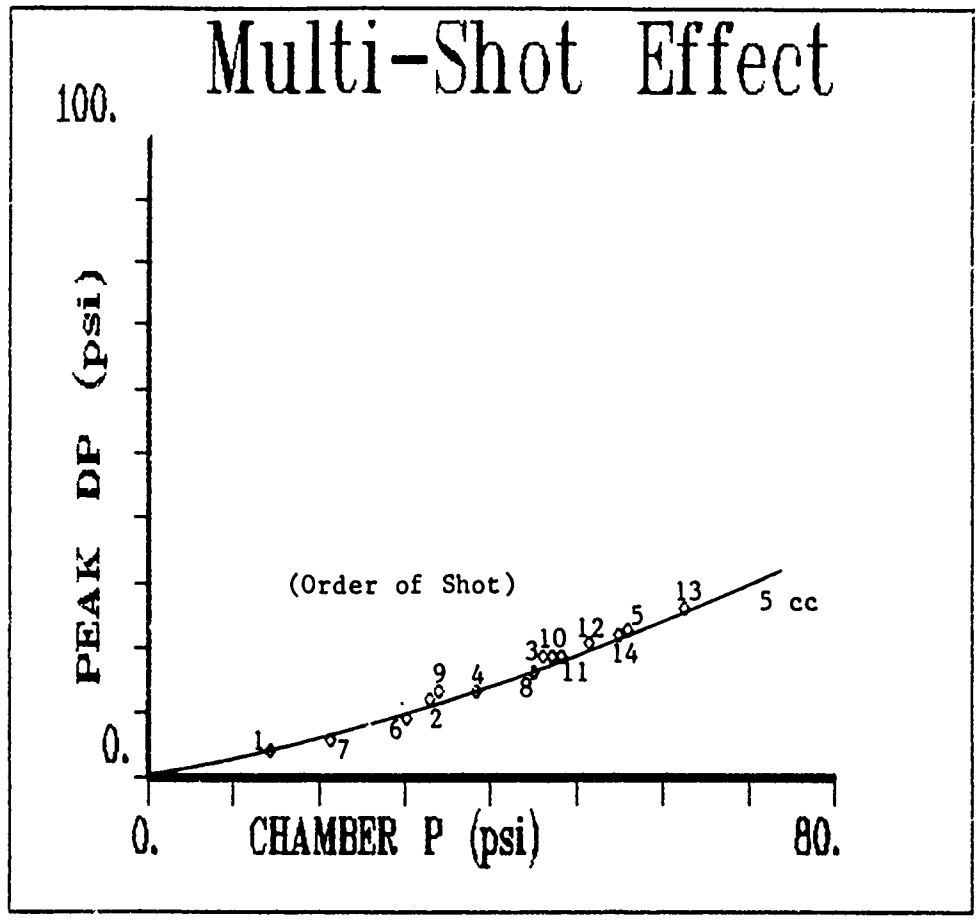

Figure 4-62. Multishot effect.

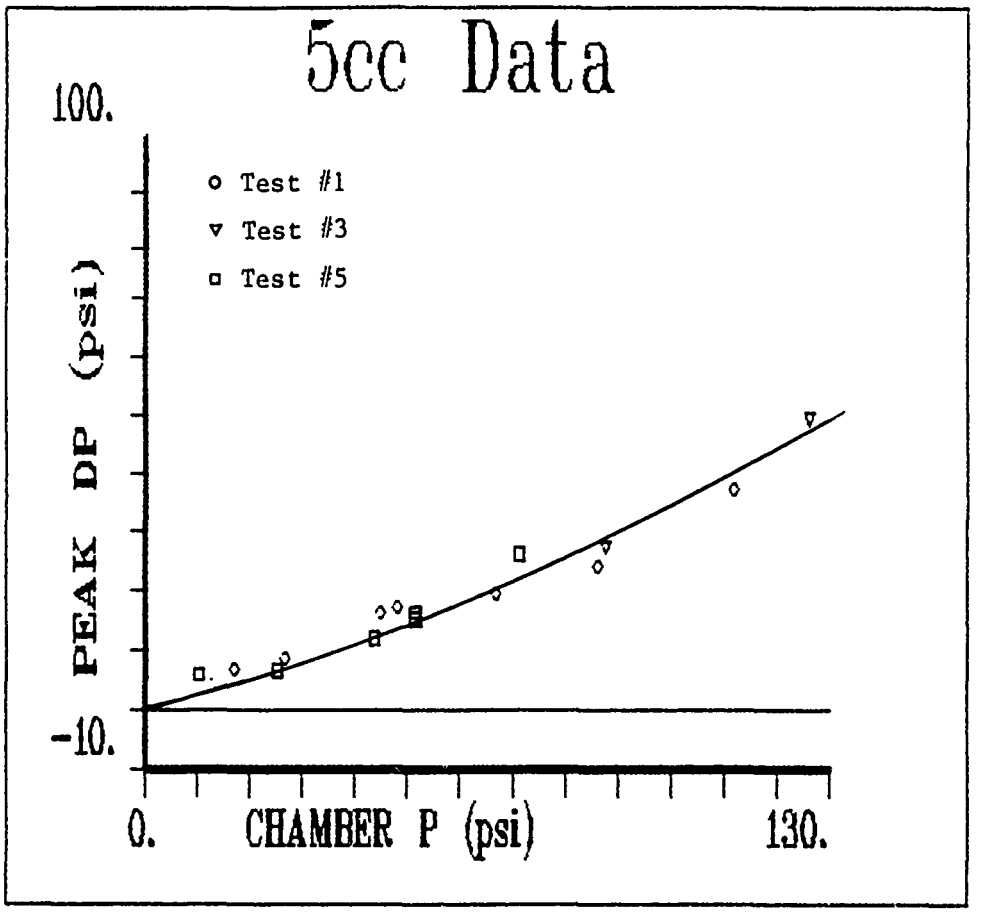

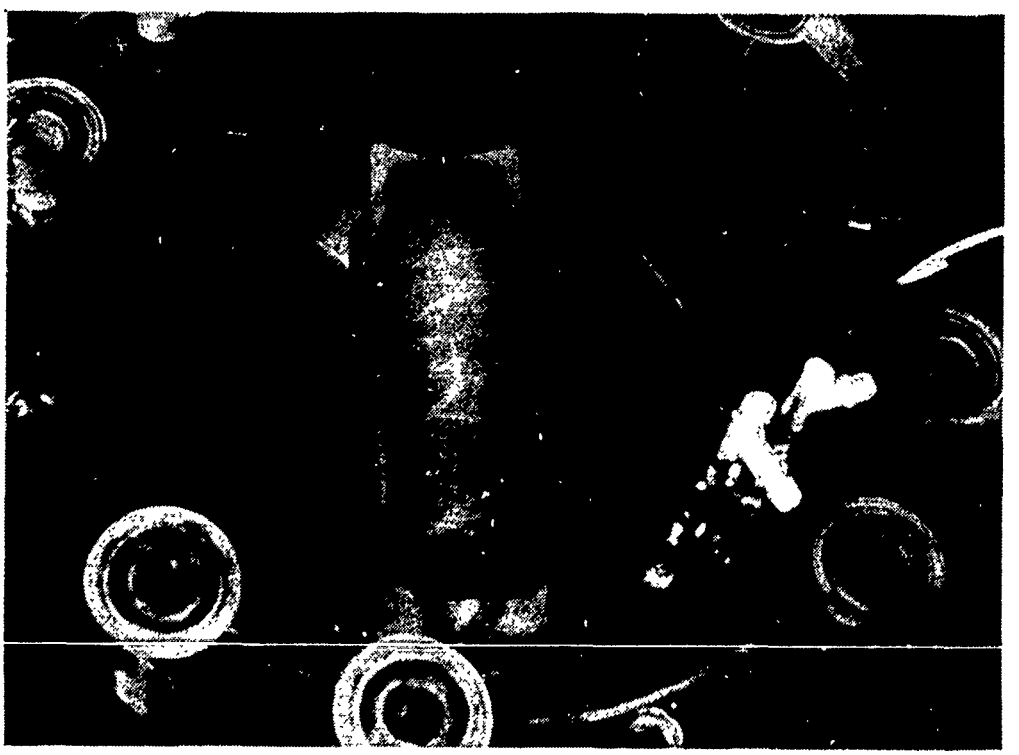

Figure 4-63. 5 cc bubble data surrogate to surrogate test setup.

The double curvature surrogate model was used to test the effect of air bubble volume on the bubble internal pressure (P_{in}) signal. Using a single surrogate sample, the air bubble volume was changed by adding air through the catheter connection and then zeroing the internal fill pressure. This technique maintained control of other test variables and allowed observation of the air bubble volume effect over a range of bubble sizes.

Figures 4-64 and 4-65 show the results of tests for 2, 5, 10 and 15 cc bubbles at similar chamber pressures. Increasing the air bubble volume primarily affects the oscillation frequency of the bubble. Smaller bubbles undergo more oscillation cycles at higher DP ($P_{bubble} - P_{chamber}$) magnitudes than larger bubbles and therefore may experience more membrane wall stress and fatiguing. This effect is most apparent when comparing 2 cc and 15 cc test results. This trend agrees with previous in vitro rabbit caecum data from reference [1], shown in Figures 4-66 and 4-67.

Figure 4-65 also shows that the 15 cc bubble has a much lower DP versus chamber pressure curve than 2, 5 and 10 cc bubbles. This may be related to the longer and thicker shape of the 15 cc bubble. Section 4.3.4 discusses this parameter.

Figures 4-68 compares the surrogate data with previous in vitro G.I. injury test data. The 5 cc surrogate and in vitro 5 cc and 10 cc data are replotted in Figure 4-68 as maximum internal bubble pressure (P_{in}) versus peak chamber pressure. As shown, excellent agreement is achieved, showing that P_{in} can be correlated to G.I. injury.

4.3.4 Air Bubble Shape Effect

The bubble shape or radius of curvature, was found to primarily affect the magnitudes of the bubble oscillation during blast. For a given air bubble volume, the smaller the membrane surface contact area (radius of curvature), the larger the membrane wall strain due to increased membrane wall displacement for a given chamber pressure.

Since the G.I. tract is composed of geometrically different sections (e.g., caecum, ascending colon, transverse colon, etc.), the shape of an air bubble is an important parameter when determining membrane wall stress during blast. Whether the bubble is long and thin or hemispherical in shape is determined by the bubble volume and radius of curvature of the surrounding G.I. structure. Surrogate tests have shown that the bubble internal pressure signal is different in magnitude for bubbles with the same volume but dissimilar curvatures.

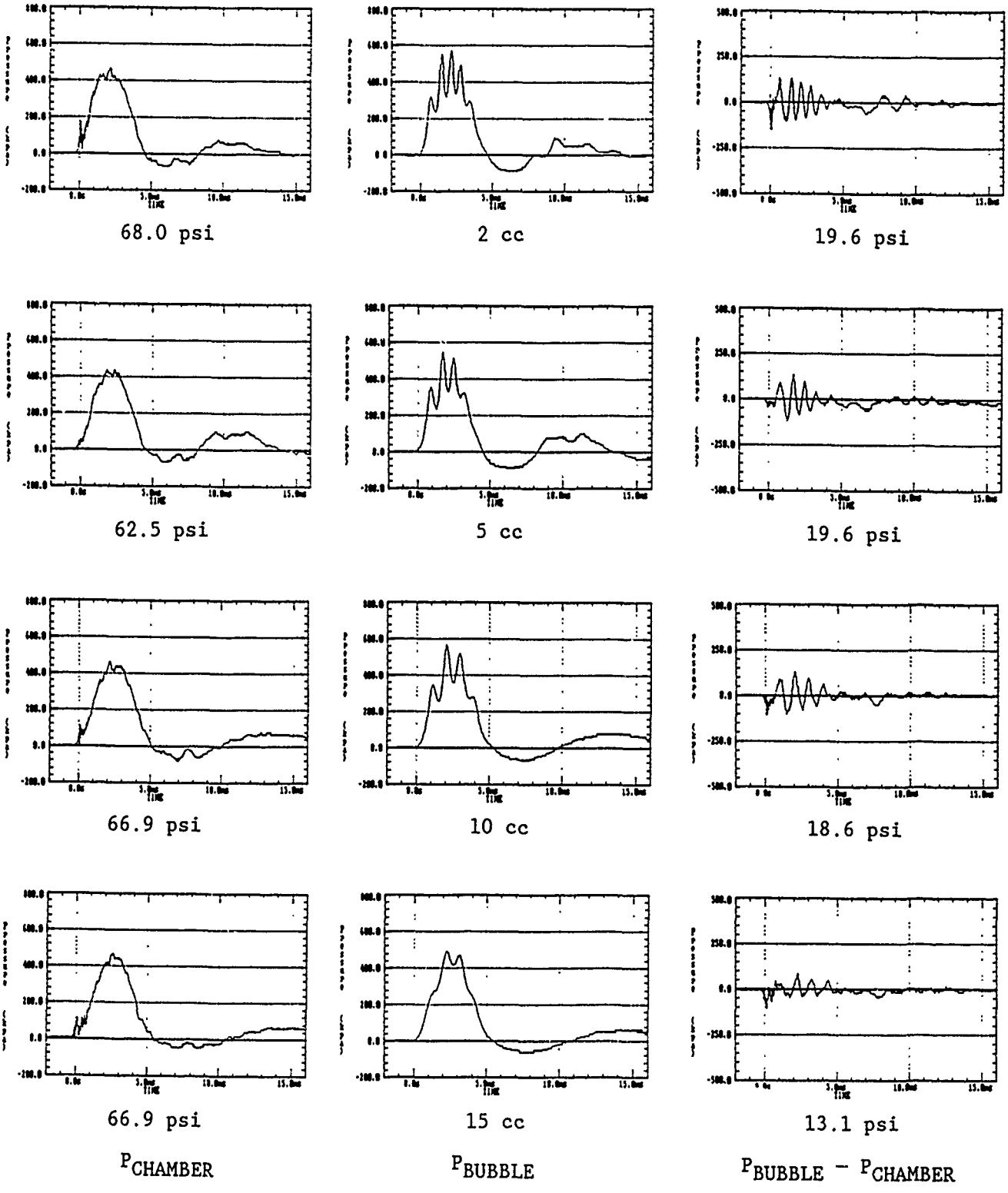

Figure 4-64. Air bubble volume effect pressure signals.

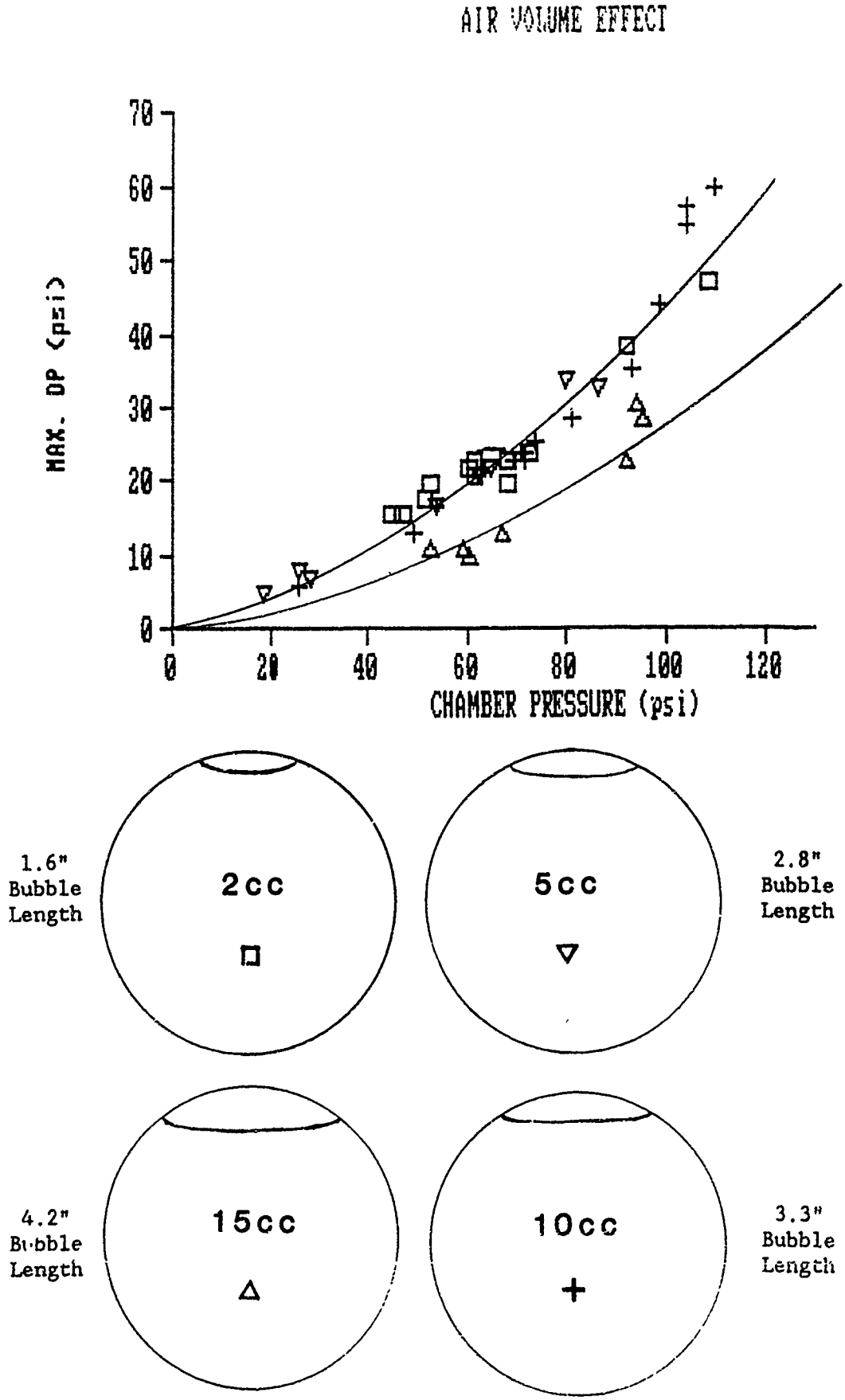

Figure 4-65. Air bubble volume effect.

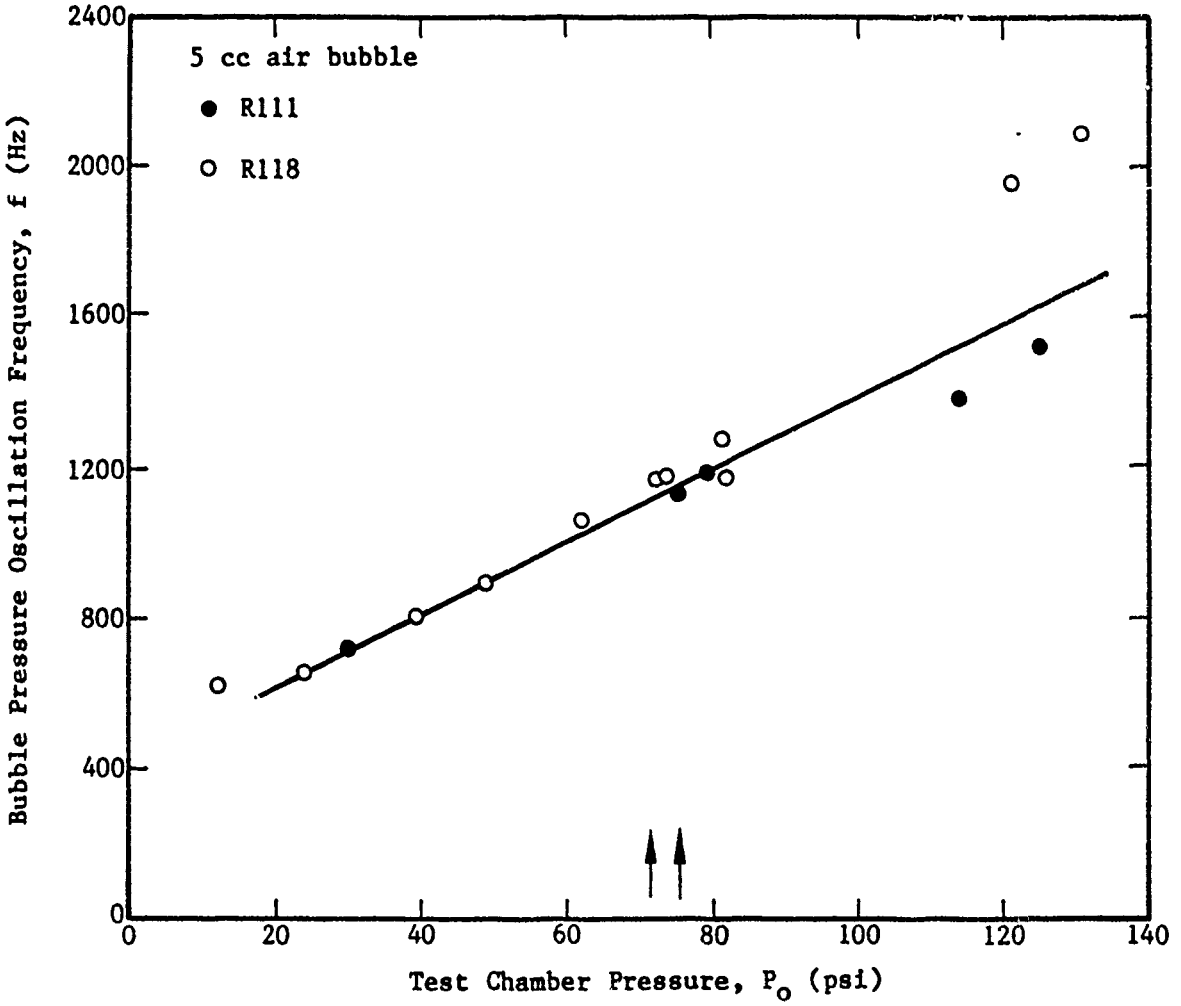

Figure 4-66. Bubble pressure oscillation frequency versus test chamber pressure for a 5 cc air bubble.

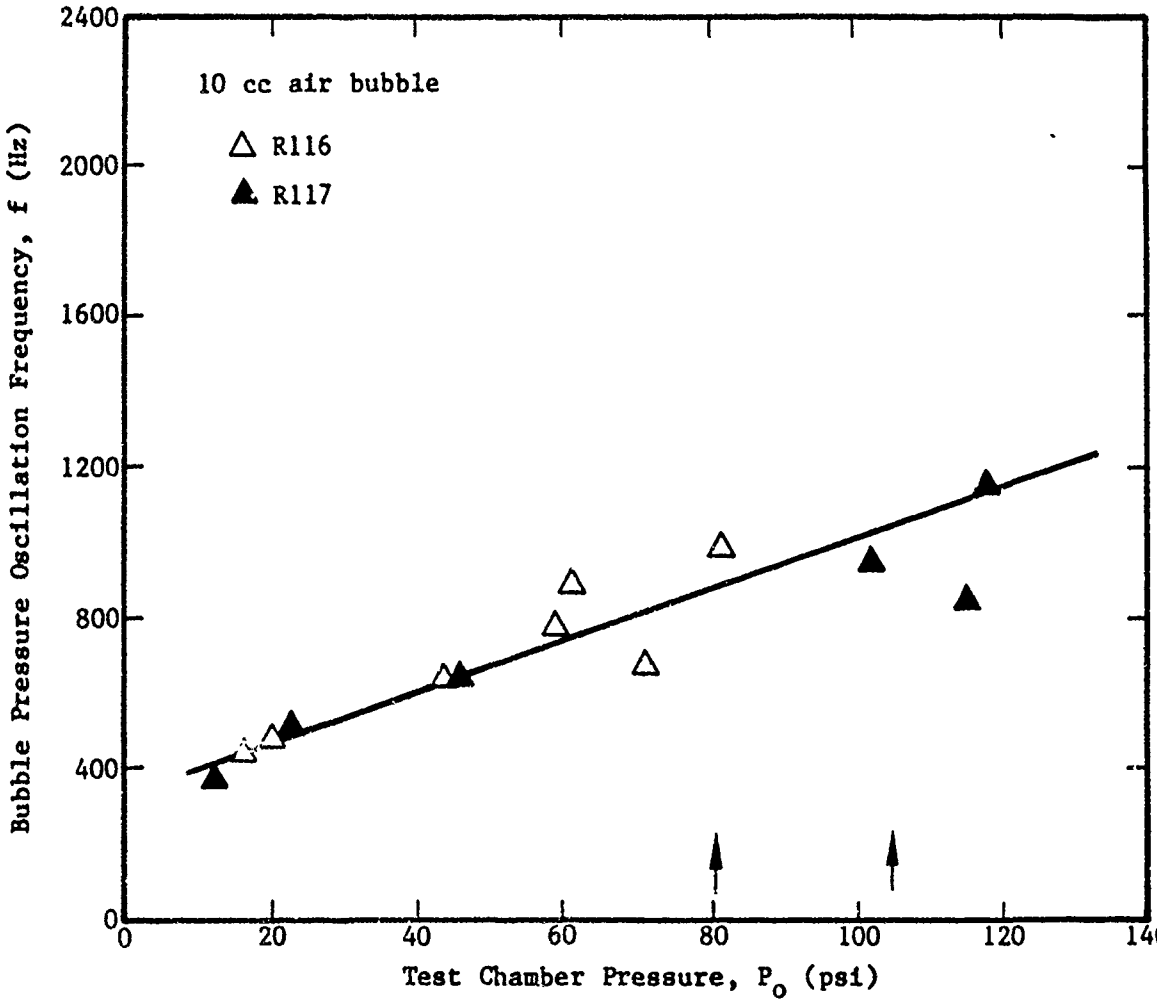

Figure 4-67. Bubble pressure oscillation frequency versus test chamber pressure for a 10 cc air bubble.

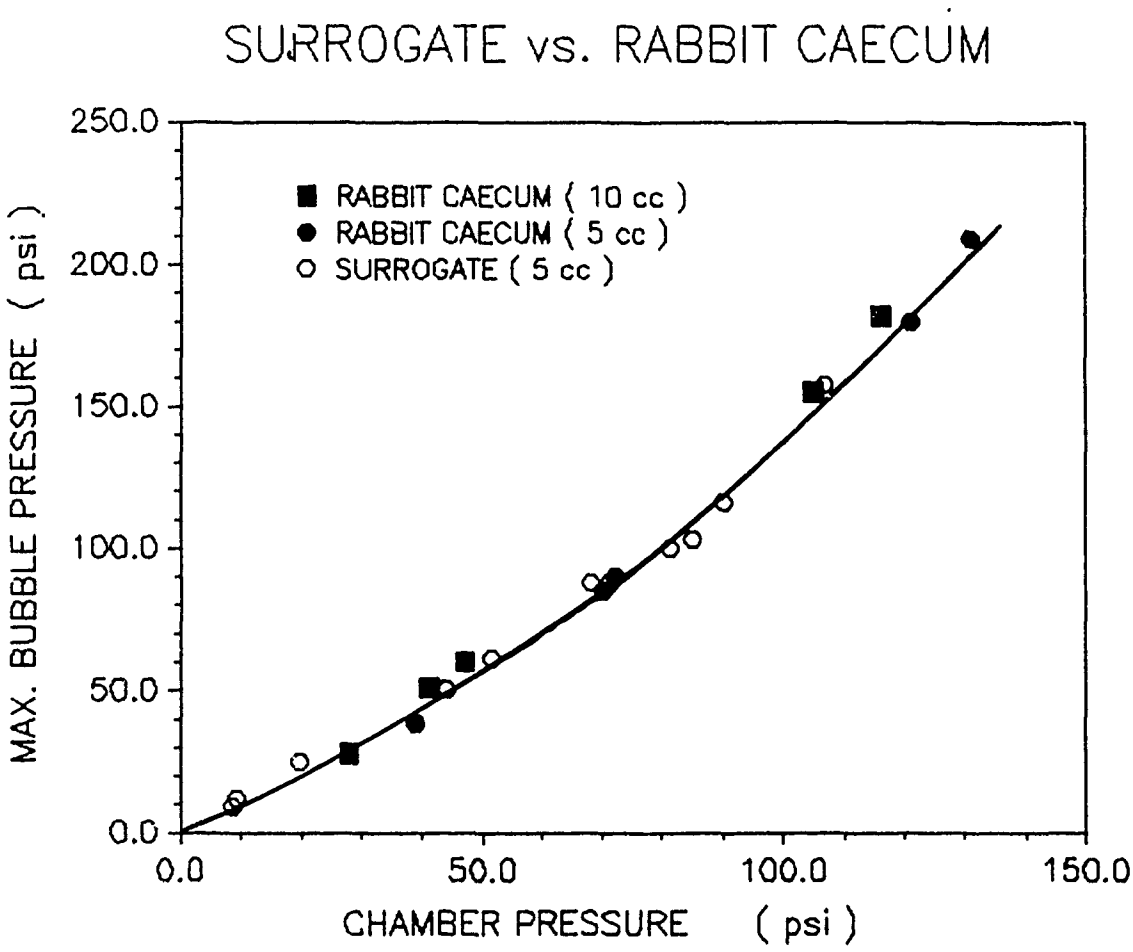

Figure 4-68. 5 cc and 10 cc volume effect in vitro data compared to surrogate data reference.

Figures 4-69 and 4-70 illustrate this point for 5 cc bubble volumes exposed to a chamber pressure of 48.3 psi. Figure 4-69 shows the two different surrogate setups for the hemispherical and double curvature (long and thin) 5 cc bubbles. The boundary conditions for both of the setups was similar with a bubble-to-chamber lid distance of 1.90". Figure 4-70 is a comparison of pressure data from inside the bubbles. The hemispherical bubble shows larger pressure differential (DP) from the chamber pressure signals than the long thin bubble. Since the bubble collapse follows the adiabatic gas law:

$$PV = P'V' \tag{3}$$

where P and V are the initial bubble pressure and volume, and P′ and V′ are the internal pressure and volume within the membrane during oscillations. The internal pressure, P′, is controlled by the net inertia of the fluid mass and membrane wall moving in and out with the bubble oscillation. Then the larger the differential pressure magnitude ($P - P'$), the greater the volume (V′) change during oscillation. The greater the volume change the larger the wall displacement and the greater the membrane wall stress. Bubbles with similar volumes but with different contact surface areas (radius of curvature) would experience different tissue stress levels. The smaller the surface contact area (smaller radius) the greater the tissue strain for a given volume change. Therefore, bubble shape which is defined by surface contact area and determined by membrane radius of curvature, is a major factor in controlling tissue stress during blast.

4.3.5 Neighboring Bodies Effect

Viscous neighboring bodies may affect the bubble internal pressure by restricting the external flow field. Preliminary data shows that the observed effect on bubble pressure for high and low viscosity neighboring bodies is negligible.

The experiments described in Section 4.2 have shown that the flow field near the collapsing bubble is coupled to the internal pressure signal shape. A restricted flow field may produce higher internal bubble pressure peaks. Current surrogate experiments use test samples surrounded by a flow field of free water. Since the in vivo condition involves a flow field of G.I. entrained fecal material of various viscosities, an experiment to model this effect was conducted.

The experiment was designed to model both the low viscosity conditions associated with the large intestine, and the high viscosity environment of the lower colon. The effects of these neighboring bodies was tested using a 5 cc bubble setup. The results were compared with the reference setup for a single unit surrounded by water shown in Figure 4-63.

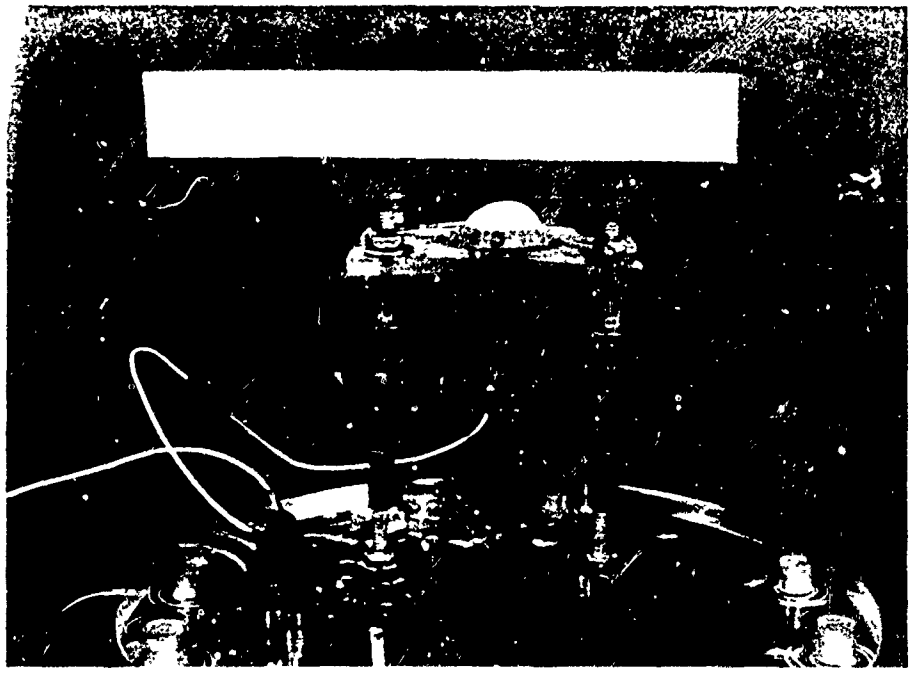

(a) Hemispherical bubble

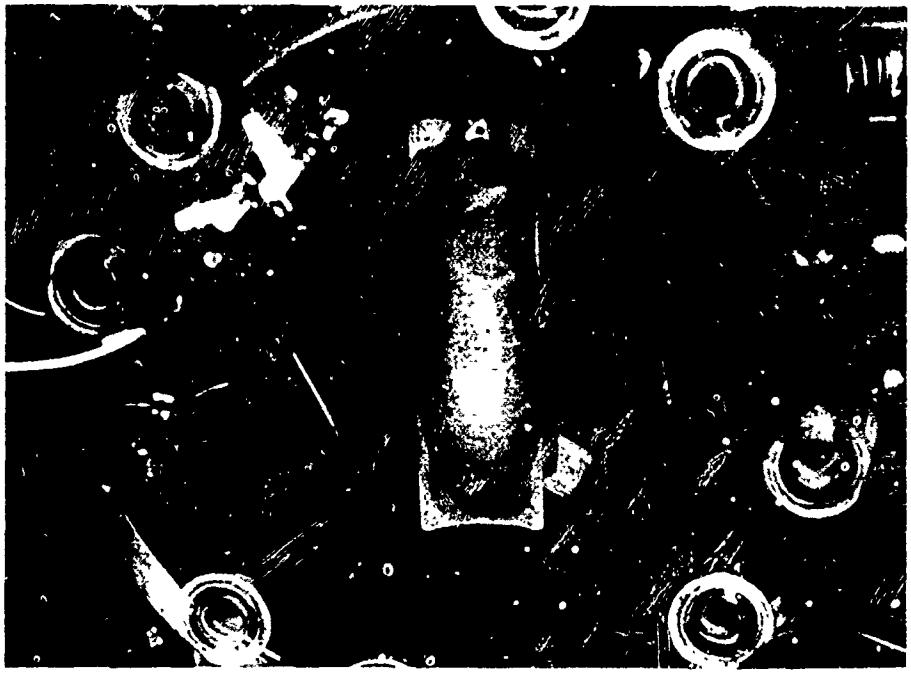

(b) Double curvature bubble

Figure 4-69. 5 cc bubble surrogate test setups.

5 cc Hemispherical Bubble

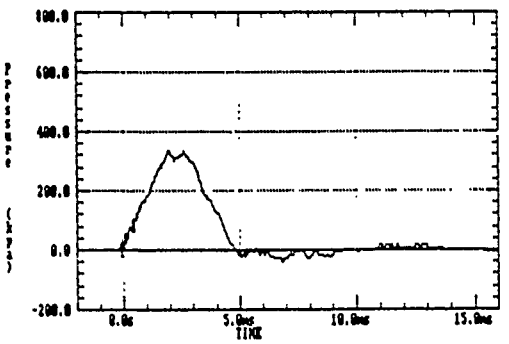

$P_{CHAMBER}$ = 48.3 psi

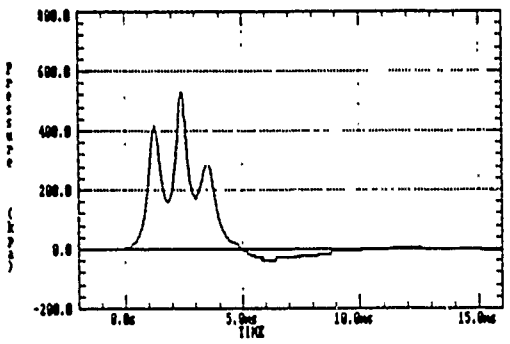

P_{BUBBLE} = 76.8 psi

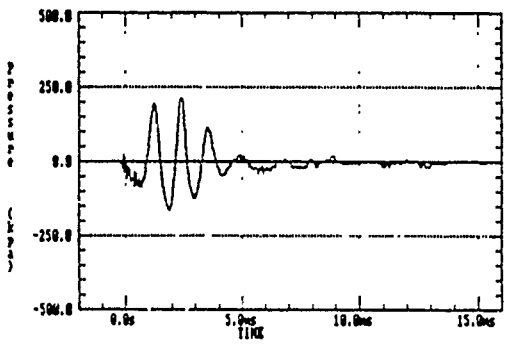

$P_{BUBBLE} - P_{CHAMBER}$ = DP
(Peak = 30.5 psi)

5 cc Double Curvature Bubble

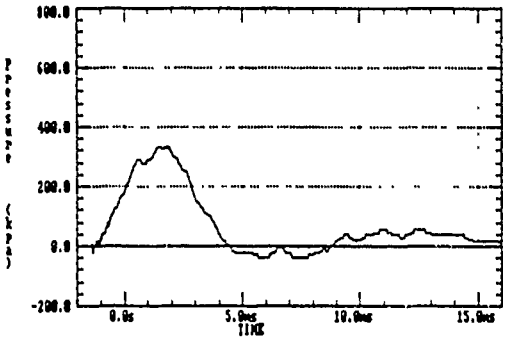

$P_{CHAMBER}$ = 48.3 psi

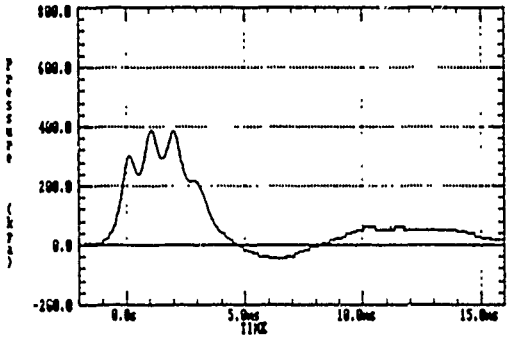

P_{BUBBLE} = 56.5 psi

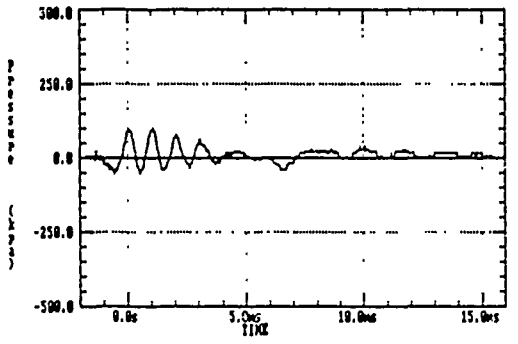

$P_{BUBBLE} - P_{CHAMBER}$ = DP
(Peak = 15.3 psi)

Figure 4-70. Comparison of pressure signals for 5 cc bubble volumes of different shapes.

Figures 4-71 and 4-72 show the setup and differential, DP, (bubble-chamber) data from the water-filled-bodies test in which eight surrogates were filled with water and placed in close proximity around the test unit. A comparison of typical single surrogate and neighboring body pressure signals is shown in Figures 4-73 and 4-74. The volume of the water in the surrounding surrogates amounted to approximately 50% of the total test chamber fluid. The nearest water-filled body was within 1/4 in. of the test bubble. For water-filled neighboring bodies, no effect is noted on internal bubble pressure magnitude or oscillation frequencies.

To test the effect of high viscosity, peanut butter was chosen to replace the fill water in the surrounding surrogates. Because of its high viscosity and nonhydroscopic properties, peanut butter more closely models the flow field in the lower colon section. Figures 4-75 and 4-76 illustrate the setup and test results. Again, the viscous surrogates constitute approximately 50% of the total chamber volume.

A comparison of the three data curves is shown in Figure 4-77, while a comparison of typical chamber pressure, internal bubble and differential (bubble-chamber) signals is given in Figure 4-78. Even though the high viscosity bodies are more rigid there appears little difference from that of water-filled surrogates in terms of bubble pressure, shape, and data curves. Within the limits of these tests, the effect of neighboring bodies appears negligible but does suggest that high viscosity may have some effect on the bubble pressures as stated in section 4.2.2. Because of this negligible effect, this experiment further validates the use of single test unit setups for G.I. surrogate model studies.

4.3.6 Internal Fill Viscosity

Membrane internal fill viscosity appears to be a major component of blast induced membrane stress. High speed movies of low and high viscosity internal fill surrogate tests showed that the higher viscosity fill affects the flow field by restricting internal fluid motion. This allows the external flow field to produce greater membrane displacements during bubble oscillations resulting in increased membrane wall strain.

The setup shown in Figure 4-79 is a single surrogate lambskin unit with viscous peanut butter as the internal fill medium. Peanut butter was chosen because of its high viscosity and low hydroscopic qualities. The peanut butter was heated in a microwave oven until a fluid state was reached. The fill material was then poured into the lambskin surrogate, a 5 cc bubble was injected and the entire setup was cooled in a water bath to room temperature. High speed movies and bubble internal pressure measurements were taken during blast exposure.

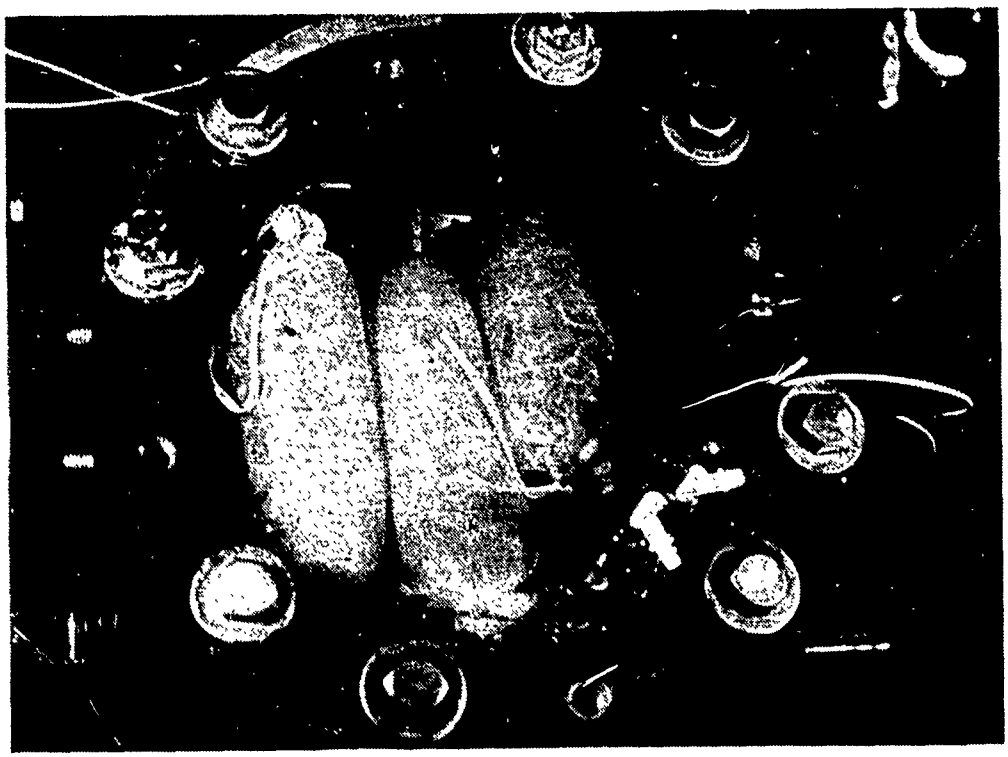

(a)

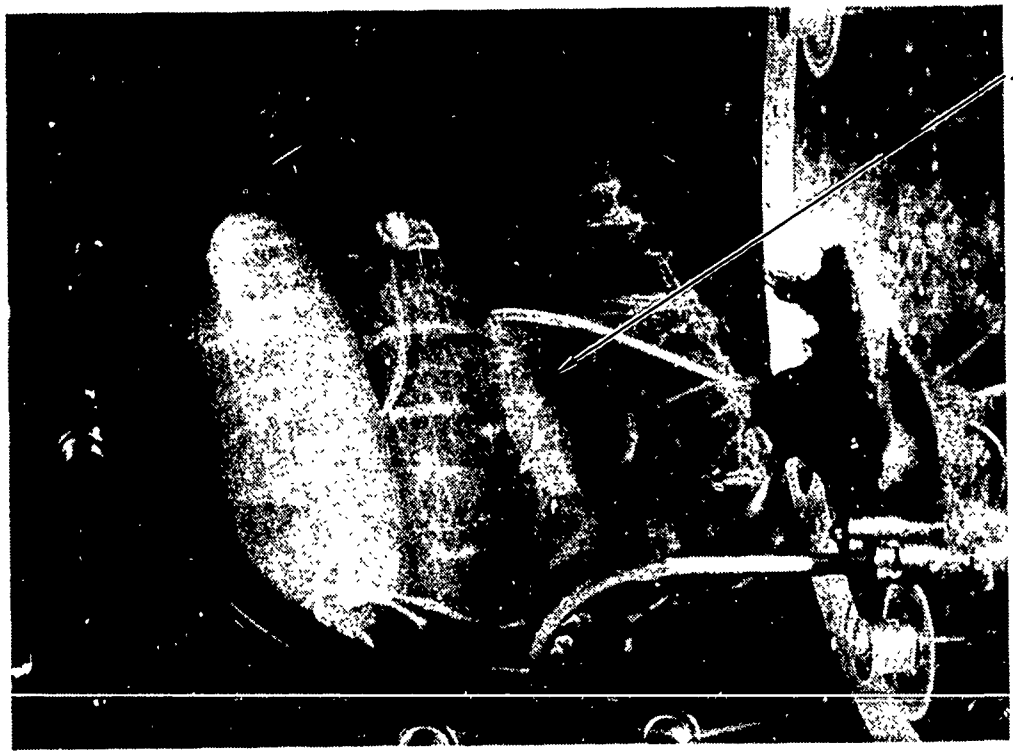

(b) One lambskin removed to show test unit

Figure 4-71. 5 cc bubble surrogate surrounded by eight water-filled lambskins.

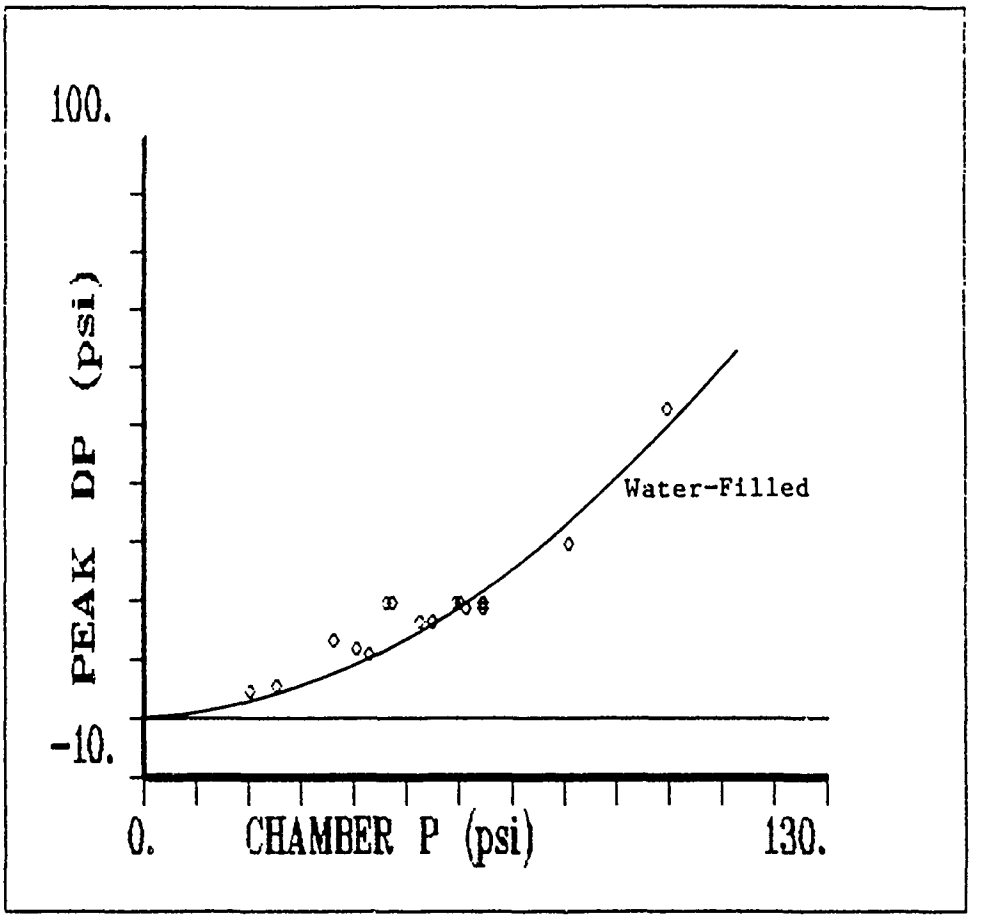

Figure 4-72. Data from a 5 cc bubble in a surrogate surrounded by eight water-filled lambskins.

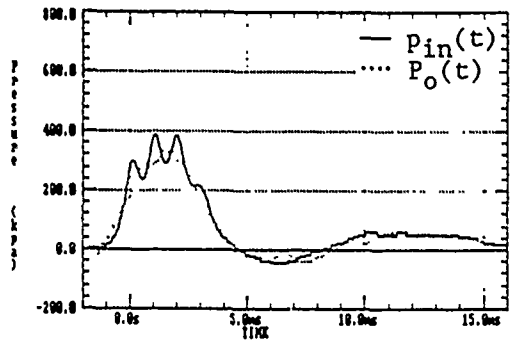

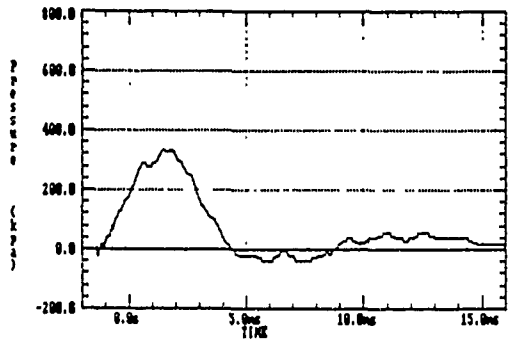

Chamber pressure = 48.3 psi

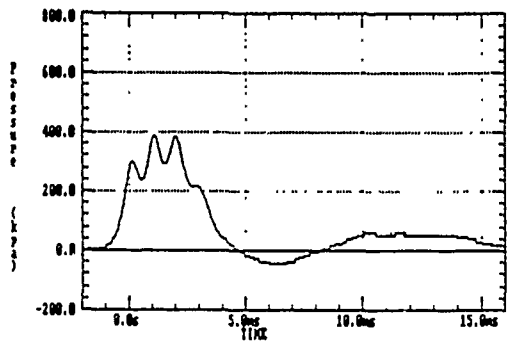

Bubble pressure = 56.5 psi

5 cc bubble test section
water-filled chamber.
Chamber pressure = 48.3 psi

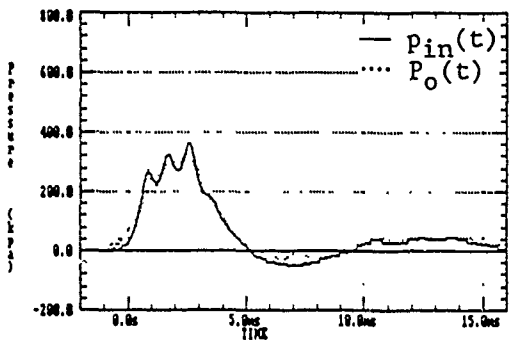

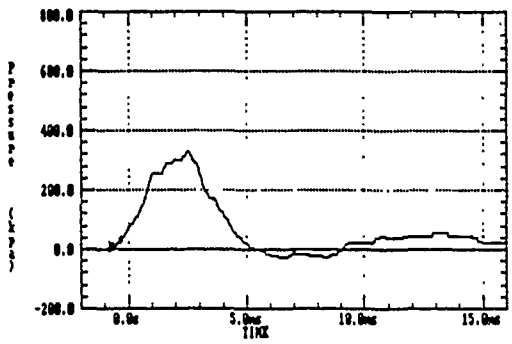

Chamber pressure = 47.2 psi

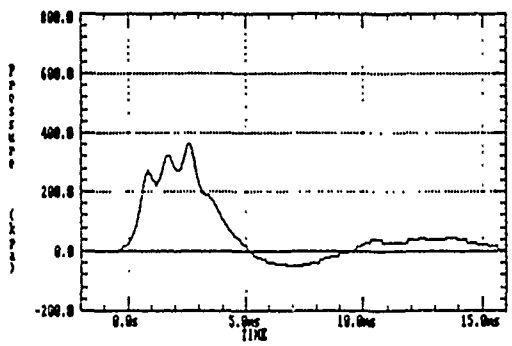

Bubble pressure = 52.1 psi

5 cc bubble setup in chamber
with 7 water-filled lambskins
surrounding test section.
Chamber pressure = 47.2 psi

Figure 4-73. Comparison of typical reference surrogate and neighboring bodies data at 48 psi chamber pressure.

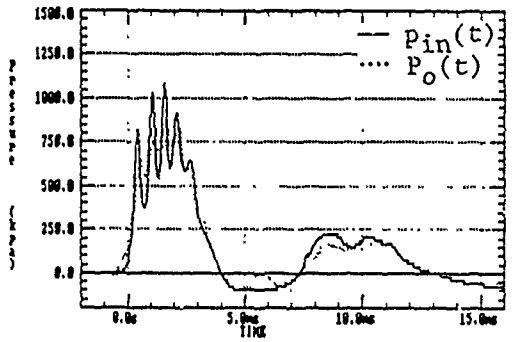

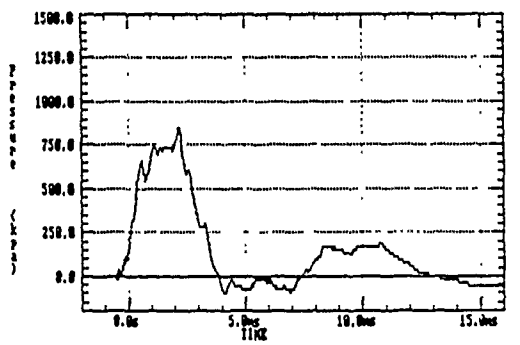

Chamber pressure = 106.9 psi

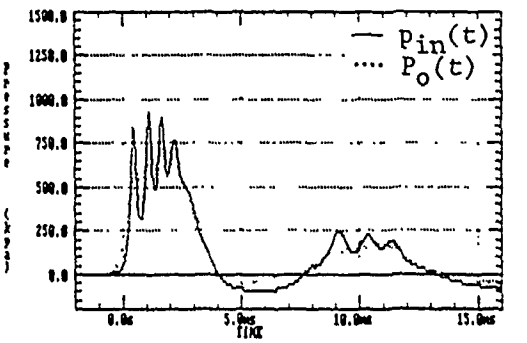

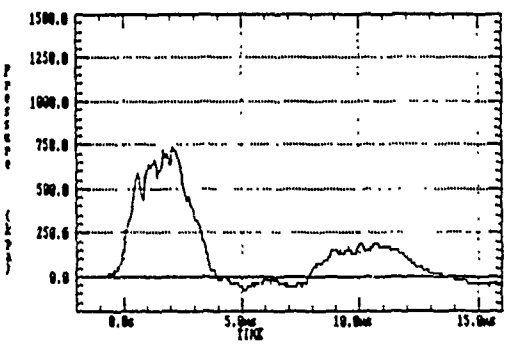

Chamber pressure = 106.9 psi

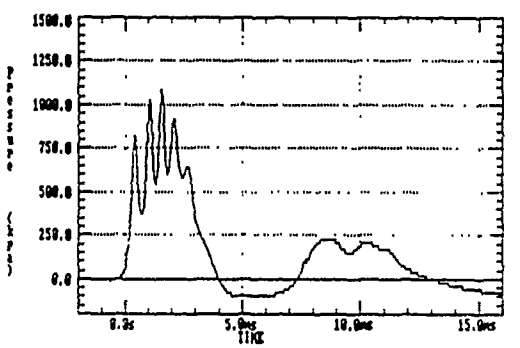

Bubble pressure = 157.5 psi

5 cc bubble test section water-filled chamber (movie). Chamber pressure = 106.9 psi

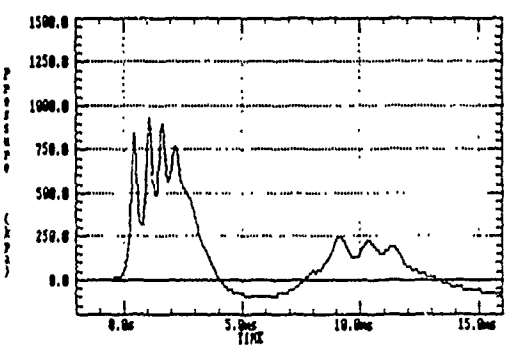

Bubble pressure = 135.8 psi

5 cc bubble setup in chamber with 7 water-filled lambskins surrounding test section. Chamber pressure = 106.9 psi

Figure 4-74. Comparison of typical reference surrogate and neighboring bodies data at 107 psi chamber pressure.

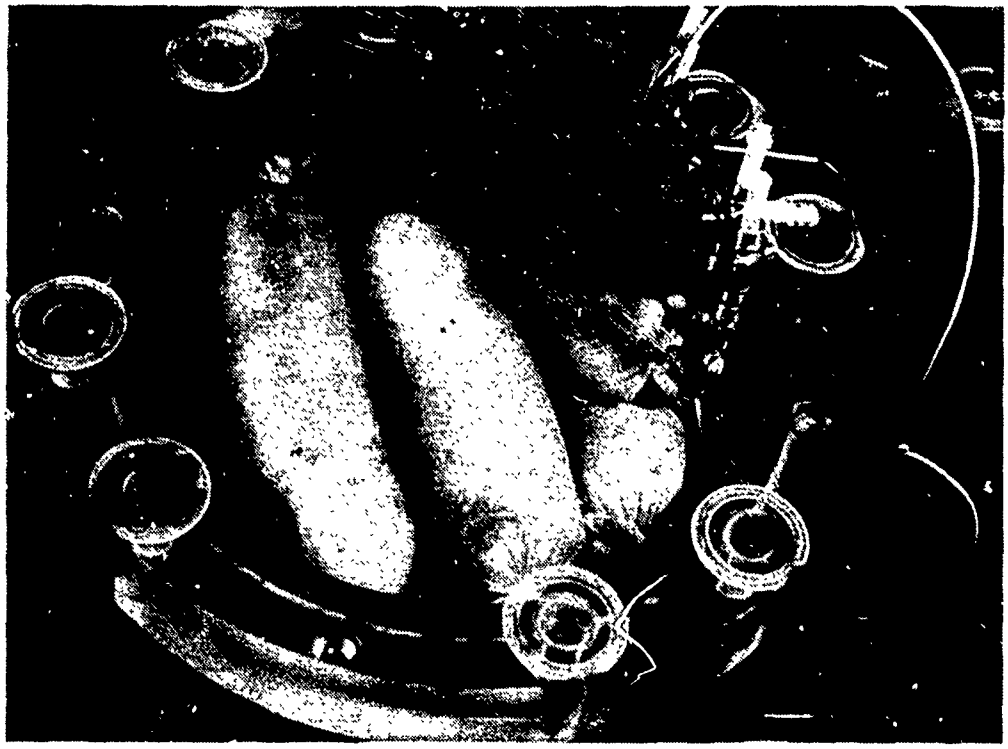

(a)

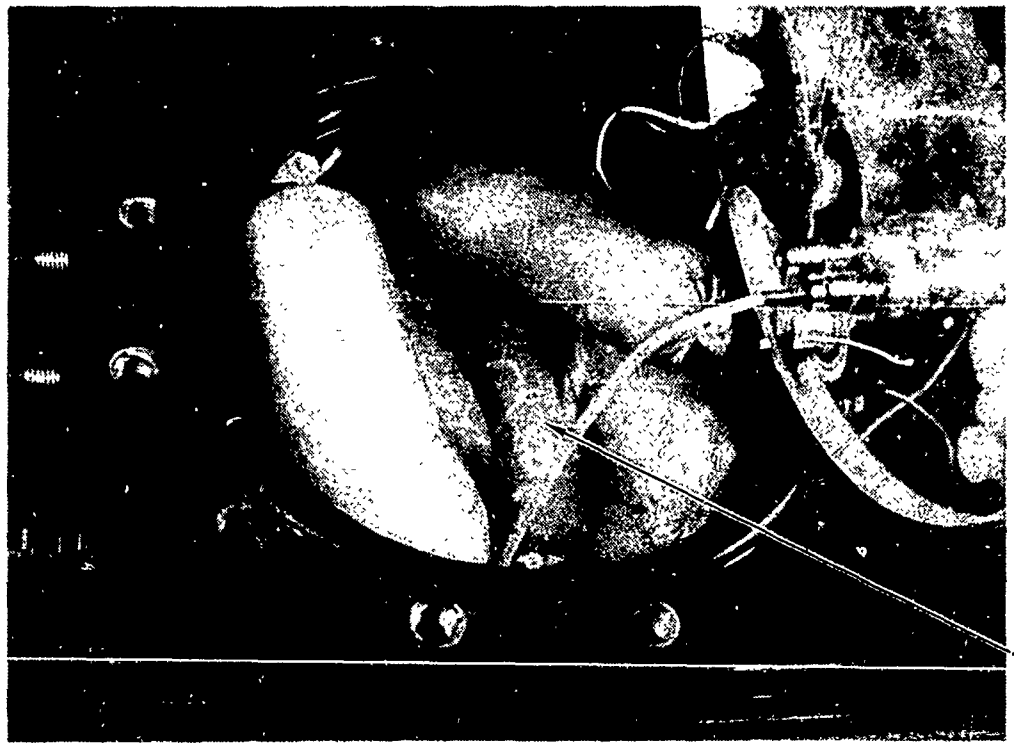

(b) One lambskin removed to show test unit

Figure 4-75. 5 cc bubble surrogate surrounded by eight viscous-filled lambskins.

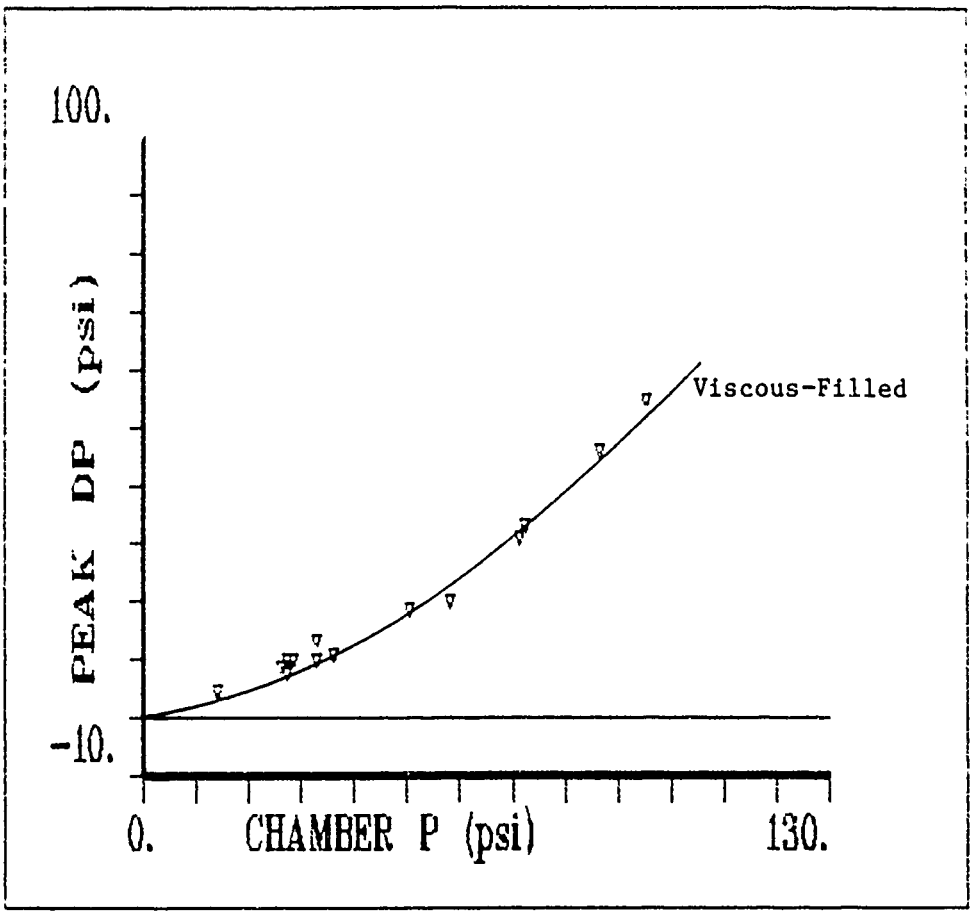

Figure 4-76. Data from a 5 cc bubble surrogate surrounded by eight viscous-filled lambskins.

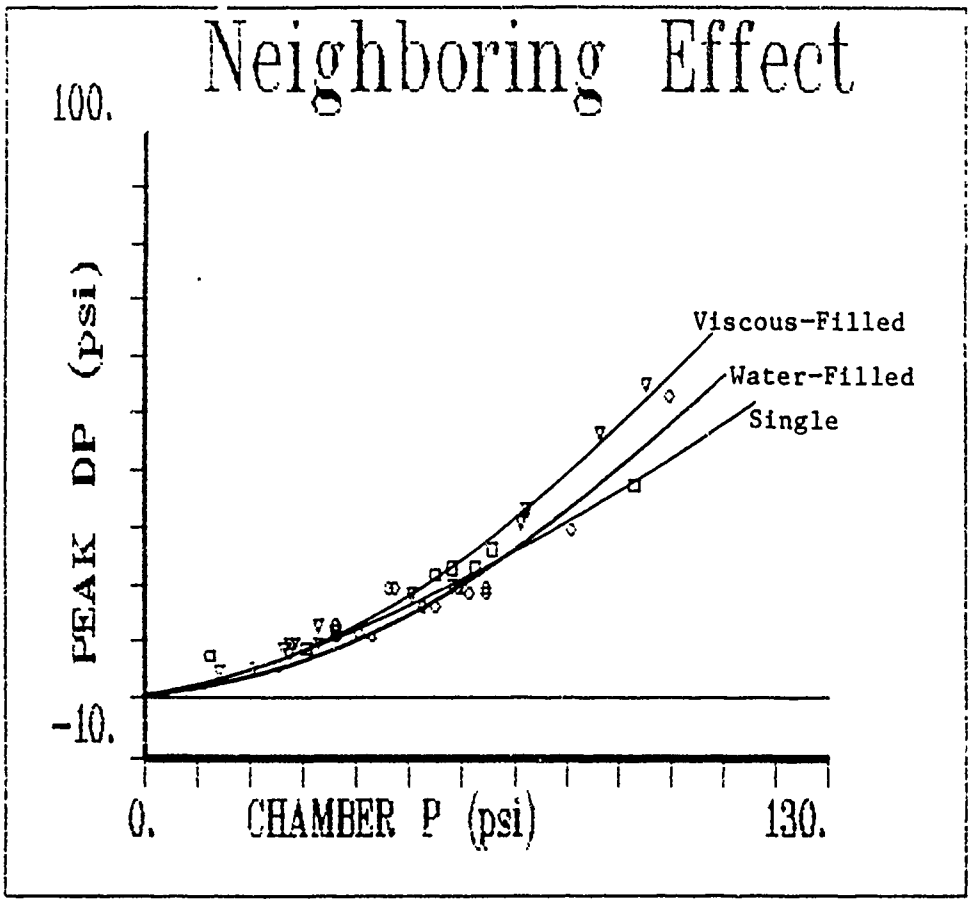

Figure 4-77. Comparison of neighboring effects data.

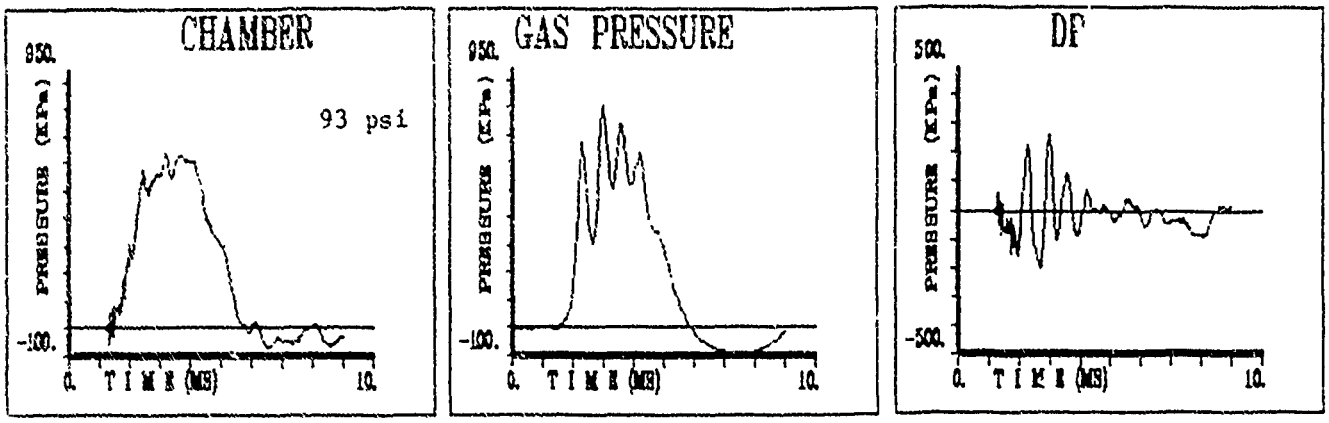

Reference

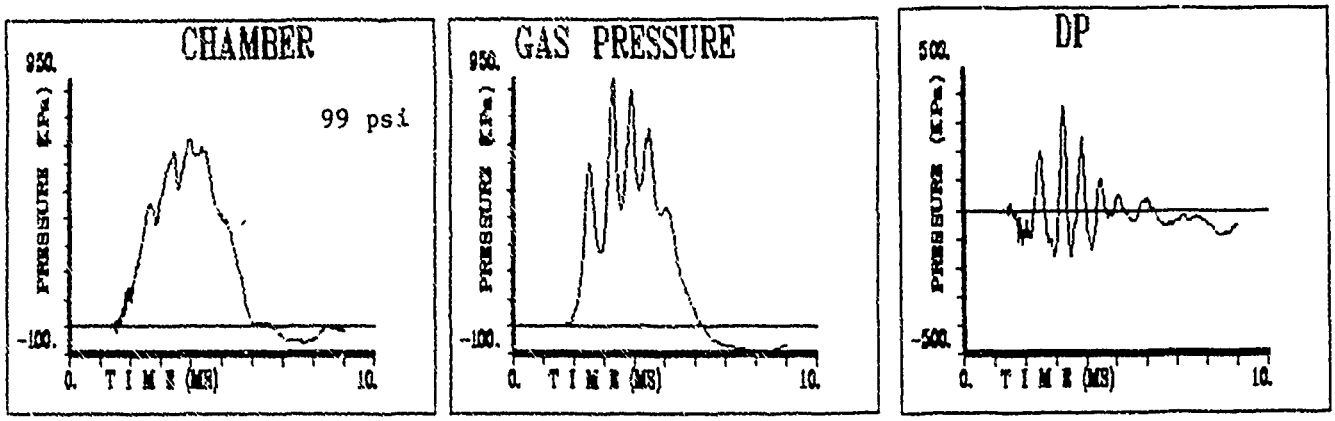

Water-Filled

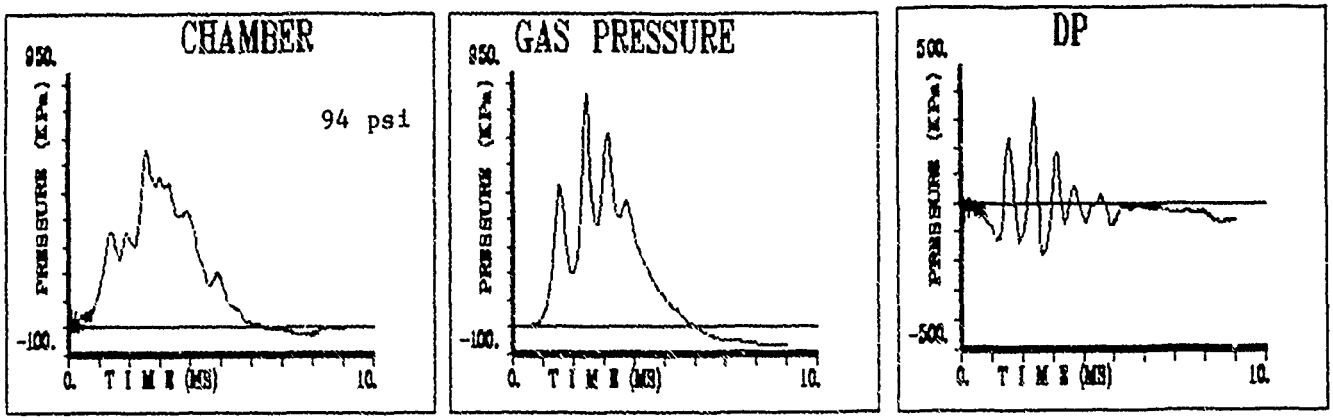

Viscous-Filled

Figure 4-78. Comparison of pressure signals.

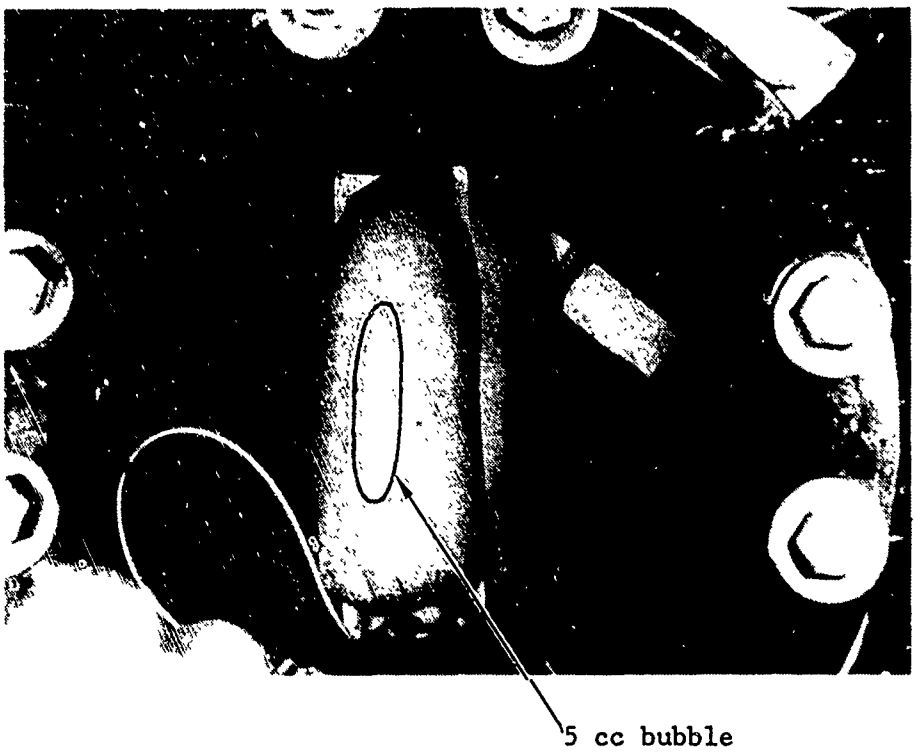

Figure 4-79. High-viscosity filled surrogate with 5 cc bubble.

Results of these tests were compared with movies and data from the water-filled surrogate test setup shown in Figure 4-63. Figures 4-80 through 4-82 illustrate this comparison.

Although the bubble internal pressure data shows no major effect on oscillation frequency and only a slight difference in magnitude attributable to internal fill viscosity, the high speed movies did show a considerable difference in apparent bubble collapse flow field. The water-filled surrogate (low viscosity) appeared to have both an internal and external flow field with the bubble shrinking and expanding in both axes as it oscillated under blast loading. The peanut butter-filled unit (high viscosity) appeared to have only an external flow field and the bubble length appeared to remain constant during oscillation. Only during the negative chamber pressure, overexpansion phase of the loading cycle did the viscous filled surrogate show a change in bubble slope to a round dome similar to the water-filled surrogate tests.

These observations indicate that high viscosity in the large intestine may experience a different flow field collapse than the low viscosity small intestine sections. This difference in flow field affects the membrane wall displacement and thus the membrane wall strain.

4.3.7 Internal Fill Pressure Effect

High membrane internal fill pressure has a slight damping effect on bubble oscillations. However, the in vivo state of the G.I. is normally in a limp condition, so that fill pressure is probably not a control parameter in practice.

An experiment was performed to determine if the internal fill condition (either limp or under pressure) has any effect on the internal bubble pressure signal.

The initial setup is shown in Figure 4-83. Two identical 5 cc PIB units, [7], were calibrated, balanced and then inserted into two separate surrogate test units. The test units were then tested for balanced response at 0 psi (full fill pressure). Additional tests in which either sample A or B was altered in internal fill pressure were then carried out. The results of these tests are illustrated in Figures 4-84 through 4-87 for internal fill pressures of 0 psi (full), 0.5 psi, 1.0 psi, and 2.0 psi, respectively. No apparent effect on maximum internal bubble pressure is seen until 2.0 psi internal fill pressure is reached. Even at this high internal pressure the effect is negligible as was also seen in section 4.1.

Since the in vivo condition of the G.I. tract usually ranges from a limp to a full condition, a partially filled surrogate was also tested as seen in Figure 4-88. This was accomplished by removing 75 cc of internal fill from sample A. Again, the data on Figure 4-89 shows no effect on maximum internal bubble pressure measurements.

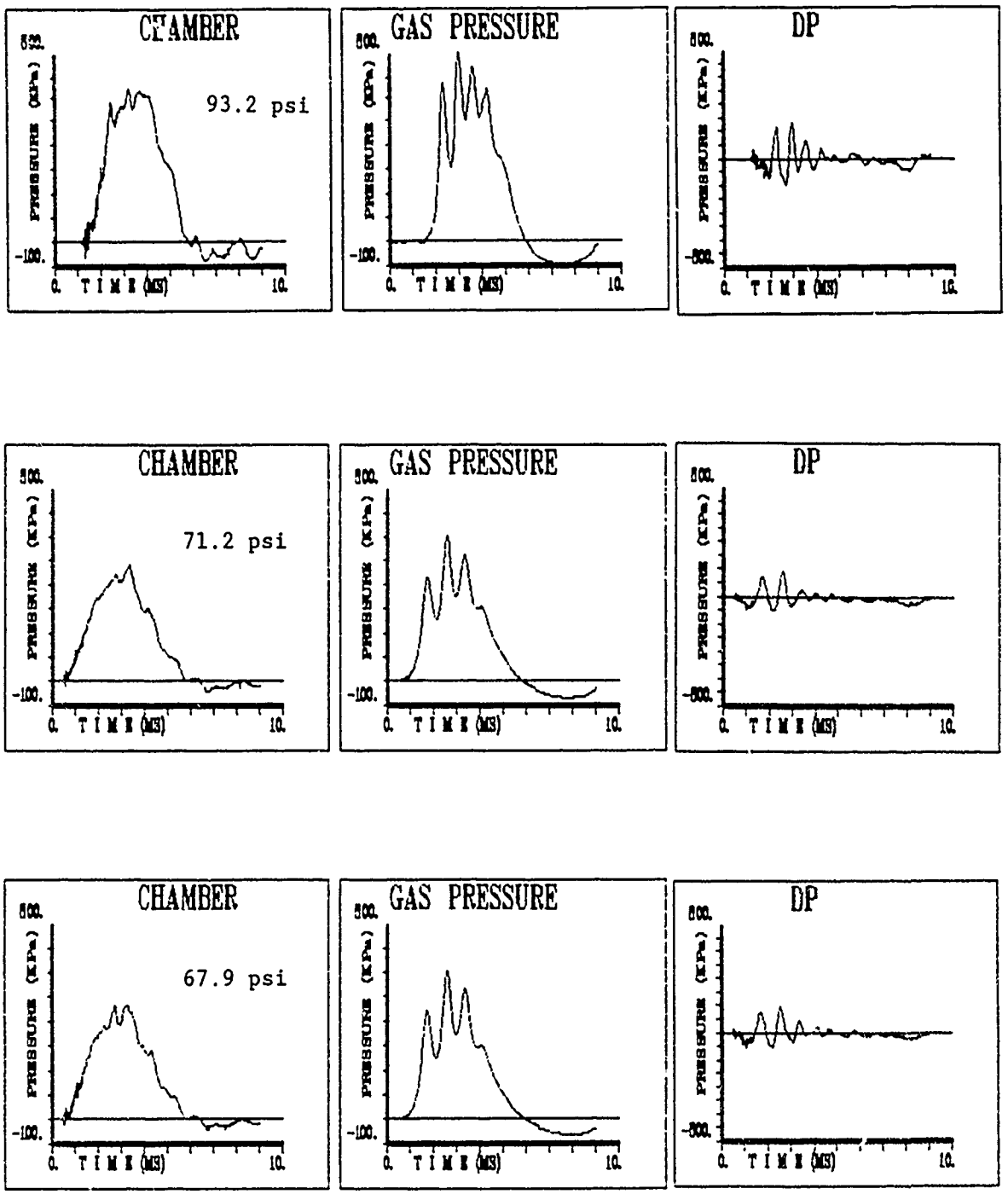

Figure 4-80. Water-filled surrogate with 5 cc bubble.

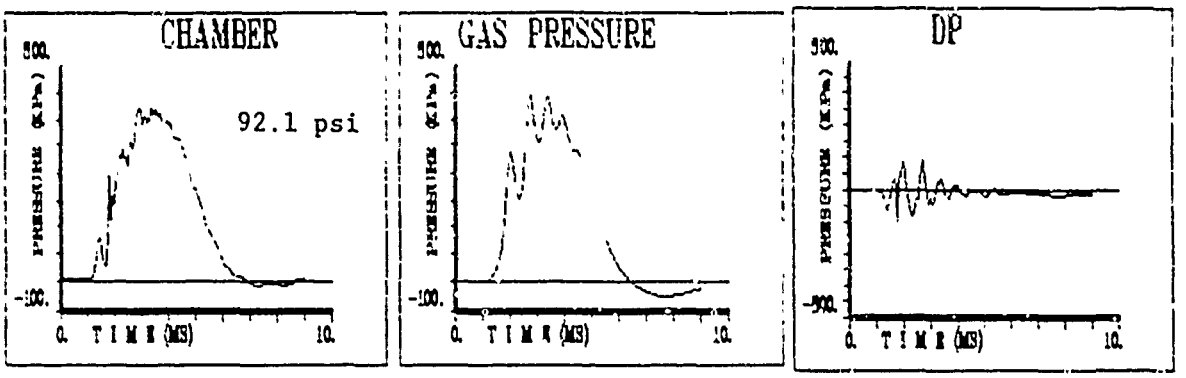

movie

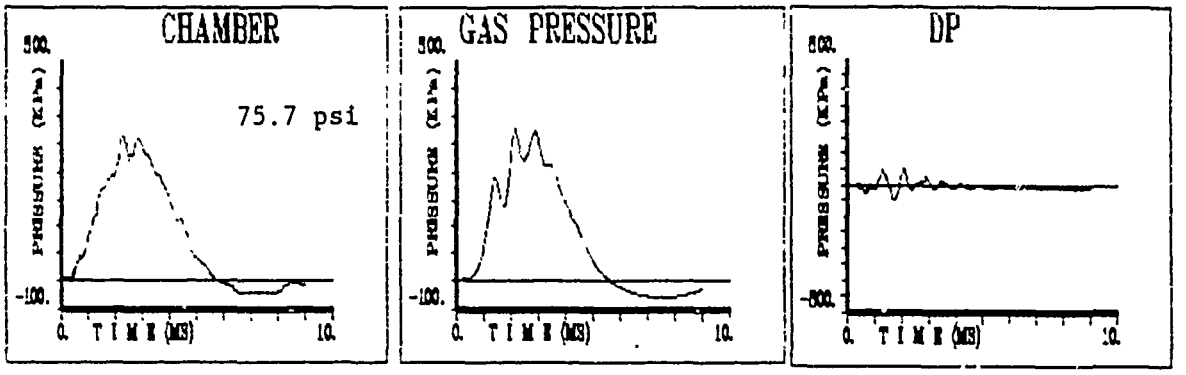

movie

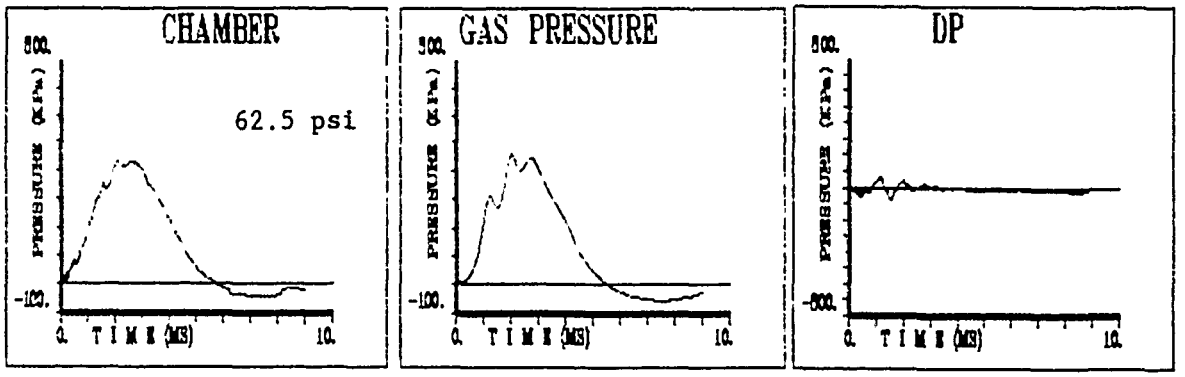

Figure 4-81. Viscous-filled surrogate with 5 cm bubble.

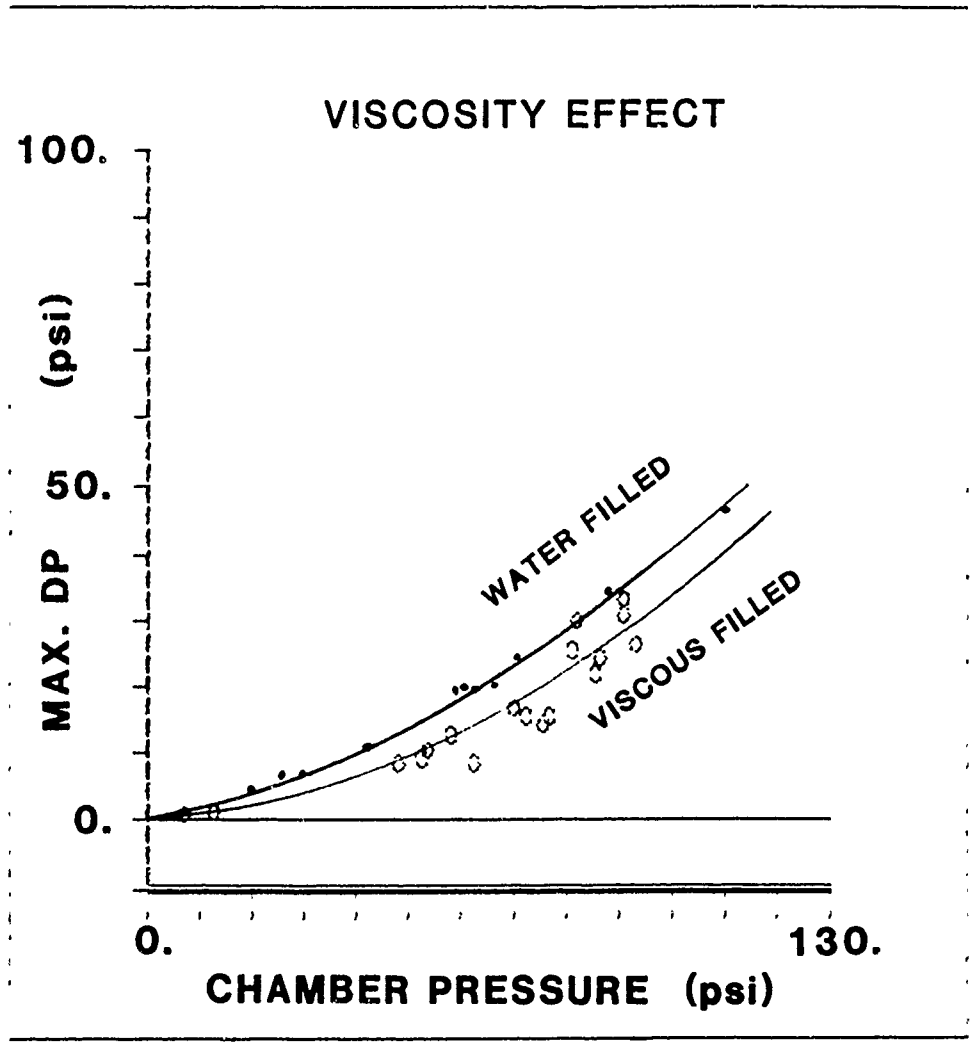

Figure 4-82. Comparison of water-filled and viscous-filled surrogates with 5 cc bubbles.

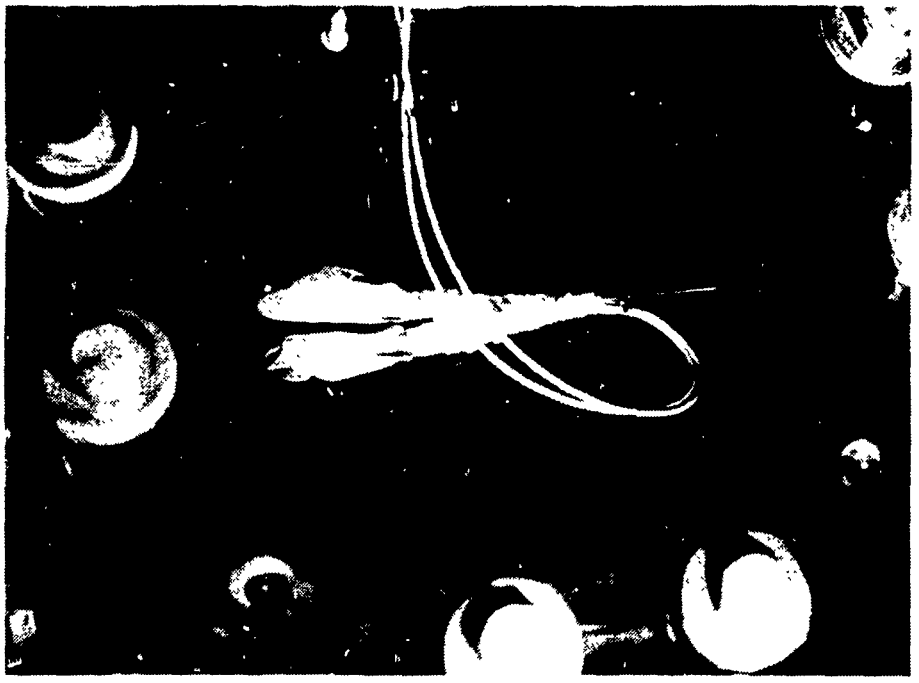

(a) PIB calibration

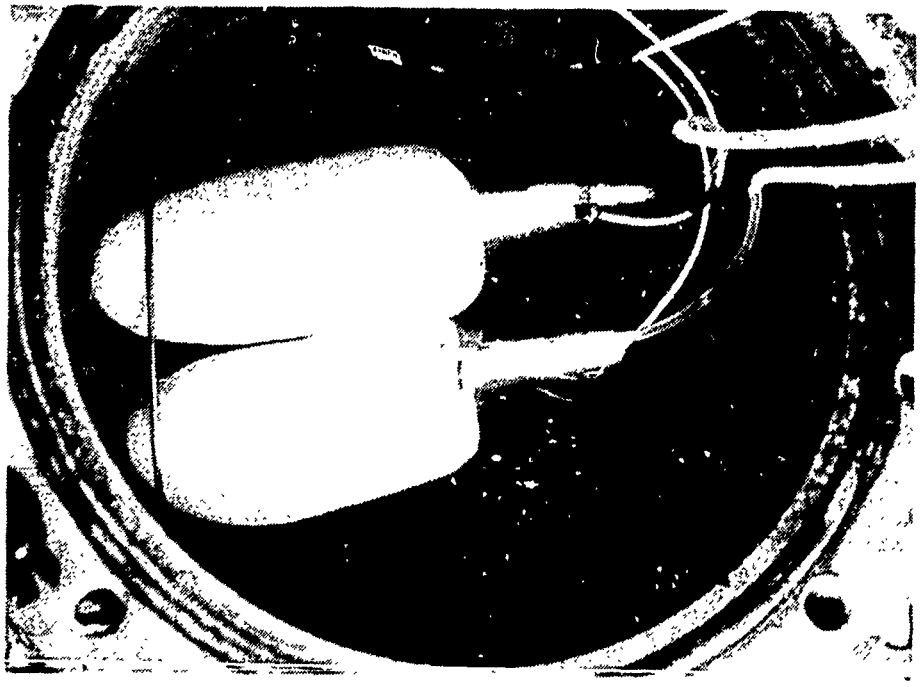

(b) Dual surrogate setup with PIBs

Figure 4-83. Setup for internal fill pressure test.

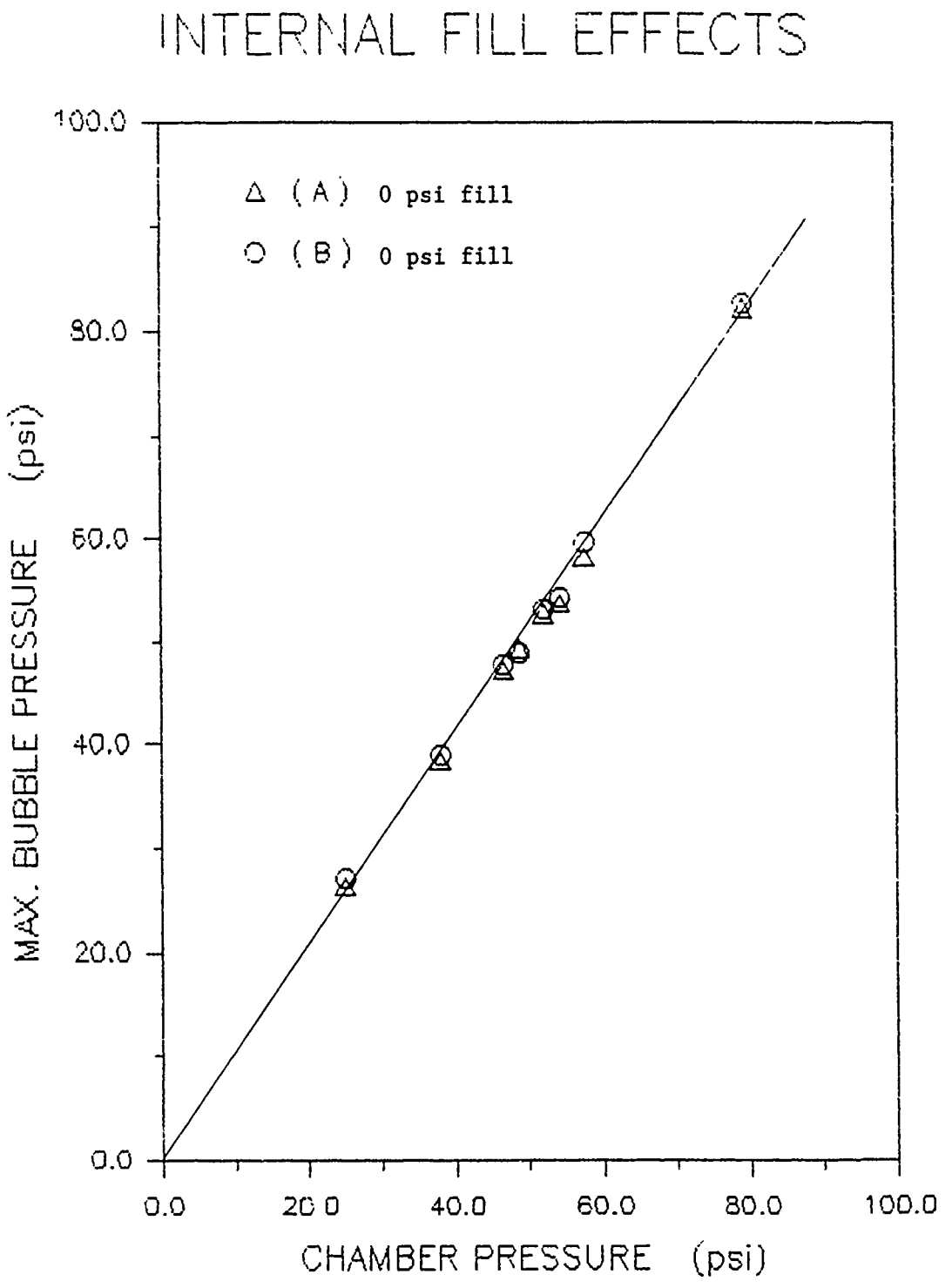

Figure 4-84. Zero internal fill pressure reference test.

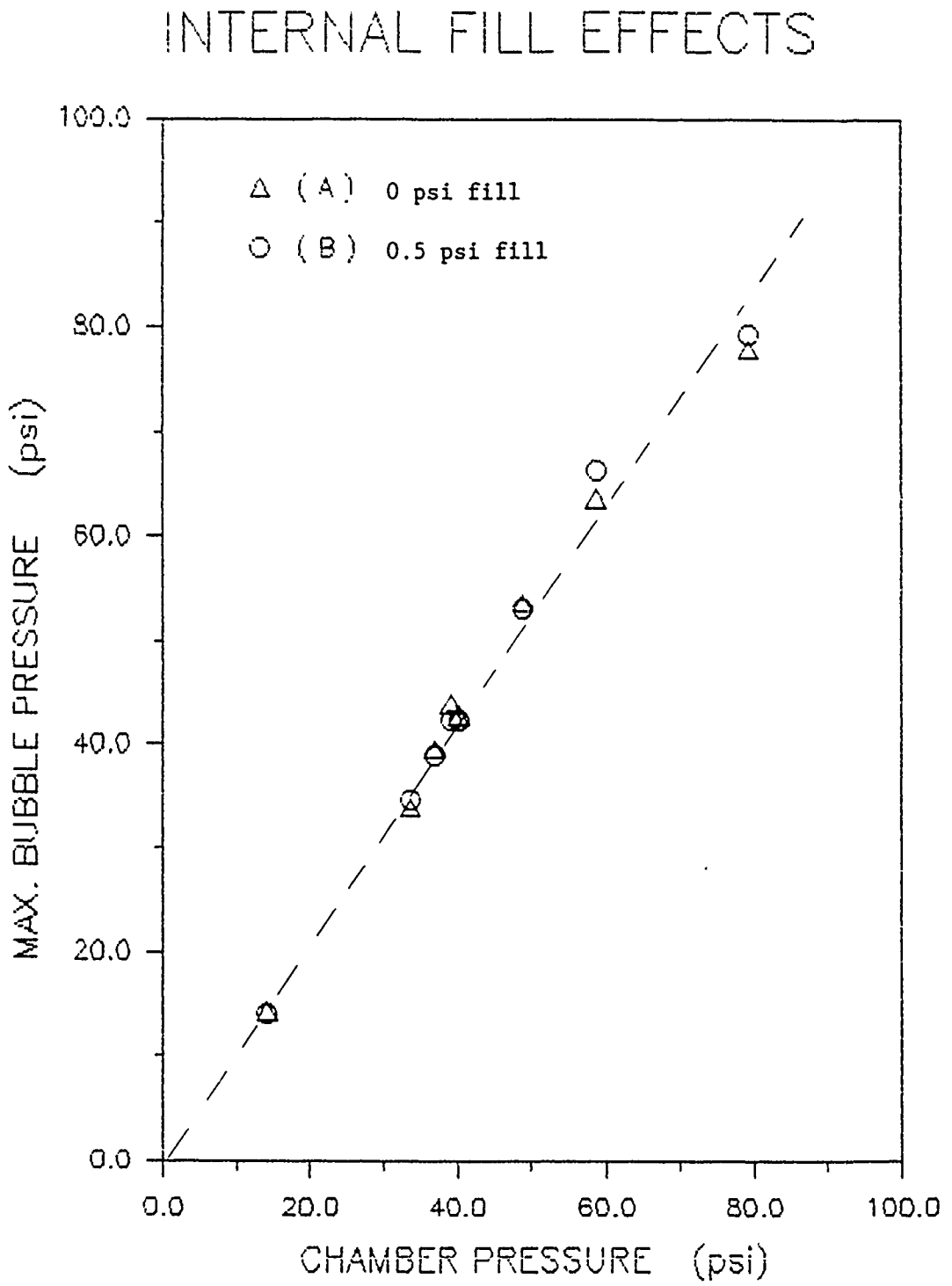

Figure 4-85. Effect of 0.5 psi internal fill pressure on maximum bubble pressure.

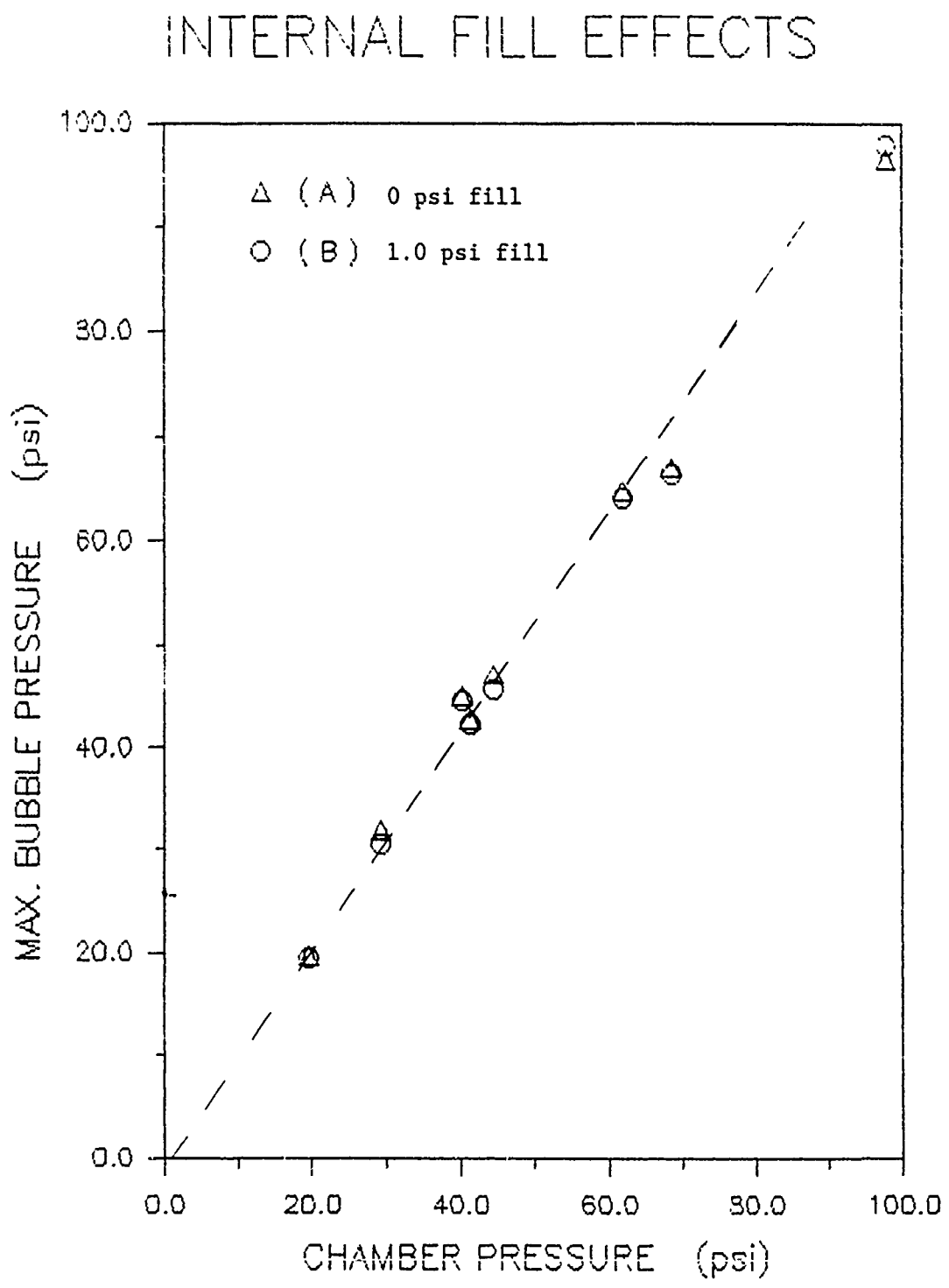

Figure 4-86. Effect of 1.0 psi internal fill pressure on maximum bubble pressure.

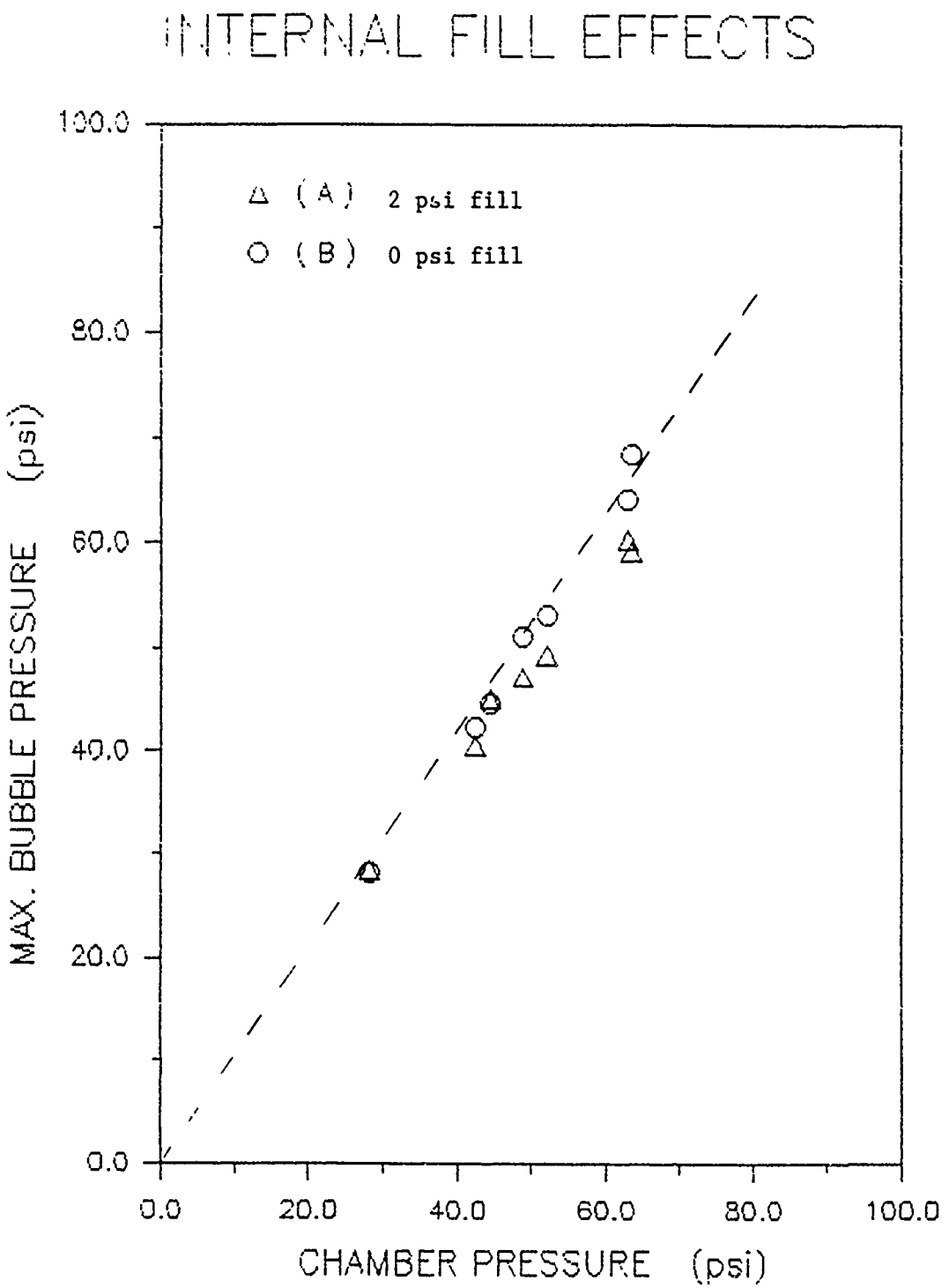

Figure 4-87. Effect of 2 psi internal fill pressure on maximum bubble pressure.

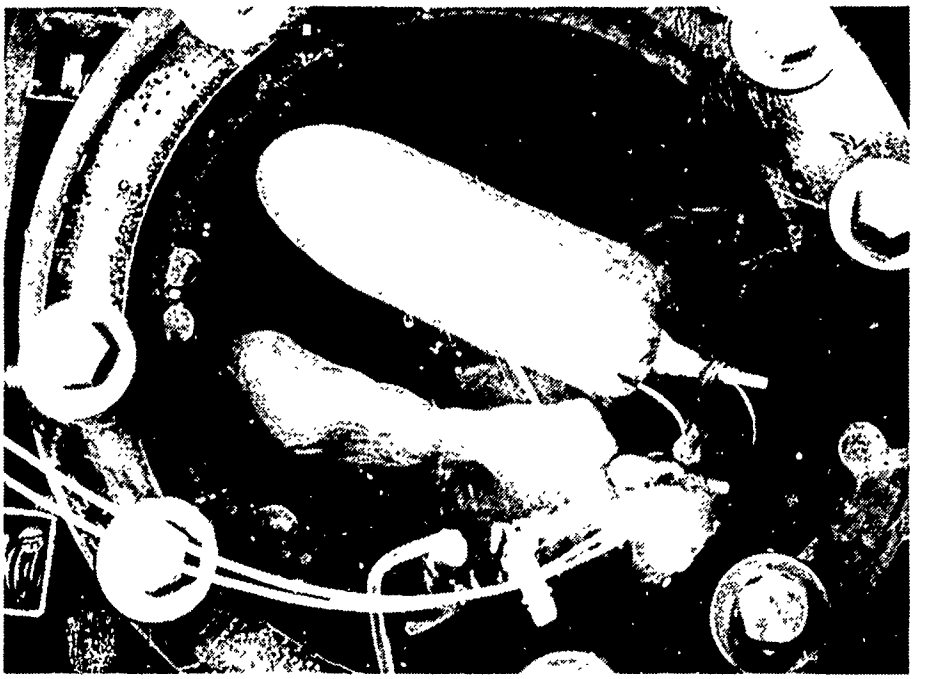

Figure 4-88. Limp fill (−75 cc) versus full fill (0 psi) test setup.

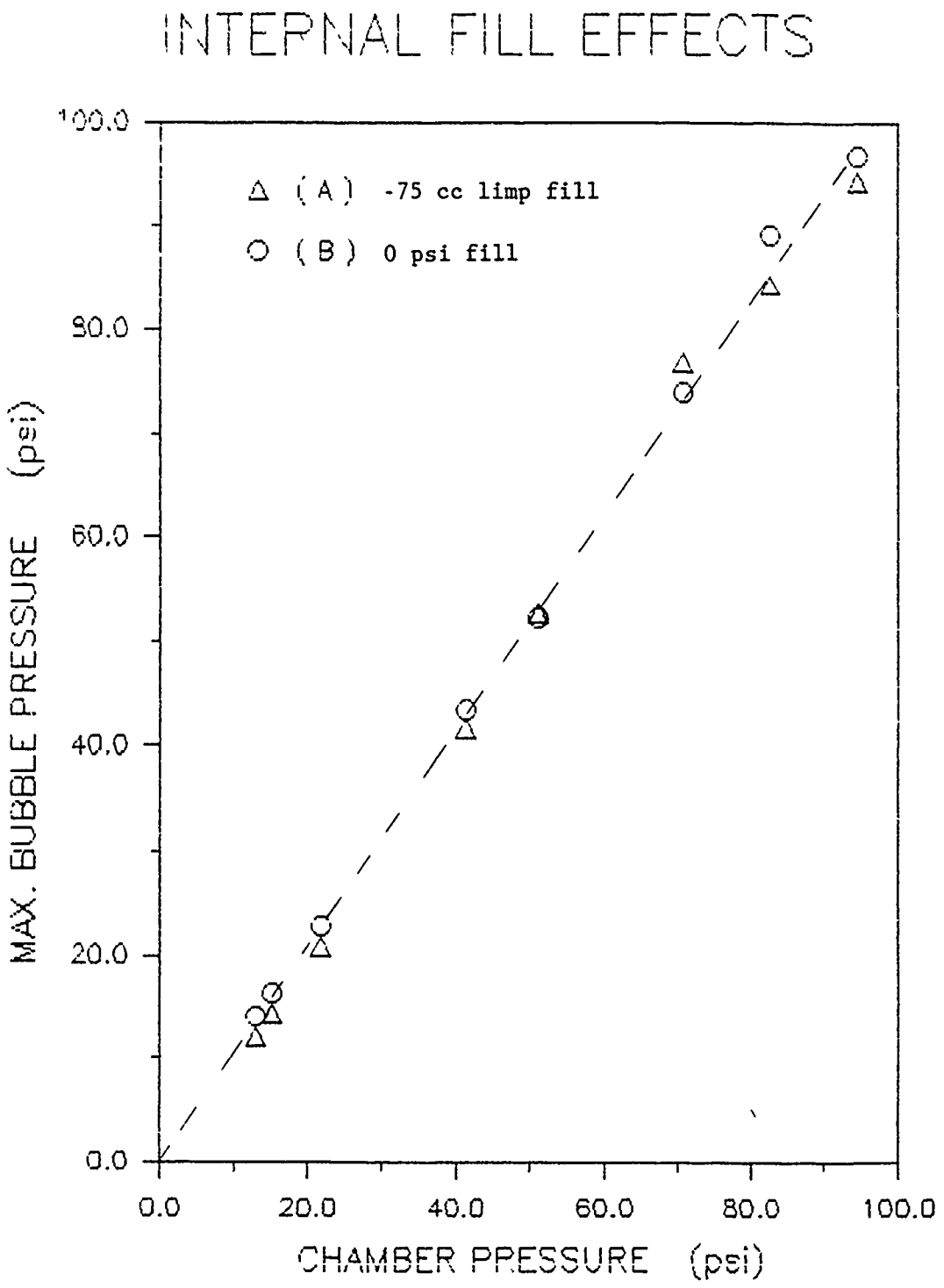

Figure 4-89. Effect of very limp fill on maximum bubble pressure.

Figure 4-90 shows that the bubble oscillation frequency is not appreciably affected by the different internal fill conditions.

Since an in vivo condition of positive fill pressure is rare, then internal fill pressure appears not to be a bubble pressure control parameter in practice. However, a limp or full condition may affect the level of tissue stress during blast loading and should therefore be tested as a factor in the small animal G.I. blast injury protocol.

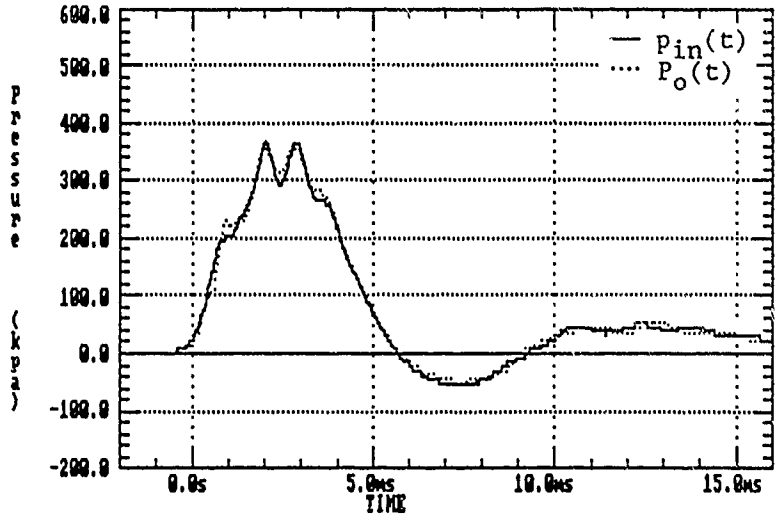

(a) PIN signals for limp fill (−75 cc) and zero fill pressure (full fill reference)

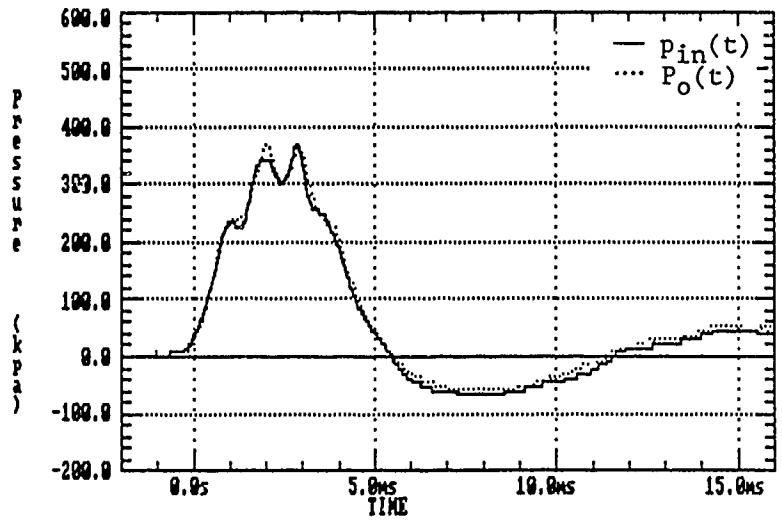

(b) PIN signals for 2 psi internal pressure fill and zero fill pressure (full fill reference)

Figure 4-90. Comparison of bubble internal pressure signals (PIN) for limp fill (−75 cc) and 2 psi internal fill pressure at chamber pressure of 53 psi.

5. CONCLUSIONS

A surrogate model to study blast dynamics of the gastrointestinal tract was developed, tested and correlated with analytical predictions. Results of each area of investigation are outlined in the Executive Summary.

REFERENCES

1. Yu, J. H.-Y. and E. J. Vasel, "Autologous Perfusion of an Isolated Rabbit Gastrointestinal Tract," JAYCOR Technical Report, August 1989.

2. Vasel, E. J., J. H.-Y. Yu, J. H. Stuhmiller, and K. T. Dodd, "Design and Field Test of a Blast Overpressure Test Module," JAYCOR Technical Report, August 1989.

3. Yu, J. H.-Y. and E. J. Vasel, "Rupture Strength of the Rabbit Large Intestine," JAYCOR Technical Report, August 1989.

4. Yu, Y. H.-Y. and E. J. Vasel, "Experimental Study of the Correlation Between Gastro-Intestinal Injury and Blast Loading," Final Report for Contract DAMD17-83-C-3221, U. S. Army Medical R&D Command, Fort Detrick, Frederick, Md., December 1984.

5. Vander Vorst, M. J., K. T. Dodd, J. H. Stuhmiller, and Y. Y. Phillips, "Calculation of the Internal Mechanical Response of Sheep to Blast Loading," in Proceedings of 10th Intl. Symposium on Military Application of Blast Simulation, Oberjettenberg, FR-Germany, September 1987.

6. Stuhmiller, J. H., J. H.-Y. Yu, E. J. Vasel, and K. T. Dodd, "Use of Surrogate and Analytical Models to Understand the Parameters Controlling Blast Injury to the Gastro-Intestinal Tract," Proceedings of the 3rd Workshop on Weapon Launch Blast Overpressure, Aberdeen Proving Ground, Md., June 9-10, 1986.

7. Vasel, E.J. and J.H.-Y. Yu, "Gastrointestinal Tract Blast Injury Laboratory Test Techniques," JAYCOR Technical Report, August 1989.

DISTRIBUTION LIST

4 copies	Director Walter Reed Army Institute of Research ATTN: SGRD-UWZ-C Washington, DC 20307-5100
1 copy	Commander US Army Medical Research and Development Command ATTN: SGRD-RMI-S Fort Detrick, Frederick, MD 21701-5012
2 copies	Defense Technical Information Center (DTIC) ATTN: DTIC-DDAC Cameron Station Alexandria, VA 22304-6145
1 copy	Dean School of Medicine Uniformed Services University of the Health Sciences 4301 Jones Bridge Road Bethesda, MD 20814-4799
1 copy	Commandant Academy of Health Sciences, US Army ATTN: AHS-CDM Fort Sam Houston, TX 78234-6100